

# Time Varying Compensator Design for Reconfigurable Structures using Non-Collocated Feedback

M. A. Scott  
*Langley Research Center, Hampton, Virginia*

October 1996

National Aeronautics and  
Space Administration  
Langley Research Center  
Hampton, Virginia 23681-0001

TIME VARYING COMPENSATOR DESIGN FOR RECONFIGURABLE  
STRUCTURES USING NON-COLLOCATED FEEDBACK

by

MICHAEL ALLEN SCOTT

MS, University of Virginia, 1989

BS, Virginia Polytechnic Institute and State University, 1984

A dissertation submitted to the  
Faculty of the Graduate School of the  
UNIVERSITY OF COLORADO  
in partial fulfillment of the requirements for the degree of  
DOCTOR OF PHILOSOPHY

in

AEROSPACE ENGINEERING SCIENCES

1995

Scott, Michael Allen (Ph.D., Aerospace Engineering Sciences)

Time Varying Compensator Design for Reconfigurable

Structures using Non-Collocated Feedback

Dissertation directed by Assistant Professor Lee Peterson

The purpose of this thesis is to develop analysis and synthesis tools to improve the dynamic performance of reconfigurable systems. For simplicity, without losing generality and physical insight, this dissertation is focused on planar motion. Various control law strategies are considered and evaluated for the non-minimum phase, non strictly positive real, time variant system. The strategies include indirect and direct model reference adaptive controllers; and fixed, robust, and optimal controllers. Particular emphasis is on enabling real time implementation and reducing the requisite number of experiments to identify the time varying system. System identification is accomplished for the kinematic nonlinear system via the observer Markov parameters using data gathering experiments of a minimum of arm orientations. In addition, the observer Markov parameters can be utilized to reduce the data and improve system identification results. The identified time varying model is augmented with a band pass filter for frequency weighting and is shown to reduce the controller size. A novel Spline Varying Optimal (SVO) controller is developed for the kinematic nonlinear system. An example problem is discussed, all controller coefficients in the SVO controller are very closely approximated by a third order polynomial in the elbow pitch angle,  $\theta$ . There are several advantages to using the SVO controller, in which the spline function approximates the system model, observer, and controller gain. They are: the spline function approximation is simply connected, thus the SVO controller is more continuous than traditional gain scheduled controllers when implemented on a

time varying plant; it is easier for real time implementations in storage and computational effort; where system identification is required, the spline function requires fewer experiments, namely four experiments; and initial startup estimator transients are eliminated. The SVO compensator was evaluated on a high fidelity simulation of the Shuttle Remote Manipulator System. The SVO controller demonstrated significant improvement over the present arm performance: (1) Damping level was improved by a factor of 3; (2) Peak joint torque was reduced by a factor of 2 following Shuttle thruster firings.

## Table of Contents

<b>1</b>	<b>Introduction</b>	1
1.1	Background and Previous Research	2
1.2	Thesis Objectives and Overview	9
1.3	Organization of Thesis	12
<b>2</b>	<b>Open Loop Manipulator Modeling</b>	15
2.1	Two Degree of Freedom Manipulator	16
2.2	Six Degree of Freedom Manipulator	28
2.3	Non-minimum Phase Zeros and Boundary Conditions	29
2.4	Frequency Dependence on Payload Mass	39
2.5	Root Locus of Open Loop System as Theta Varies	43
2.6	Modal Open Loop Infinity Norm	45
2.7	Summary	48
<b>3</b>	<b>System Identification</b>	50
3.1	Markov Parameters and the State Space Model	52
3.2	Observer Markov Parameters	53
3.3	Identification of Linear Systems	56
3.4	Identification of Time Varying Systems	58
3.5	Numerical Experimental Results	60
3.6	Observer Canonical State Space Model	70
3.7	Summary	73
<b>4</b>	<b>Compensator Design</b>	75
4.1	Controller Implementation Strategy	76

4.2	Fixed Optimal Compensator.....	77
4.3	Fixed Robust Dynamic Compensator .....	83
4.4	Gain Scheduled Compensator.....	89
4.5	Spline Varying Optimal (SVO) Compensator .....	97
4.6	Performance Comparison.....	100
4.7	Summary .....	113
<b>5</b>	<b>Active Vibration Damping of the Space Shuttle Remote Manipulator System.....</b>	<b>115</b>
5.1	Shuttle Remote Manipulator System .....	116
5.2	Collocated Versus Non-Collocated Control .....	123
5.3	Spline Varying System Identification .....	126
5.4	Spline Varying Optimal Controller Design and Implementation in RMS Software .....	132
5.5	Active Damping Results .....	135
5.6	Summary .....	137
<b>6</b>	<b>Conclusion and Recommendations .....</b>	<b>138</b>
	<b>List of References.....</b>	<b>144</b>
	<b>Appendix.....</b>	<b>150</b>
A	Hyperstability and Positive Definite Systems - Definitions.....	150

## List of Tables

1.1	Summary of Controller Design Techniques .....	9
2.1	Definition of Variables used in Model Generation.....	18
2.3.1	Non Dimensional Parameters used in Experiment.....	33
2.3.2	Poles and Zeroes with No Base Constraint.....	34
2.3.3	Poles and Zeroes with Gearbox Model Inserted .....	35
2.3.4	Poles and Zeroes with Gearbox Model and Rate Command Inserted ....	37
2.4.1	Frequency Versus Non Dimensional Payload Mass Ratio.....	42
2.5.1	Root location for 1st and 2nd Modes as Theta Varies.....	44
2.6.1	Non Dimensional Parameters used in Zero Payload Experiment .....	47
3.5.1	Non Dimensional Parameters used in Numerical Experiment.....	60
3.5.2	Identified Observer Markov Parameters - $p = 2$ .....	61
3.5.3	Identified Observer Markov Parameters - $p = 4$ .....	65
4.6.1	SVO Compensator Parameters.....	106
4.6.2	Cost Comparisons.....	112
5.1.1	Slew Rate Limits of SRMS.....	118
5.3.1	Identified Observer Markov Parameters .....	128

## List of Figures

2.1	Flexible Manipulator .....	17
2.2.1	Six Degree of Freedom Manipulator .....	29
2.3.1	Control Block Diagram with Rate Command .....	31
2.3.2	Two Link Model with Rate Command.....	32
2.3.3	Root Locus of Poles and Zeroes - No Base Constraint.....	34
2.3.4	Root Locus of Poles and Zeroes with Gearbox Model.....	35
2.3.5	Pulse Time History with Gearbox Model.....	36
2.3.6	Root Locus of Poles and Zeroes with Gearbox Model and Rate Command.....	37
2.3.7	Pulse Time History with Gearbox Model and Rate Command.....	38
2.4.1	Cantilever Hinged Problem.....	41
2.4.2	Theoretical Frequency Separation for Cantilever Free Boundary Condition .....	41
2.4.3	Frequency Ratio Versus Payload Mass Ratios for Various Modes.....	43
2.5.1	First Mode Poles as a Function of Theta.....	44
2.5.2	Second Mode Poles as Function of Theta .....	45
2.6.1	Infinity Norm of Bode Response as a Function of Mode Number and Theta - Heavy Payload.....	46
2.6.2	Infinity Norm Ratio of 2nd vs 1st Mode as a Function of Theta.....	46
2.6.3	Infinity Norm Ratio of 3rd vs 1st Mode as a Function of Theta .....	47
2.6.4	Infinity Norm of Bode Response as a Function of Mode Number and Theta - Zero Tip Mass.....	48
3.1	Two Link Model used for System Identification.....	51
3.1.1	Markov Parameters as Weights in a Linear Network.....	53
3.2.1	A Single Layer of a Recurrent Network .....	55

3.4.1	A Single Layer Time Varying Recurrent Network.....	59
3.5.1	Identified Polynomial $\hat{\beta}_1(\theta)$ .....	62
3.5.2	Identified Polynomial $\hat{\alpha}_1(\theta)$ .....	62
3.5.3	Identified Polynomial $\hat{\beta}_2(\theta)$ .....	63
3.5.4	Identified Polynomial $\hat{\alpha}_2(\theta)$ .....	63
3.5.5	Identified Exponential Function $\hat{\beta}_1(\theta) - p = 4$ .....	66
3.5.6	Identified Exponential Function $\hat{\alpha}_1(\theta) - p = 4$ .....	66
3.5.7	Identified Exponential Function $\hat{\beta}_2(\theta) - p = 4$ .....	67
3.5.8	Identified Exponential Function $\hat{\alpha}_2(\theta) - p = 4$ .....	67
3.5.9	Identified Exponential Function $\hat{\beta}_3(\theta) - p = 4$ .....	68
3.5.10	Identified Exponential Function $\hat{\alpha}_3(\theta) - p = 4$ .....	68
3.5.11	Identified Exponential Function $\hat{\beta}_4(\theta) - p = 4$ .....	69
3.5.12	Identified Exponential Function $\hat{\alpha}_4(\theta) - p = 4$ .....	69
4.2.1	Fixed Dynamic Compensator .....	79
4.3.1	Fixed Robust Compensator - Nominal Stability .....	84
4.3.2	Fixed Robust Compensator with Large Plant Variations .....	85
4.3.3	Additive Model Errors .....	87
4.3.4	Universal Diagram for Gain-Phase Margin Evaluation .....	88
4.4.1	Gain Scheduled Compensator.....	89
4.4.2	Diagonal Gain and Phase Change Matrix at Plant Input .....	96
4.5.1	SVO Compensator Block Diagram .....	99
4.6.1	Open and Closed Loop Cost Comparison as a Function of Theta - Fixed Compensator.....	101
4.6.2	Bode Response of Nominal Plant Model $G_n(s)$ at $40^\circ$ .....	103

4.6.3	Maximum Bound on the Additive Model Error $E_a(j\omega)$ .....	103
4.6.4	Open and Closed Loop Cost Comparison as a Function of Theta - Fixed Robust Compensator .....	104
4.6.5	SVO Compensator Parameter $\alpha_1(\theta)$ .....	107
4.6.6	SVO Compensator Parameter $\alpha_2(\theta)$ .....	107
4.6.7	SVO Compensator Parameter $\beta_1(\theta)$ .....	108
4.6.8	SVO Compensator Parameter $\beta_2(\theta)$ .....	108
4.6.9	SVO Compensator Parameter $C_{c1}(\theta)$ .....	109
4.6.10	SVO Compensator Parameter $C_{c2}(\theta)$ .....	109
4.6.11	SVO Compensator Parameter $K_{y1}(\theta)$ .....	110
4.6.12	SVO Compensator Parameter $K_{y2}(\theta)$ .....	110
4.6.13	Open and Closed Loop Cost Comparison as a Function of Theta - SVO Compensator.....	111
4.6.14	Open and Closed Loop Cost Comparison as a Function of Theta .....	112
5.1.1	Space Shuttle Remote Manipulator System (RMS).....	117
5.1.2	SRMS Configuration $\theta = 0^\circ$ .....	120
5.1.3	SRMS Configuration $\theta = 30^\circ$ .....	120
5.1.4	SRMS Configuration $\theta = 60^\circ$ .....	120
5.1.5	SRMS Configuration $\theta = 90^\circ$ .....	120
5.1.6	Typical RMS Response and Sensor Outputs.....	121
5.1.7	RMS Second Structural Mode Shape .....	122
5.1.8	RMS Structural Mode Contributions.....	122
5.2.1	The SISO System Identification Results for the y Axis of the Simulated Tip Accelerometer.....	124
5.2.2	The SISO System Identification Results for the y Axis of the Simulated Shoulder-Yaw Tachometer.....	124

5.2.3	Damping as a Function of Scaled Gain Using the Shoulder-Yaw Joint.....	125
5.2.4	Damping as a Function of Scaled Gain Using the Shoulder-Pitch Joint .....	126
5.3.1	SVO SRMS Compensator Parameter $\beta_1(\theta)$ .....	128
5.3.2	SVO SRMS Compensator Parameter $\alpha_1(\theta)$ .....	129
5.3.3	SVO SRMS Compensator Parameter $\beta_2(\theta)$ .....	129
5.3.4	SVO SRMS Compensator Parameter $\alpha_2(\theta)$ .....	130
5.3.5	System Identification Results for the Tip Displacement.....	131
5.3.6	System Identification Results for the Tip Accelerometer (y axis).....	131
5.4.1	Proposed SVO Controller Implementation in Shuttle Software.....	134
5.5.1	Tip Position Following 3-Second Pulse Command.....	136
5.5.2	Shoulder Pitch Servo Torque Following 3-Second Pulse Command. After 90 Seconds the Shuttle Thrusters are Fired for 6 Seconds.....	136
A.1	Geometric Interpretation of $\bar{A} + \bar{A}^T < 0$ .....	152

## Nomenclature

$a_i$	$i^{\text{th}}$ time dependent generalized coordinate of link 1
$A$	System matrix
$A_{ai}$	Cross sectional area of link $i$
$A_c$	Controller system matrix
$\hat{A}_{ob}$	Observer system matrix $\hat{A}_{ob} = T_{ob}^{-1}AT_{ob}$
$B$	System input influence matrix
$B_c$	Controller system input influence matrix
$\hat{B}_{ob}$	Observer system input influence matrix $\hat{B}_{ob} = T_{ob}^{-1}B$
$c_j$	$j^{\text{th}}$ time dependent generalized coordinate of link 2
$C$	System output matrix
$C_c$	Controller system output matrix
$\hat{C}_{ob}$	Observer system output matrix $\hat{C}_{ob} = CT_{ob}$
$D$	Direct transmission matrix
$D_c$	Controller direct transmission matrix
$e(k)$	State estimation error
$E_a(j\omega)$	Additive error bound
$E_i$	Modulus of elasticity of link $i$
$f$	Non dimensional frequency
$G_{ave}(s)$	Average model transfer function
$G_c(s)$	Compensator transfer function
$G_n(j\omega)$	Design model
$h_k$	Discrete Markov parameters
$h_k$	Pulse response
$i$	$\sqrt{-1}$
$I_i$	Area moment of inertia of link $i$
$J$	Linear quadratic regulator cost function

$K$	Observer gain
$L$	Lagrangian
$L_i$	Longitudinal length of link i
$m_i$	Mass at end of link i
$m_p$	Payload mass
$\bar{M}$	Non-dimensional mass
$p_i$	i <sup>th</sup> pole of transfer function
$q$	Generalized coordinate vector
$Q$	Output weight matrix
$Q_w$	Process noise covariance
$\dot{\vec{r}}_{2,x}$	Velocity of elemental mass $x_2$ on link 2
$r_L$	Link length ratio: length of link 2 relative to link 1
$R$	Input weight matrix
$R_v$	Measurement noise covariance
$s$	Laplace Variable
$t$	Time
$tr( )$	Trace Operator
$T$	Kinetic energy
$T_J(G_c)$	Total cost for compensator $G_c(s)$
$T_n(s)$	Loop transfer function matrix
$T_{ob}$	Change of state matrix
$u$	System inputs
$U$	Potential energy
$w'_{1,L_1}$	First spatial derivative of link 1 evaluated at $L_1$
$\dot{w}_{2,L_2}$	First time derivative of link 2 evaluated at $L_2$
$w_i(x_i, t)$	Transverse deflection of link i
$\bar{x}$	Augmented state vector
$\hat{x}(k)$	State estimate
$\bar{x}_0$	Initial augmented state vector
$x_i$	Spatial variable for link i
$y$	System outputs

$\bar{Y}(k)$	Observer Markov parameters
$z_i$	i <sup>th</sup> zero of transfer function
$z^{-1}$	Time delay operator

### Greek

$\hat{\alpha}_k, \hat{\beta}_k$	Identified Markov parameters
$\alpha_k, \beta_k$	Markov Parameters
$\xi$	Damping
$\phi_i$	i <sup>th</sup> admissible spatial function of link 1
$\phi^*$	Normalized deflection function of link 1
$\eta_i$	Mass ratio of link i; end mass to link mass
$\eta_L$	Link mass ratio: mass of link 2 relative to link 1
$\lambda$	Eigenvalues
$\mu_i$	Non-dimensional stiffness properties of link i
$\rho_i$	Volumetric density of link i
$\theta_i$	Rigid body orientation of link i relative to link i+1
$\underline{\sigma}$	Minimum singular value
$\bar{\sigma}$	Maximum singular value
$\omega_n$	Natural frequency
$\xi_i$	Normalized spatial variable of link i
$\psi_j$	j <sup>th</sup> admissible spatial function of link 2
$\psi^*$	Normalized deflection function of link 2

### Math

1,2	Subscript denotes link 1 or link 2
$\  \cdot \ _{\infty}$	Infinity norm
$(\cdot)^*$	Complex conjugate transpose
$(\cdot)^{-1}$	Inverse operator
$(\cdot)^+$	Pseudo-inverse
$(\cdot)^T$	Transpose of matrix or vector

## **CHAPTER 1**

### **INTRODUCTION**

One of the fundamental problems in the operations of flexible manipulators in space is the duration and rate of decay of their oscillatory motions. Robotic manipulator arms have traditionally been modeled as composed of rigid links, with collocated actuators and sensors, to ensure stable and reliable control. In order for the arms to remain rigid while carrying a payload, they must typically be made with heavy elements, requiring in turn larger and heavier actuators. These facts have motivated the recent interest in using lightweight, higher performance robots for both commercial and space-based applications. The advantages of such lightweight manipulators are many, including faster system response, lower energy consumption, smaller actuators and trimmer mechanical design. Obvious tradeoffs, however, complicate the problem of flexible manipulator control, which focuses primarily on the controller design to compensate for flexible effects.

Traditionally, ground based manipulators designed to handle payloads in the presence of gravity weigh 100-200 times the weight of the assigned payload. However, space-based robots such as the Shuttle Remote Manipulator System (RMS), are designed to maneuver payloads in the absence of gravity. Due to mass and volume constraints these manipulators have relatively thin (low stiffness) booms, yet they maneuver payloads weighing 30-40,000 lb. The corresponding manipulator to payload weight ratio is 0.005:1. In addition, space-based robots tend to be much longer than their terrestrial counterparts. The fundamental bending frequency of these structural systems

is proportional to the square root of the stiffness to payload mass, thus the robotic systems exhibit long periods of oscillatory motion following routine operational maneuvers. As a result, the Shuttle RMS safety operational constraints require astronauts to wait extended periods of time before they are allowed to command the next maneuver.

## **1.1 Background and Previous Research**

There are two distinct approaches to reduce residual motions of robotic manipulators following commanded motions. One approach is to reduce the residual oscillations by using input command shaping techniques (Seering and Singer, 1990 ). An adaptive precompensator can be implemented by combining a frequency domain identification scheme which is used to estimate on-line the modal frequencies and subsequently update the band stop interval or the spacing between the impulses (Tzes, 1989). The advantages of the input shaping approach are that accurate identification of plant parameters, such as frequency and damping, is not critical, and there is no knowledge requirement for the controller influence coefficients. One disadvantage is a significant phase lag between the desired input and corresponding motion of the manipulator. This move time penalty is on the order of one period of the first mode of vibration. The operator commands the arm to stop, but the end point will continue to move for a few seconds. As a result, the manipulator does not have the same “feel” as the current manipulator when used by a trained operator, which could be detrimental when precise positioning is required. Another disadvantage of command shaping is that it cannot reject unknown disturbances. For example, oscillations of the Shuttle RMS that result from the Shuttle thruster firings cannot be damped by an input shaping method applied solely to the Shuttle RMS.

The second approach of employing output feedback to reduce vibration has been selected for this thesis. In this approach, output feedback of measurements of the system response is used in a compensator to derive joint commands designed to damp the residual motions. An example of this second approach is the work by Prakash, Adams and Appleby (1989), who used a detailed analytical model of the manipulator to design model based compensators. Other methods for robust controller design of flexible link arms and nonlinear control methods were suggested by Korolov, Chen (1989) and Kreutz and Jamieson, respectively. In Juang (1993) and Feddema (1990) a model-independent controller for large angle position control of a two and six-degree of freedom robot was developed. However, in these methods the passive controller requires collocation of sensor and actuator. Kanoh and Lee (1985) studied a single link flexible arm with a concentrated mass at the tip; similarly a 12.5 foot steel beam was constructed at the Jet Propulsion Laboratory (Schaechter, 1982). Both of these studies used collocated sensors and actuators in their experiments.

Shoenwald (1991) and Eisler (1990) analyzed the experimental results of a minimum time trajectory control scheme for a two link flexible robot. An off line optimization routine determined a minimum time, straight line tip trajectory, which stayed within the torque constraints of the motor. The control strategy used a linear quadratic regulator to determine the feedback gains based on a finite element model linearized about the straight line tip trajectory. At some points along the trajectory the gains varied considerably. When the set of gains was used to control the system, the results were less than satisfactory. Although the arm did reach the desired end point, there was considerable error in the tip position along the way. In an attempt to reduce the sensitivity of the feedback gains to modeling errors, a single gain matrix, optimized for the average of the workspace, was used. The author (Eisler, 1990) felt that a better

solution would be to use a set of three to four gains that would be scheduled to become active when major changes in the states occurred.

Optimal control has been applied to the nonlinear multilink problem using end point measurement (non-collocation) with limited success. Oakley (1989, 1990b) explores a modeling and mode-selection technique to improve the prediction of the manipulator end-point position. The nonlinear end-point controller based on end-point sensing incorporates a linear quadratic regulator and a nonlinear estimator. Experiments show that this technique significantly improves manipulator position tracking over commonly used collocated control techniques. End point sensing is achieved using a CCD television camera to track special reflectivity targets located at the manipulator end-point. The nonlinear rigid-flex equations of motion were linearized about an elbow angle of  $75^\circ$  in the constant regulator and estimator gain matrices, thus constraining the usable workspace to small perturbations around the linearized plant. In Oakley (1990a) a 278 state controller was able to operate over a large workspace while sacrificing on performance. The authors indicated that if the controller were gain scheduled, the performance would be much improved for operating points far from the linearization point. In Seraji (1986) and Hasting (1985), multivariable control is applied to a two-link robot. The control design is based on a linearized model of the robot dynamics, and it was noted that perturbations of variables from their nominal values must be kept small. When large excursions of variables are expected, the controller must be updated at suitable intermediate positions in order to improve the performance of the control system.

In Matsuno (1990) a control law is developed for a 6 degree of freedom robot using acceleration feedback. Matsuno showed that the end effector tip trajectories were superior in terms of residual motion over the open loop trajectories, although the

available workspace was constrained within small perturbations around the linearized plant. In Yurkovich (1990), identified models of a two link manipulator were used in static and dynamic fixed controller design, where end point accelerations were used. The controller performance was found to be unsatisfactory for large system parameter variations, especially the elbow joint angle.

It has been known for some time (Gevarter, 1970) that if a flexible structure is controlled by locating every sensor exactly at the actuator it will control, then stable operation is easy to achieve. Nearly all commercial robots and most flexible spacecraft are controlled in this way for this reason. Conversely, when one attempts to control a flexible structure by applying control torques at one end that are based on a sensor at the other end, the problem of achieving stability is severe. Solving it is an essential step for better control in space; the space-shuttle arm is a cogent example. The next generation of industrial robots will also need such control capability, since they will need to be much lighter in weight (to achieve quick response with less power), and they will need to achieve greater precision by employing end-point sensing (Cannon, 1984). A direct-drive, laser cutting robot, for example, tracks a curved trajectory, while the tracking error at the arm tip is required to be less than  $\pm 0.2$  mm (Asada, 1987). Extremely heavy arm inertia resulted when one tries to make the arm construction sufficiently stiff so that the elastic deformation is less than  $\pm 0.2$  mm at the arm tip (Asada, 1990).

It has been shown (Hillsley, 1991; Yurkovich, 1990; Oakley, 1988; Kotnik, 1988) that rigid dynamics control alone cannot achieve accurate and steady link endpoint position. Kotnik (1988) and Wells present single link laboratory results for a flexible manipulator in which four separate control strategies are compared and contrasted. Namely, the control schemes compared are: compensation using classical root locus techniques with

endpoint position feedback, a full state feedback, observer-based design, and compensation using endpoint acceleration feedback. The results indicated that acceleration feedback has great potential in flexible manipulator control. The study pointed out that the use of acceleration feedback for flexible robot arm control has intuitive appeal from an engineering design viewpoint. Primary advantages include the fact that sensing acceleration for control implementation is accomplished with structure mounted devices so that camera position or field of view are not issues, and that from a practical viewpoint implementation is easy and inexpensive.

A similar study was performed in Scott (1993), where arm tip acceleration feedback was used in a model-based compensator for the six degree of freedom Shuttle RMS, augmented with a mounted 3000 pound payload. However, in this study the workspace was constrained to small perturbations about a linearized plant. In another study by Demeo (1992) the workspace of the RMS was extended by developing a single controller optimized over a range of workspaces using a Quasi-Newton numerical optimization routine. The control design presented here was relatively simple in nature, with a motor shaft position feedback loop for rigid body motion control and the endpoint acceleration feedback loop for flexible motion control. System identification studies were employed in lieu of analytical modeling exercises because system identification would become increasingly necessary as the level of complexity for such systems increases. In this study the sensor dynamics and actuator dynamics were lumped into a single aggregate system. The use of digital filtering techniques enhanced the quality of the signals used in the control design, and was equivalent to an a-priori frequency weighted design.

Other feedback methods to reduce vibration include adaptive control algorithms which is an attractive feedback approach since the plant is changing in time (Lucibello, 1990,

Balestrino, 1983, and Nicosia, 1984, Harashima and Ueshiba, 1986). Adaptive control can be divided into two subcategories; indirect and direct. Indirect (or explicit) identifies explicit parameters of the plant. Direct (or implicit) has no parameter identification. The indirect Model Reference Adaptive Controller (MRAC) does not solve the non-collocated actuators and sensor problem well for non-minimum phase plants (Liang, 1990). The ‘one step ahead control law’ inverts the plant transfer function, thus non-minimum phase plants are not stable for this control law. Even one-link flexible arms, where linear dynamic models are appropriate (Cannon, 1984), standard inversion techniques aimed at output trajectory reproduction fail, due to the non-minimum phase nature of the transfer function from joint torque to tip position. A similar difficulty is present when working with the full nonlinear dynamics of a two or multilink arm, due to the presence of an unstable zero dynamics (De Luca, 1989). The Direct MRAC requires the plant to be Strictly Positive Real (SPR) when the plant model states are not available for feedback. A new version of the Direct MRAC has been developed (Galvez, 1991) which does not require the SPR property of the plant. With this technique a Dynamic Projection Model (DPM) is adaptively designed so that it shares a common point on the Nyquist plot at zero frequency with the plant. The definition of positive definite systems is summarized in Appendix A.

Dissipative compensators offer an attractive alternative because they circumvent the sensitivity problems associated with model-based compensators. However, the practical usefulness of these controllers is limited because stability depends on the system parameters to be “passive.” In the context of network theory, a passive system represents the driving point impedance of a dissipative network. A network is called dissipative if it consists only of resistors, lossy inductors, and lossy capacitors, which dissipate energy. Dissipative compensators use collocated compatible actuators and sensors (Joshi, 1991).

Table 1.1 summarizes several control design techniques. Each control technique is evaluated in terms of constraints, assumptions, and performance models required. For a reconfigurable system, this thesis proposes the Spline Varying Optimal (SVO) Compensator, which is outlined in Chapter 5.

On the left hand side of Table 1.1, the constraints and fundamental assumptions include non-minimum phase and Strictly Positive Real (SPR) requirements on the plant and/or the controller (Liang, 1990). The reference or performance model refers to the requirement of a dynamic model which the controller is required to track. Adaptive plant realization refers to the requirement of real time plant realizations. To be fair to the non proposed controllers depicted in Table 1.1, some of the constraints are theoretical in nature, as opposed to practical. For example, although sufficient stability theory is not yet available, these controllers have performed well for certain systems that violate the plant and or controller constraints. Thus the conditions are sufficient, but not necessary as outlined (Liang, 1990). In addition, there are operational conditions of the SVO controller which are required. These conditions are outlined in section 4.1.

As shown in Table 1.1, both the direct and indirect MRAC require a reference or performance model. How one derives such a model for a time varying system is not clear. In addition, requiring a plant to follow such a reference model may result in moving plant poles unnecessarily large distances in the root locus plane to achieve model following properties. Both the indirect and direct adaptive control methodologies require extensive use of on-board computer hardware.

Table 1.1 Summary of Controller Design Techniques				
	IMRAC	CGT-DRMAC	DPM DRMAC	Proposed in this thesis
Type of Controller	Model Following Feed forward	Model Following Feed forward	Model Following Feedback	Spline Varying Optimal (SVO)
Plant Constraints	Non-minimum phase	SPR	None	None
Fundamental Assumption		$A_c = A + B G(t) C$ remains SPR for all time	None	None
Reference or Performance Model Required	Yes	Yes	Yes	None
Adaptive Plant realization Required	Yes	None	Yes	None

## 1.2 Thesis Objectives and Overview

The primary objective of this thesis is to develop analysis and synthesis tools which do not demand the plant constraints, and adaptive realizations as outlined in Table 1.1. The focus is to improve the dynamic performance of a nonlinear flexible reconfigurable structure, while minimizing hardware and software modifications to the overall system. Minimal hardware in this sense implies using few and lightweight sensors and actuators, for example, taking advantage of the actuators that are already on a reconfigurable structure to improve dynamic performance, and using inexpensive flight qualified sensors such as accelerometers. Minimal software implies using adroit techniques to minimize the computational burden of the dynamic controller (i.e., small order controller). In addition, a major emphasis is to reduce the requisite number of system identification experiments to characterize the system for control law

development. Particular attention is focused on the type of manipulator used on the Shuttle Remote Manipulator System.

The approach taken for control law design relies on identifying mathematical models from data. Identified models eliminate the need to develop accurate models of operational safety functions, sensor, and actuator transfer functions of the system under control. Experience with complex hardware in the NASA Langley lab has shown that as system complexity increases, analytical model based controllers require a large order compensator, and may not be as accurate for control law development as identified reduced order mathematical models (Belvin, 1991).

In this thesis the dynamic behavior of a space robot maneuvering a heavy payload is exploited to design several very small order compensators that improve robot dynamic performance over a large workspace. There are two main categories of nonlinearities associated with a multidegree of freedom manipulator; kinetic and kinematic. The kinetic nonlinearities are associated with nonlinear energy dissipation in the joints, for example gearbox stiction, friction and backlash. The kinematic nonlinearities include the nonlinear behavior induced by large angle motion of the manipulator joints, resulting in configuration changes, which alter the open loop dynamics of the system. Addressing the kinematic nonlinearities is the main focus of this thesis; although the nonlinear controllers will be evaluated on a high fidelity simulator which includes the aforementioned kinetic nonlinearities. A two link planar model will be used to address the kinematic nonlinear problem. The high fidelity simulator is utilized to investigate various collocated and non-collocated control strategies, and to evaluate the low order controller on a highly nonlinear system. Another objective of this thesis is to identify sensor locations on the structure that enable a time varying non-collocated controller to operate over a wide variety of arm orientations.

It is shown that the wait time penalty incurred by operators is largely dominated by the modal damping of the lowest fundamental mode of the manipulator dynamics. The damping of this fundamental mode is increased by minimizing a cost performance index evaluated over the workspace of the manipulator. A non-dimensional parameter dependent mathematical model of a two link manipulator is analyzed to investigate various control law designs. Three different compensators that utilize non-collocated measurement of the time varying system are investigated. The compensators include fixed, robust, and spline varying optimal (SVO) compensators. This thesis develops a method to implement each of the compensators in a manner which reduces the computational burden of real time implementations.

The objectives of the compensator design are as follows:

- To determine the performance and limitations of collocated control versus non-collocated control.
- To determine how a traditional fixed gain dynamic compensator performs for a plant that is changing in time.
- To determine the performance of a fixed compensator, and if the resultant stability margins are sufficient to work over a large workspace.
- To determine the performance of traditional robust compensator designs over a large workspace.
- To determine what the optimal state dependent compensator is for the time varying plant. What is its performance in relation to the fixed and robust compensator.
- To determine what type and number of experiments are required to design a SVO compensator. To determine how many different arm

orientations are necessary to characterize the dynamics over the workspace.

To aid this investigation, the time varying optimal compensator is implemented on a Draper simulation of the Shuttle Remote Manipulator System (Gray, 1985) . The fixed gain compensator developed by the author was evaluated by astronauts at the Johnson Space Center. The astronaut/operator's assessment of the fixed gain compensator noted that there was a "significant increase in damping" (Lepanto, 1992). It was noted that "Our (NASA/Draper) philosophy has been to design a single compensator that improves the performance of the RMS for a wide range of configurations, and it is clear that the increase in damping at any one configuration will be less with this 'one size fits all' compensator than with a compensator tuned to that specific configuration." Loads reduction for the RMS with the fixed gain compensator was also cited as an important factor several times during the sessions. The time varying compensator demonstrated significant improvement over the present arm performance (Scott, 1993): (1) Damping level was improved by a factor of 3 and (2) Peak joint torque was reduced by a factor of 2 following Shuttle thruster firings. It is expected that with an optimal time varying compensator the damping and the loads will be improved for a larger workspace of the manipulator.

### **1.3 Thesis Organization**

Chapter 2 introduces a mathematical model of a manipulator that can be used to investigate various control law strategies. Lagrangian dynamics are applied to determine the kinetic and potential energies for the two link system. The resultant dynamic equations are then organized into a state space model suitable for use in linear

control system design. First a two link manipulator is discussed. The equations of motion are non-dimensionalized to provide a greater understanding of how physical parameters affect the open loop dynamics. A six degree of freedom manipulator is used to indicate, and discuss the relative sensitivity of the various input-output transfer functions to the joint degrees of freedom, and indicate why the two degree of freedom model approximates the larger degree of freedom system. Some fundamental mathematical properties of manipulators such as the frequency separation and the modal contribution to the open loop infinity norm are discussed.

In Chapter 3 the nonlinear system is identified using the observer Markov Parameters. Data is gathered from four experiments as the elbow joint angle is moved from 0 degrees to 90 degrees. System identification is then applied to the data to identify the observer Markov parameters. The observer Markov Parameters are then used to obtain the system state space matrices as a function of  $\theta$ .

In Chapter 4 the compensator design is discussed and the control strategy is introduced. Three compensators are investigated: a fixed gain compensator, a robust dynamic compensator, and the Spline Varying Optimal (SVO) compensator. An example problem is included to discuss the performance and stability comparisons of the various controller strategies.

In Chapter 5 various control strategies are applied to a high fidelity simulation of the shuttle manipulator system. The approach to the RMS active damping feasibility study is developed as follows. First, a set of payloads and arm configuration combinations consistent with the types of payloads expected during Space Station assembly were defined. Second, RMS dynamics and operational characteristics were examined using the nonlinear Draper RMS Simulator (DRS) code (Gray, 1985). The determination of

active damping augmentation feasibility involved the design and simulation of candidate damping augmentation control laws. For this purpose, system identification methods were employed on output data from the DRS to identify time varying models which closely match the DRS response. With the nonlinear control design models, various active control law design concepts were evaluated, as were the requirements for feedback sensors to measure arm motions. The final step was the simulation of the active damping control laws in a modified version of the DRS, to determine the effects of system nonlinearities and computer time delays. Chapter 6 includes Conclusion and Recommendations.

## **CHAPTER 2**

### **OPEN LOOP MANIPULATOR MODELING**

The problem of modeling articulated flexible mechanical systems has been studied extensively. Cannon and Schmitz (1984) published the pioneer work in the area of control and modeling of flexible robot arms. In that work, the mathematical modeling and the initial experiments have been carried out to address the control of a one link flexible robot arm where the position of the end effector (tip) is controlled by measuring that position and using the measurement as a basis for applying control torque to the other end of the arm (joint). Book, Maizza-Neto and Whitney (1975) directly approximate a two link flexible robot with a linear model derived from a nonlinear distributed parameter model. In the papers of Balas (1978) and Karkkainen and Halme (1985) a modal approach to the problem of approximating a general flexible mechanical system is used. Book (1979) uses a special technique called lumping approximation to analyze flexible mechanical systems, assuming that the links bend in a first mode of vibration. Judd and Falkenburg (1985) apply this method to non rigid articulated robots; the same technique is adopted by Sunada and Dubowsky (1983) and modified in such a way that more vibration modes are allowed. Chassiakos and Bekey (1985) approximate the distributed parameter system response. Truckenbrodt (1982) analyzes the deformation of a chain of elastic links using the Ritz-Kantorovitch method and studies the dynamic behavior linearizing the related differential equations.

No attempt is made in this thesis to improve the modeling techniques for flexible manipulators. Including high order effects such as foreshortening of the beam only obfuscate the issues discussed in the control law design.

This chapter discusses the open loop manipulator modeling. First a two link manipulator is discussed. The equations of motion are non-dimensionalized to provide a greater understanding of how physical parameters affect the open loop dynamics (Smart, 1993). A six degree of freedom manipulator model is presented to discuss the relative sensitivity of the various input-output transfer functions to the joint degrees of freedom, and to indicate why the two degrees of freedom model approximates the larger degree of freedom system. The frequency dependence on the payload mass is then introduced. It is noted that for heavier payloads there is a larger separation between the first and higher order or residual modes. If a payload 100 times the mass of the arm is considered, the 2nd modal frequency is 98 times the frequency of the 1st mode. In Section 2.4 the open loop infinity norm is utilized to indicate the predominance of the fundamental mode to the overall performance of the open loop manipulator.

## **2.1 Two Degree of Freedom Manipulator**

The material in this section describes a time varying linear model of a flexible two link manipulator (Figure 2.1). The mathematical model forms the basis for investigating various control strategies covered in later sections.

The mechanical joint corresponding to  $\theta_1$  angle is referred to as the shoulder joint, and the joint corresponding to the  $\theta_2$  angle is referred to as the elbow joint. In Figure 2.1,  $m_1$  and  $m_2$  refer to point masses at the first and second links respectively. The method

employed to generate the model utilizes a separable formulation of assumed modes to represent the transverse displacement due to bending. Lagrangian dynamics are applied to determine the kinetic and potential energies for the two link system (Smart, 1993). The resultant dynamic equations are then organized into a state space model suitable for use in linear control system design.

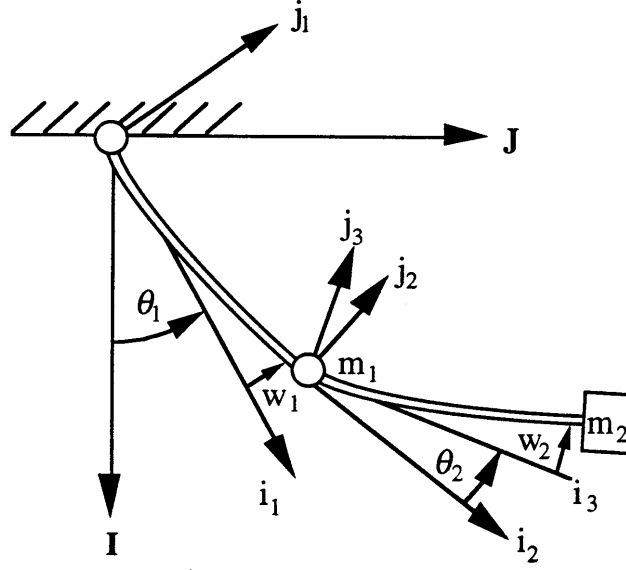


Figure 2.1 Flexible Manipulator

The slenderness ratio of each link is such that rotary inertia and shear deformation effects may be neglected (i.e. assuming Euler-Bernoulli beam theory). In the following analysis it is assumed that the squared flexible deflections are negligible compared to the axial dimension squared (Hasting, 1986). The definition of the variables used in the model generation are shown in Table 2.1.

The coordinate systems are defined as follows.

$$\begin{Bmatrix} i_1 \\ j_1 \end{Bmatrix} = \begin{bmatrix} \cos(\theta_1) & \sin(\theta_1) \\ -\sin(\theta_1) & \cos(\theta_1) \end{bmatrix} \begin{Bmatrix} I \\ J \end{Bmatrix} \quad (2.1.1)$$

$$\begin{Bmatrix} i_2 \\ j_2 \end{Bmatrix} = \begin{bmatrix} \cos(w'_{1,L_1}) & \sin(w'_{1,L_1}) \\ -\sin(w'_{1,L_1}) & \cos(w'_{1,L_1}) \end{bmatrix} \begin{Bmatrix} i_1 \\ j_1 \end{Bmatrix} \quad (2.1.2)$$

$$\begin{Bmatrix} i_3 \\ j_3 \end{Bmatrix} = \begin{bmatrix} \cos(\theta_2) & \sin(\theta_2) \\ -\sin(\theta_2) & \cos(\theta_2) \end{bmatrix} \begin{Bmatrix} i_2 \\ j_2 \end{Bmatrix} \quad (2.1.3)$$

<p style="text-align: center;"><i>Table 2.1</i> Definition of Variables used in Model Generation</p>	
$\rho_i$	Volumetric density of link i
$E_i$	Modulus of elasticity of link i
$A_{ai}$	Cross sectional area of link i (constant)
$I_i$	Area moment of inertia of link i
$L_i$	Length of link i
$w_i(x_i, t)$	Transverse deflection of link i
$w'_{1,L_1}$	First spatial derivative of link 1 evaluated at $L_1$
$\dot{w}_{2,L_2}$	First time derivative of link 2 evaluated at $L_2$
$x_i$	Spatial variable for link i
t	Time

In Equation (2.1.2) it is implicitly assumed that the geometric angle at the tip of link 1 created by the elastic deformation of the link is approximately  $(\partial w_1 / \partial x_1)_{x_1=L_1}$ . In addition, note that the rigid body rotation of the second member is relative to the slope at the end of the first link. The coordinate axis in (2.1.1-3) are depicted in Figure 2.1.  $I$ , and  $J$  represent the local vertical and horizontal axis respectively. The coordinates  $i_1$ , and  $j_1$  represent the rigid body motion of link 1 with respect to the local vertical axis  $I$ , and  $J$ . The coordinates  $i_2$ , and  $j_2$  represent the rigid body rotation of link 2 with respect to  $i_1$ , and  $j_1$ .

Using the coordinate transformations of equations (2.1.2) and (2.1.3), the position for an elemental mass on link 2 at  $x_2$  takes the form

$$\vec{r}_{2,x} = L_1 \hat{i}_1 + w_{1,L_1} \hat{j}_1 + x_2 \hat{i}_3 + w_2 \hat{j}_3 \quad (2.1.4)$$

The corresponding velocity for an elemental mass on link 2 at  $x_2$  is

$$\dot{\vec{r}}_{2,x} = \left( L_1 \dot{\theta}_1 + w_{1,L_1} \right) \hat{j}_1 - w_{1,L_1} \dot{\theta}_1 \hat{i}_1 + (x_2 \omega + \dot{w}_2) \hat{j}_3 - w_2 \omega \hat{i}_3 \quad (2.1.5)$$

where

$$\omega = \theta_1 + \theta_2 + \dot{w}'_{1,L_1} \quad (2.1.6)$$

the dot product of the element velocity is given by

$$\begin{aligned} \dot{\vec{r}}_{2,x} \cdot \dot{\vec{r}}_{2,x} = & L_1^2 \dot{\theta}_1^2 + 2L_1 \dot{\theta}_1 \dot{w}_{1,L_1} + \dot{w}_{1,L_1}^2 + x_2^2 \omega^2 + 2x_2 \omega \dot{w}_2 + \dot{w}_2^2 \\ & + 2L_1 \dot{\theta}_1 x_2 \omega \cos(\theta_2) + 2L_1 \dot{\theta}_1 \dot{w}_2 \cos(\theta_2) \\ & + 2\dot{w}_{1,L_1} x_2 \omega \cos(\theta_2) + 2\dot{w}_{1,L_1} \dot{w}_2 \cos(\theta_2) \end{aligned} \quad (2.1.7)$$

In accordance with the small angle approximation made in (2.1.2), it is assumed that

$w'_{1,L_1}$  is small such that  $\cos(w'_{1,L_1}) \cong 1$ ,  $\sin(w'_{1,L_1}) \cong w'_{1,L_1}$ . Thus

$$\begin{aligned} \cos(\Omega + w'_{1,L_1}) &\approx \cos(\Omega) - w'_{1,L_1} \sin(\Omega) \\ \sin(\Omega + w'_{1,L_1}) &\approx \sin(\Omega) + w'_{1,L_1} \cos(\Omega) \end{aligned} \quad (2.1.8)$$

where  $\Omega$  is some linear combination of the rigid body rotations. Furthermore, it is assumed that terms involving the deflection functions and their derivatives with powers greater than two are negligible, and the kinetic and potential energies may be reduced to a quadratic form. The above assumptions were made in Smart (1992) where experimental results were used to confirm the assumption.

In determining the kinetic energy of the two link system, only the transverse elastic deformation of each link,  $w_i(x_i, t)$ ,  $i=1,2$ , relative to a known rigid body rotation,  $\theta_i$ ,

i=1,2, is considered. Using Equation (2.1.8) with  $\Omega = \theta_2$ , the quadratic form of the kinetic energy for the first and second link,  $T$ , is

$$\begin{aligned}
T &= T_{L_1} + T_{L_2} \\
&= \frac{1}{2} \int_0^{L_1} (\rho A)_1 (\dot{\vec{r}}_{1,x} \cdot \dot{\vec{r}}_{1,x}) dx_1 + \frac{1}{2} m_1 (\dot{\vec{r}}_{1,x} \cdot \dot{\vec{r}}_{1,x}) \Big|_{x_1=L_1} \\
&\quad + \frac{1}{2} \int_0^{L_2} (\rho A)_2 (\dot{\vec{r}}_{2,x} \cdot \dot{\vec{r}}_{2,x}) dx_2 + \frac{1}{2} m_2 (\dot{\vec{r}}_{2,x} \cdot \dot{\vec{r}}_{2,x}) \Big|_{x_2=L_2}
\end{aligned} \tag{2.1.9}$$

In Equation (2.1.9) the tip masses are modeled as lumped masses without rotary inertia. The potential energy is derived assuming: isotropic beams are in a state of pure bending, plane sections remain plane after bending, Hooke's Law is applicable and only small displacements are considered. In addition, the assumptions of Equation (2.1.8) are used whereby  $\Omega = \theta_1 + \theta_2$ .

The equations of motion are developed using the assumed modes method in conjunction with Lagrange's equation. In doing so, the transverse deflection functions of each beam are written as a linear combination of admissible functions of the spatial coordinate multiplied by time-dependent generalized coordinates (Meirovitch, 1967). That is,

$$\begin{aligned}
w_1(x, t) &= \sum_{i=0}^{\infty} \phi_i(x_1) a_i(t) = \phi^T a = a^T \phi \\
w_2(x, t) &= \sum_{j=0}^{\infty} \psi_j(x_2) c_j(t) = \psi^T c = c^T \psi
\end{aligned} \tag{2.1.10}$$

The quadratic form of the kinetic energy for the first link,  $T_{L_1}$ , is

$$T_{L_1} = \frac{1}{2} J_1^{(1)} \dot{\theta}_1^2 + \frac{1}{2} \dot{a}^T M_a^{(1)} \dot{a} + \dot{\theta}_1 \dot{a}^T M_{1a}^{(1)} \tag{2.1.11}$$

where

$$J_1^{(1)} = \int_0^{L_1} (\rho A)_1 x_1^2 dx_1 + m_1 x_1^2 \Big|_{x_1=L_1} \quad (2.1.12)$$

$$M_a^{(1)} = \int_0^{L_1} (\rho A)_1 \phi \phi^T dx_1 + m_1 \phi \phi^T \Big|_{x_1=L_1} \quad (2.1.13)$$

$$M_{1a}^{(1)} = \int_0^{L_1} (\rho A)_1 x_1 \phi dx_1 + m_1 x_1 \phi \Big|_{x_1=L_1} \quad (2.1.14)$$

where  $J_1^{(1)}$  is the inertia term for the first link,  $M_{1a}^{(1)T}$  is the feedforward term from the joint angle  $\theta$  to the generalized coordinate or tip displacement term  $q$ .  $M_{1a}^{(1)}$  is the feedback term from the generalized tip displacement to the joint angle  $\theta$ , and  $u$  is the generalized input.

The quadratic form of the kinetic energy for the second link,  $T_{L_2}$ , is

$$\begin{aligned} T_{L_2} = & \frac{1}{2} J_1^{(2)} \dot{\theta}_1^2 + J_{12} \dot{\theta}_1 \dot{\theta}_2 + \frac{1}{2} J_2^{(2)} \dot{\theta}_2^2 + \dot{\theta}_1 \dot{a}^T M_{1a}^{(2)} \\ & + \dot{\theta}_2 \dot{a}^T M_{2a} + \frac{1}{2} \dot{a}^T M_a^{(2)} \dot{a} + \dot{\theta}_1 \dot{c}^T M_{1c} + \dot{\theta}_2 \dot{c}^T M_{2c} \\ & + \frac{1}{2} \dot{c}^T M_c \dot{c} + \dot{c}^T M_{ca} \dot{a} \end{aligned} \quad (2.1.15)$$

where

$$\begin{aligned} J_1^{(2)} = & \int_0^{L_2} (\rho A)_2 (L_1^2 + x_2^2 + 2L_1 x_2 \cos(\theta_2)) dx_2 \\ & + m_2 (L_1^2 + x_2^2 + 2L_1 x_2 \cos(\theta_2)) \Big|_{x_2=L_2} \end{aligned} \quad (2.1.16)$$

$$J_2 = \int_0^{L_2} (\rho A)_2 x_2^2 dx_2 + m_2 x_2^2 \Big|_{x_2=L_2} \quad (2.1.17)$$

$$J_{12} = \int_0^{L_2} (\rho A)_2 (x_2^2 + L_1 x_2 \cos(\theta_2)) dx_2 + m_2 (x_2^2 + L_1 x_2 \cos(\theta_2)) \Big|_{x_2=L_2} \quad (2.1.18)$$

$$\begin{aligned} M_{1a}^{(2)} = \int_0^{L_2} (\rho A)_2 & \left( L_1 \phi_{L_1} + x_2^2 \phi'_{L_1} + L_1 x_2 \phi'_{L_1} \cos(\theta_2) + x_2 \phi_{L_1} \cos(\theta_2) \right) dx_2 \\ & + m_2 \left( L_1 \phi_{L_1} + x_2^2 \phi'_{L_1} + L_1 x_2 \phi'_{L_1} \cos(\theta_2) + x_2 \phi_{L_1} \cos(\theta_2) \right) \Big|_{x_2=L_2} \end{aligned} \quad (2.1.19)$$

$$\begin{aligned} M_{2a} = \int_0^{L_2} (\rho A)_2 & \left( x_2^2 \phi'_{L_1} + x_2 \phi_{L_1} \cos(\theta_2) \right) dx_2 \\ & + m_2 \left( x_2^2 \phi'_{L_1} + x_2 \phi_{L_1} \cos(\theta_2) \right) \Big|_{x_2=L_2} \end{aligned} \quad (2.1.20)$$

$$\begin{aligned} M_a^{(2)} = \int_0^{L_2} (\rho A)_2 & \left( \phi_{L_1} \phi_{L_1}^T + x_2^2 \phi'_{L_1} \phi_{L_1}^T + 2 \phi_{L_1} \phi_{L_1}'^T \cos(\theta_2) \right) dx_2 \\ & + m_2 \left( \phi_{L_1} \phi_{L_1}^T + x_2^2 \phi'_{L_1} \phi_{L_1}^T + 2 \phi_{L_1} \phi_{L_1}'^T \cos(\theta_2) \right) \Big|_{x_2=L_2} \end{aligned} \quad (2.1.21)$$

$$M_{1c} = \int_0^{L_2} (\rho A)_2 (x_2 \psi + L_1 \psi \cos(\theta_2)) dx_2 + m_2 (x_2 \psi + L_1 \psi \cos(\theta_2)) \Big|_{x_2=L_2} \quad (2.1.22)$$

$$M_{2c} = \int_0^{L_2} (\rho A)_2 x_2 \psi dx_2 + m_2 x_2 \psi \Big|_{x_2=L_2} \quad (2.1.23)$$

$$M_c = \int_0^{L_2} (\rho A)_2 \psi \psi^T dx_2 + m_2 \psi \psi^T \Big|_{x_2=L_2} \quad (2.1.24)$$

$$M_{ca} = \int_0^{L_2} (\rho A)_2 \left( x_2 \psi \phi'_{L_1}{}^T + \psi \phi_{L_1}^T \cos(\theta_2) \right) dx_2 + m_2 \left( x_2 \psi \phi'_{L_1}{}^T + \psi \phi_{L_1}^T \cos(\theta_2) \right) \Big|_{x_2=L_2} \quad (2.1.25)$$

The quadratic form of the potential energy  $U$  is

$$U = \frac{1}{2} \int_0^{L_1} (EI)_1 (w_1'')^2 dx_1 + \frac{1}{2} \int_0^{L_2} (EI)_2 (w_2'')^2 dx_2 \quad (2.1.26)$$

However

$$K_a = \int_0^{L_1} ((EI)_1 \phi'' \phi''^T) dx_1$$

$$K_c = \int_0^{L_2} ((EI)_2 \psi'' \psi''^T) dx_2 \quad (2.1.27)$$

Substituting the relations of (2.1.10) into the kinetic and potential energies, the Lagrangian  $L$ , is

$$L = T - U$$

$$= \frac{1}{2} J_1^{(1)} \dot{\theta}_1^2 + \frac{1}{2} \dot{a}^T M_a^{(1)} \dot{a} + \dot{\theta}_1 \dot{a}^T M_{1a}^{(1)}$$

$$+ \frac{1}{2} J_1^{(2)} \dot{\theta}_1^2 + J_{12} \dot{\theta}_1 \dot{\theta}_2 + \frac{1}{2} J_2^{(2)} \dot{\theta}_2^2 + \dot{\theta}_1 \dot{a}^T M_{1a}^{(2)}$$

$$+ \dot{\theta}_2 \dot{a}^T M_{2a} + \frac{1}{2} \dot{a}^T M_a^{(2)} \dot{a} + \dot{\theta}_1 \dot{c}^T M_{1c} + \dot{\theta}_2 \dot{c}^T M_{2c}$$

$$+ \frac{1}{2} \dot{c}^T M_c \dot{c} + \dot{c}^T M_{ca} \dot{a} - \frac{1}{2} \dot{a}^T K_a a - \frac{1}{2} \dot{c}^T K_c c$$

$$- \frac{1}{2} a^T K_a a - \frac{1}{2} c^T K_c c \quad (2.1.28)$$

The equations of motion are determined according to Lagrange's equation, which for conservative systems states

$$\frac{\partial}{\partial t} \left[ \frac{\partial L}{\partial \dot{q}_i} \right] - \frac{\partial L}{\partial q_i} = 0 \quad (2.1.29)$$

where

$$q = \begin{bmatrix} \theta_1 & \theta_2 & a^T & c^T \end{bmatrix}^T \quad (2.1.30)$$

Assuming the squared flexible deflections are negligible compared to the axial dimension squared, and the square of the rigid body angular velocity are small (Hasting, 1986), the Lagrangian reduces to

$$\bar{M}\ddot{q} + \bar{K}q = 0 \quad (2.1.31)$$

where  $\bar{M}$  and  $\bar{K}$  are given by

$$\bar{M} = \begin{bmatrix} J_1^{(1)} + J_1^{(2)} & J_{12} & (M_{1a}^{(1)} + M_{1a}^{(2)})^T & M_{1c}^T \\ J_{12} & J_2 & M_{2a}^T & M_{2c}^T \\ M_{1a}^{(1)} + M_{1a}^{(2)} & M_{2a} & M_a^{(1)} + \frac{1}{2}(M_a^{(2)} + M_a^{(2)})^T & M_{ca}^T \\ M_{1c} & M_{2c} & M_{ca} & M_c \end{bmatrix} \quad (2.1.32)$$

$$\bar{K} = \begin{bmatrix} 0 & 0 & 0 & 0 \\ 0 & 0 & 0 & 0 \\ 0 & 0 & K_a & 0 \\ 0 & 0 & 0 & K_c \end{bmatrix} \quad (2.1.33)$$

The following variables are used to non-dimensionalize the equations of motion.

$$\eta_1 = \frac{m_1}{(\rho AL)_1}, \quad \eta_2 = \frac{m_2}{(\rho AL)_2}, \quad \eta_L = \frac{(\rho AL)_2}{(\rho AL)_1}, \quad \eta_e = \eta_1 + \eta_L(1 + \eta_2), \quad r_L = \frac{L_2}{L_1},$$

$$\mu_i = \left( \frac{EI}{\rho AL^4} \right)_i, \quad M_i = (\rho AL)_i, \quad \phi^* = \frac{\phi}{L_1}, \quad \psi^* = \frac{\psi}{L_2}, \quad \xi_1 = \frac{x_1}{L_1}, \quad \text{and} \quad \xi_2 = \frac{x_2}{L_2}$$

Where  $\eta_1$  and  $\eta_2$  are non-dimensional parameters which relate the mass at the end of the link to the mass of the link.  $\eta_L$  represents the mass ratio between the first and second

link and  $\eta_e$  is a non-dimensional parameter which simplifies the equations.  $r_L$  is the non-dimensional parameter which relates the length ratio between the two links.  $\mu_i$  are the non-dimensional stiffness properties of the respective links.  $M_i$  are the mass of the respective links.  $\phi^*$  and  $\psi^*$  are the normalized admissible functions of the spatial coordinates  $\phi$  and  $\psi$ .  $\xi_1$  and  $\xi_2$  are the normalized displacement along the axis of the link.

Accordingly, the matrices defined in (2.1.32) and (2.1.33) become

$$\begin{aligned} J_1 &= \left\{ \frac{1}{3} + \eta_e + \eta_L r_L^2 \left( \frac{1}{3} + \eta_2 \right) \right\} + \left\{ \eta_L r_L (1 + 2\eta_2) \right\} \cos(\theta_2) \\ &= J_{1,i}^* + J_{1,ii}^* \cos(\theta_2) \end{aligned} \quad (2.1.34)$$

$$\begin{aligned} J_{12}^* &= \left\{ \frac{1}{3} + \eta_2 \right\} + \left\{ \frac{1}{r_L} \left( \frac{1}{2} + \eta_2 \right) \right\} \cos(\theta_2) \\ &= J_2^* + J_{12,ii}^* \cos(\theta_2) \end{aligned} \quad (2.1.35)$$

$$J_2^* = \frac{1}{3} + \eta_2 \quad (2.1.36)$$

$$\begin{aligned} M_{1a}^* &= \left\{ \int_0^1 \xi_1 \phi^* d\xi_1 + \eta_e \phi_1^* \right\} + \left\{ \eta_L r_L^2 \left( \frac{1}{3} + \eta_2 \right) \phi_1'^* \right\} \\ &\quad + \left\{ \eta_L r_L \left( \frac{1}{2} + \eta_2 \right) (\phi_1^* + \phi_1'^*) \right\} \cos(\theta_2) \\ &= M_{1a,i}^* + M_{1a,ii}^* + M_{1a,iii}^* \cos(\theta_2) \end{aligned} \quad (2.1.37)$$

$$\begin{aligned}
M_{2a}^* &= \left\{ \left( \frac{1}{3} + \eta_2 \right) \phi_1'^* \right\} + \left\{ \frac{1}{r_L} \left( \frac{1}{2} + \eta_2 \right) \right\} \cos(\theta_2) \phi_1^* \\
&= M_{2a,i}^* + M_{2a,ii}^* \cos(\theta_2)
\end{aligned} \tag{2.1.38}$$

$$\begin{aligned}
M_a^* &= \left\{ \int_0^1 \phi^* \phi'^{*T} d\xi_1 + \eta_e \phi_1^* \phi_1'^{*T} \right\} + \left\{ \eta_L r_L^2 \left( \frac{1}{3} + \eta_2 \right) \phi_1'^* \phi_1'^{*T} \right\} \\
&\quad + \left\{ \eta_L r_L (1 + 2\eta_2) \phi_1^* \phi_1'^{*T} \right\} \cos(\theta_2) \\
&= M_{a,i}^* + M_{a,ii}^* + M_{a,iii}^* \cos(\theta_2)
\end{aligned} \tag{2.1.39}$$

$$\begin{aligned}
M_{1c}^* &= \left\{ \int_0^1 \xi_2 \psi^* d\xi_2 + \eta_2 \psi^* \right\} + \left\{ \frac{1}{r_L} \left( \int_0^1 \psi^* d\xi_2 + \eta_2 \psi_1^* \right) \right\} \cos(\theta_2) \\
&= M_{1c,i}^* + M_{1c,ii}^* \cos(\theta_2)
\end{aligned} \tag{2.1.40}$$

$$M_{2c}^* = \int_0^1 \xi_2 \psi^* d\xi_2 + \eta_2 \psi_1^* \tag{2.1.41}$$

$$\begin{aligned}
M_{ca}^* &= \left\{ r_L M_{2c}^* \phi_1'^{*T} \right\} + \left\{ \left( \int_0^1 \psi^* d\xi_2 + \eta_2 \psi_1^* \right) \phi_1'^{*T} \right\} \cos(\theta_2) \\
&= M_{ca,i}^* + M_{ca,ii}^* \cos(\theta_2)
\end{aligned} \tag{2.1.42}$$

$$M_c^* = M_2 L_2^2 \left[ \int_0^1 \psi^* \psi'^{*T} d\xi_2 + \eta_2 \psi_1^* \psi_1'^{*T} \right] \tag{2.1.43}$$

$$K_a^* = \left( \frac{EI}{L} \right)_1 \left[ \int_0^1 \phi''^* \phi''^{{*T}} d\xi_1 \right] \tag{2.1.44}$$

$$K_c^* = \left( \frac{EI}{L} \right)_2 \left[ \int_0^1 \psi''^* \psi''^{{*T}} d\xi_2 \right] \tag{2.1.45}$$

Where  $\phi'^*$  denotes the derivatives with respect to the non-dimensional spatial variable  $\xi_1$ , and  $\phi_1^*$  denotes the evaluation of  $\phi^*$  at  $\xi_1 = 1$ .  $\psi'^*$  denotes the derivatives with respect to the non-dimensional spatial variable  $\xi_2$ , and  $\psi_1^*$  denotes the evaluation of  $\psi^*$  at  $\xi_2 = 1$ .

The non-dimensional matrices defined in 2.1.37 - 2.1.45 are used to create the non-dimensional system matrices.

$$M_{sys,i}^* = \begin{bmatrix} J_{1,i}^* & \eta_L r_L^2 J_2^* & (M_{1a,i}^* + M_{1a,ii}^*)^T & \eta_L r_L^2 M_{2c}^{*T} \\ \eta_L r_L^2 J_2^* & \eta_L r_L^2 J_2^* & \eta_L r_L^2 M_{2a,i}^{*T} & \eta_L r_L^2 M_{2c}^{*T} \\ M_{1a,i}^* + M_{1a,ii}^* & \eta_L r_L^2 M_{2a,i}^* & M_{a,i}^* + M_{a,ii}^* & \eta_L r_L^2 M_{ca,i}^{*T} \\ \eta_L r_L^2 M_{2c}^* & \eta_L r_L^2 M_{2c}^* & \eta_L r_L^2 M_{ca,i}^* & \eta_L r_L^2 M_c^* \end{bmatrix} \quad (2.1.46)$$

$$M_{sys,ii}^* = \begin{bmatrix} J_{1,ii}^* & \eta_L r_L^2 J_{12,ii}^* & M_{1a,iii}^{*T} & \eta_L r_L^2 M_{1c,ii}^{*T} \\ \eta_L r_L^2 J_{12,ii}^* & 0 & \eta_L r_L^2 M_{2a,ii}^{*T} & 0 \\ M_{1a,iii}^* & \eta_L r_L^2 M_{2a,ii}^* & \frac{1}{2}(M_{a,iii}^* + M_{a,iii}^{*T}) & \eta_L r_L^2 M_{ca,ii}^{*T} \\ \eta_L r_L^2 M_{1c,ii}^* & 0 & \eta_L r_L^2 M_{ca,ii}^* & 0 \end{bmatrix} \quad (2.1.47)$$

$$M_{sys}^* = M_{sys,i}^* + M_{sys,ii}^* \cos(\theta_2) \quad (2.1.48)$$

$$K_{sys}^* = \begin{bmatrix} 0 & 0 & 0 & 0 \\ 0 & 0 & 0 & 0 \\ 0 & 0 & \mu_1^2 K_a^* & 0 \\ 0 & 0 & 0 & \eta_L r_L^2 \mu_2^2 K_c^* \end{bmatrix} \quad (2.1.49)$$

which results in the second order form

$$\left[ M_{sys,i}^* + M_{sys,ii}^* \cos(\theta_2) \right] (\ddot{q}) + M_{sys}^*(q) = fu \quad (2.1.50)$$

where

$$q = \begin{bmatrix} \theta_1 & \theta_2 & a^T & c^T \end{bmatrix}^T \quad (2.1.51)$$

The second order system matrices can be put in first order state-space form

$$\dot{x} = Ax + Bu \quad (2.1.52)$$

where

$$x = \begin{bmatrix} \theta_1 & \theta_2 & a^T & c^T & \dot{\theta}_1 & \dot{\theta}_2 & \dot{a}^T & \dot{c}^T \end{bmatrix}^T \quad (2.1.53)$$

The first order state space form of (2.1.50) is given by (2.1.54)

$$\begin{bmatrix} \dot{\theta}_1 \\ \dot{\theta}_2 \\ \dot{\phi}_L \\ \dot{\psi}_L \\ \ddot{\theta}_1 \\ \ddot{\theta}_2 \\ \ddot{\phi}_L \\ \ddot{\psi}_L \end{bmatrix} = \begin{bmatrix} 0 & I \\ -inv(M_{sys}^*)K_{sys} & 0 \end{bmatrix} \begin{bmatrix} \theta_1 \\ \theta_2 \\ \phi_L \\ \psi_L \\ \dot{\theta}_1 \\ \dot{\theta}_2 \\ \dot{\phi}_L \\ \dot{\psi}_L \end{bmatrix} + \begin{bmatrix} 0 \\ inv(M_{sys}^*)f \end{bmatrix} u \quad (2.1.54)$$

## 2.2 Six Degree of Freedom Manipulator

The dynamics of a six degree of freedom manipulator are substantially more complicated than those for the two degree of freedom manipulator shown in the above section. However, it is worth noting that much of the nonlinear kinematics of the manipulator are dependent on the elbow pitch joint (2.1.48).

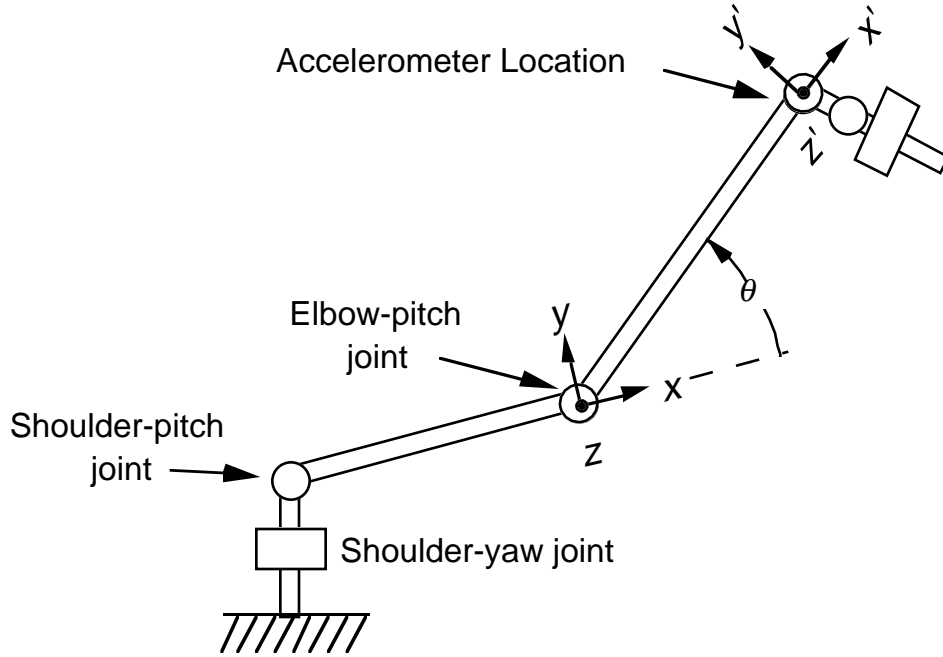


Figure 2.2.1 Six Degree of Freedom Manipulator

For example, in Figure 2.2.1 the transfer function which relates the shoulder-pitch joint to an accelerometer located inboard of the  $x'$ ,  $y'$ ,  $z'$  reference frame, is not sensitive to the shoulder yaw or shoulder-pitch joint angle. This thesis will thus focus on the controller sensitivities of the elbow-pitch angle. In Figure 2.2.1 a schematic of the RMS system with the placement of the accelerometers located at the end of the second boom is illustrated. This sensor location is used in the SRMS example of Chapter five.

### 2.3 Non-minimum Phase Zeroes and Boundary Conditions

This analysis shows the effect of the base boundary conditions on the poles and zeroes of the transfer function of the two link model. The base constraint (or boundary condition at the shoulder joint) experienced on the SRMS is essentially a fixed

constraint due to the gearbox ratio of 1842:1. To model the physics of the SRMS with the high gearbox ratio, the feedback dynamics of the two link arm flexibility were prevented mathematically from driving the shoulder joint, while the elbow joint remained fixed. This can be accomplished by eliminating those dynamic feedback terms from the flexible modes which drive the shoulder joint. Thus the mass matrix of the two link model is modified as shown below (Juang, 1986). Note that this representation results in a non-symmetric mass matrix, and is an accurate representation for very high gearbox ratios.

$$\underline{M}_{sys,i}^* = \begin{bmatrix} J_{1,i}^* & 0 & 0 & 0 \\ \eta_L r_L^2 J_2^* & \eta_L r_L^2 J_2^* & \eta_L r_L^2 M_{2a,i}^{*T} & \eta_L r_L^2 M_{2c}^{*T} \\ M_{1a,i}^* + M_{1a,ii}^* & \eta_L r_L^2 M_{2a,i}^* & M_{a,i}^* + M_{a,ii}^* & \eta_L r_L^2 M_{ca,i}^{*T} \\ \eta_L r_L^2 M_{2c}^* & \eta_L r_L^2 M_{2c}^* & \eta_L r_L^2 M_{ca,i}^* & \eta_L r_L^2 M_c^* \end{bmatrix} \quad (2.3.1)$$

and

$$\underline{M}_{sys,ii}^* = \begin{bmatrix} J_{1,ii}^* & 0 & 0 & 0 \\ \eta_L r_L^2 J_{12,ii}^* & 0 & \eta_L r_L^2 M_{2a,ii}^{*T} & 0 \\ M_{1a,iii}^* & \eta_L r_L^2 M_{2a,ii}^* & \frac{1}{2}(M_{a,iii}^* + M_{a,iii}^{*T}) & \eta_L r_L^2 M_{ca,ii}^{*T} \\ \eta_L r_L^2 M_{1c,ii}^* & 0 & \eta_L r_L^2 M_{ca,ii}^* & 0 \end{bmatrix} \quad (2.3.2)$$

The total system mass matrix is given by

$$\underline{M}_{sys}^* = \underline{M}_{sys,i}^* + \underline{M}_{sys,ii}^* \cos(\theta_2) \quad (2.3.3)$$

Notice these mass matrices (2.3.1) and (2.3.2) are similar to those shown in Equations (2.1.46) and (2.1.47). However, now all feedback terms to  $\theta_1$  in the top row of the mass matrix  $\underline{M}_{sys}^*$  and to the right of the inertia terms  $J_{1,i}^*$  and  $J_{1,ii}^*$  have been set to zero to prevent the arm from back driving the joint at  $\theta_1$ . Thus, as shown in first order

form, the forward dynamics are retained while preventing backward effects. The state space model is shown in (2.3.4) with  $M_{sys}^*$  replaced by  $\underline{M}_{sys}^*$ .

$$\begin{bmatrix} \dot{\theta}_1 \\ \dot{\theta}_2 \\ \dot{\phi}_L \\ \dot{\psi}_L \\ \ddot{\theta}_1 \\ \ddot{\theta}_2 \\ \ddot{\phi}_L \\ \ddot{\psi}_L \end{bmatrix} = \begin{bmatrix} 0 & I \\ -inv(\underline{M}_{sys}^*)K_{sys} & -inv(\underline{M}_{sys}^*)D \end{bmatrix} \begin{bmatrix} \theta_1 \\ \theta_2 \\ \phi_L \\ \psi_L \\ \dot{\theta}_1 \\ \dot{\theta}_2 \\ \dot{\phi}_L \\ \dot{\psi}_L \end{bmatrix} + \begin{bmatrix} 0 \\ inv(\underline{M}_{sys}^*)f \end{bmatrix} u \quad (2.3.4)$$

### Rate Command

To mathematically model velocity (or rate) command of the two link model, a servo loop is inserted into the open loop model as was done on the SRMS (Ravindran, 1982).

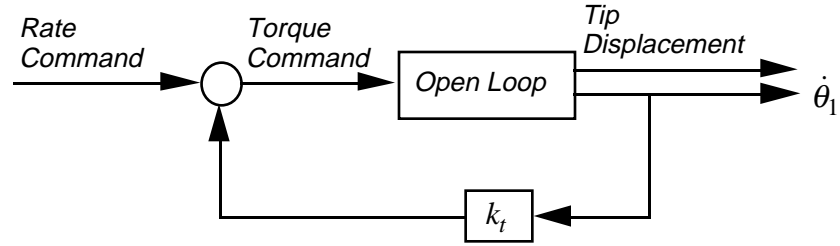


Figure 2.3.1 Control Block Diagram with Rate Command

The servo loop provides the ability to command angular rates as opposed to commanding torques. It is not advisable to command torque's in space based or terrestrial manipulators due to high angular rates they may induce. Thus a servo loop is added to the mathematical model as shown in Figure 2.3.1. A proportional gain  $k_t$  is

introduced which feeds back to provide sufficient torque to maintain the commanded velocity as shown in Figure 2.3.2.

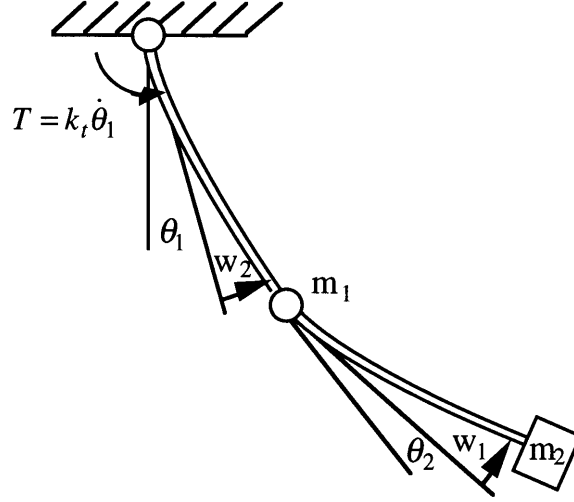


Figure 2.3.2 Two Link Model with Rate Command

To examine the effect of the rate command on the open loop poles and zeroes, several example dynamic responses are shown. In the following plots, the two link model is used with  $\theta_2$  locked at  $0^\circ$ . The following non-dimensional parameters are used in a Matlab (Matlab, 1992) simulation of the system modeled in Section 2.2. These non-dimensional parameters represent an example problem where both links have the same mass and stiffness properties. A very heavy mass at the end of the second link is used for example purposes only (Table 2.3.1). The structural damping used is  $\zeta = 0.02$ .

Three sets of analysis are shown in the following section. The first analysis is for the above model with no base constraint. The second includes the mathematical model of the gearbox, in which feedback dynamics are prevented from driving the joint corresponding to  $\theta_1$ . The third analysis includes the rate command servo *in addition* to

<p style="text-align: center;"><i>Table 2.3.1</i> Non-Dimensional Parameters used in Experiment</p>	
$\eta_1 = \frac{m_1}{M_1} = 0$	Mass ratio of link 1; end mass to link 1 mass
$\eta_2 = \frac{m_2}{M_2} = 200$	Mass ratio of link 2; tip mass to link 2 mass
$\eta_L = \frac{M_2}{M_1} = 1$	Link mass ratio: mass of link 2 relative to link 1
$r_L = \frac{L_2}{L_1} = 1$	Link length ratio: length of link 2 to link 1
$\mu_i = \left( \frac{E_i I_i}{M_i L_i^3} \right) = 18$	Non-dimensional stiffness properties of link i

the gearbox model. All the transfer functions indicated show the response from the input command to the shoulder joint and a sensor located at the arm tip. In this manner the non-collocation, non-minimum phase system can be explored. All poles and zeroes shown in the following tables correspond to the transfer function pole zero form shown here.

$$H(s) = C(sI - A)^{-1}B + D = k \frac{(s - z_1)(s - z_2) \dots (s - z_n)}{(s - p_1)(s - p_2) \dots (s - p_n)} \quad (2.3.5)$$

To simplify discussion only four system modes are shown. The four non-zero pole locations are the lowest frequency modes. Table 2.3.2 shows the poles and zeroes with no base constraint. These poles and zeroes are shown in Figure 2.3.3 in the root locus with no base constraint. Notice in this example there are two open loop zeroes.

<p style="text-align: center;"><i>Table 2.3.2</i> Poles and Zeroes with No Base Constraint</p>	
$z_i$	$p_i$
-4.3125e+02	0
4.2503e+02	0
-7.8737e-01+3.4913e+02i	-3.2062e+01+9.5380e+02i
-7.8737e-01-3.4913e+02i	-3.2062e+01-9.5380e+02i
-6.8055e+01	-6.7239e+00+4.9055e+02i
6.9064e+01	-6.7239e+00-4.9055e+02i
0	-1.8390e+00+1.7813e+02i
0	-1.8390e+00-1.7813e+02i
	-1.5754e-01+4.7325e+01i
	-1.5754e-01-4.7325e+01i

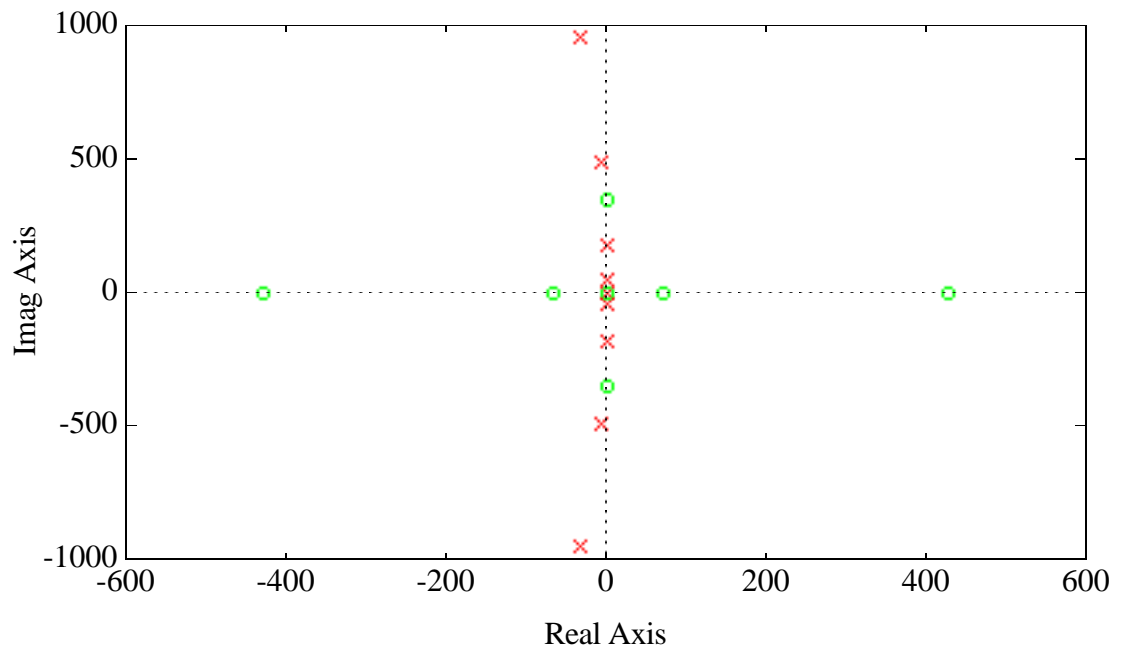


Figure 2.3.3 Root Locus of Poles and Zeroes - No Base Constraint

When the gearbox model is inserted, Table 2.3.3 indicates that the poles have significantly changed, while leaving the zeroes unchanged. The poles have a considerably higher frequency compared to Table 2.3.2. Figure 2.3.4 is a diagram of

the poles and zeroes in the root locus domain. Notice that the zeroes are left unchanged. In Figure 2.3.5 the pulse response from an input command to the shoulder joint and a sensor located at the arm tip is shown.

<p style="text-align: center;"><i>Table 2.3.3</i> Poles and Zeroes with Gearbox Model Inserted</p>	
$z_i$	$p_i$
-4.3125e+02	0
4.2503e+02	-4.7843e+00+5.6088e+02i
-7.8737e-01+3.4913e+02i	-4.7843e+00-5.6088e+02i
-7.8737e-01-3.4913e+02i	-7.1962e-01+2.2726e+02i
-6.8055e+01	-7.1962e-01-2.2726e+02i
6.9064e+01	-3.8345e-01+7.2709e+01i
0	-3.8345e-01-7.2709e+01i
0	-5.6805e-05+7.9551e-01i
	-5.6805e-05-7.9551e-01i

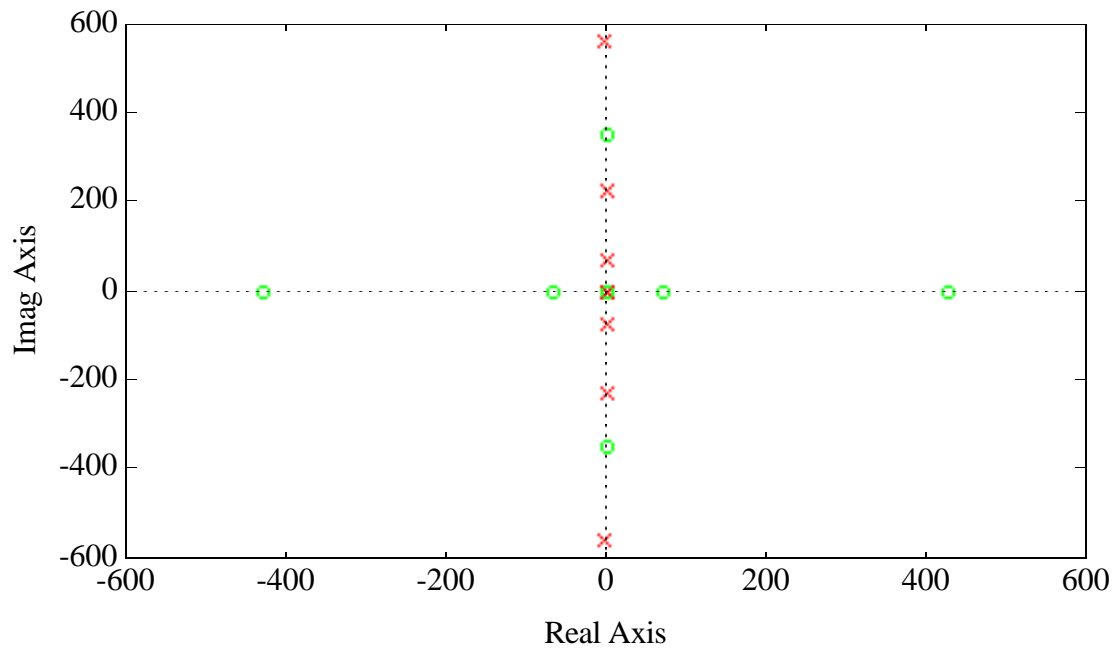


Figure 2.3.4 Root Locus of Poles and Zeroes with Gearbox Model

In Figure 2.3.5, the response is shown for a unit pulse input at the base. The high frequency dynamics have been replaced with lower frequency dynamics, corresponding to the insertion of the gearbox model. In this case the constraint at the base is constrained do to the gearbox model versus the pinned condition earlier. There still exists a rigid body mode corresponding to the poles at zero.

When the rate servo is inserted, Table 2.3.4 indicates that the poles have significantly changed, while leaving the zeroes unchanged. One of the rigid body poles is removed when compared with the poles and zeroes with the gearbox model inserted.

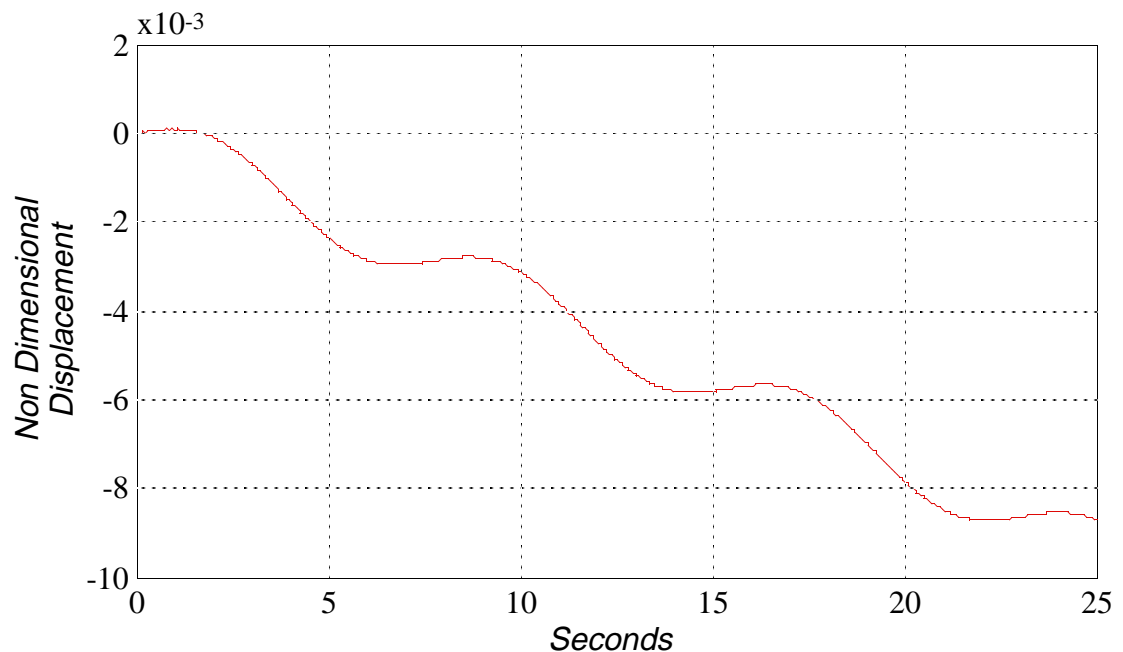


Figure 2.3.5 Pulse Time History with Gearbox Model

These poles and zeroes with the gearbox mode and rate command inserted are shown in Figure 2.3.6 in the root locus plane. Notice the zeroes remain unchanged yet again.

<p style="text-align: center;"><i>Table 2.3.4</i></p> <p style="text-align: center;">Poles and Zeroes with Gearbox Model and Rate Command Inserted</p>	
$z_i$	$p_i$
-4.3125e+02	0
4.2503e+02	-4.7843e+00+5.6088e+02i
-7.8737e-01+3.4913e+02i	-4.7843e+00-5.6088e+02i
-7.8737e-01-3.4913e+02i	-7.1962e-01+2.2726e+02i
-6.8055e+01	-7.1962e-01-2.2726e+02i
6.9064e+01	-7.1338e-01+7.1338e+01i
0	-7.1338e-01-7.1338e+01i
0	-7.8896e-03+7.8896e-01i
	-7.8896e-03-7.8896e-01i
	-1.2458e+01

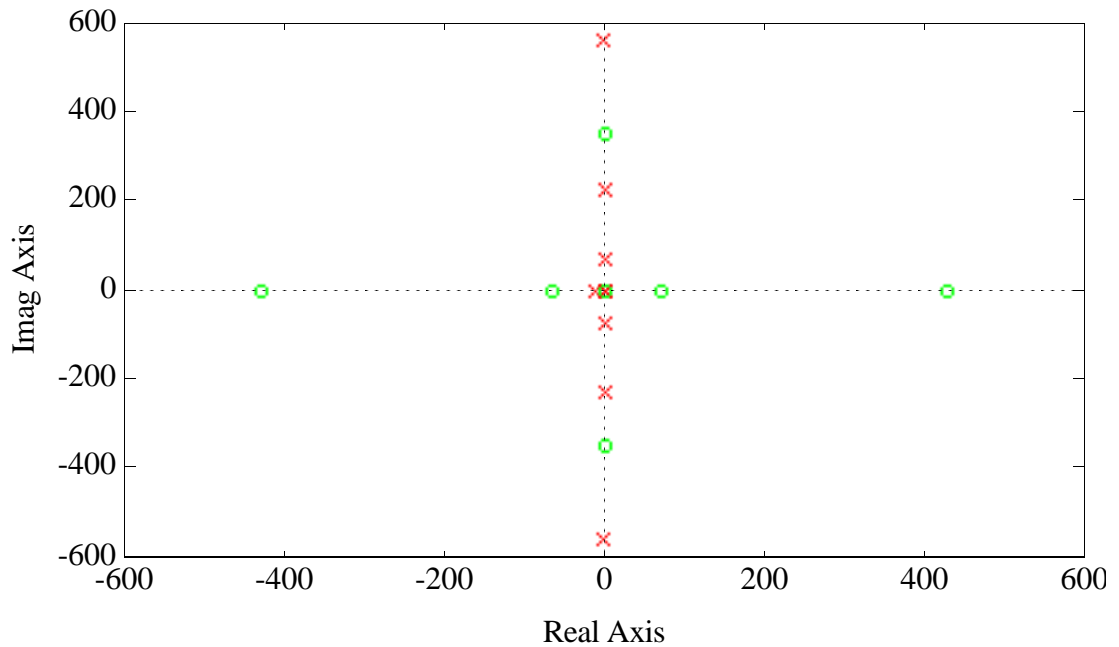


Figure 2.3.6 Root Locus of Poles and Zeroes with Gearbox Model and Rate Command

In Figure 2.3.7 the high frequency dynamics have been replaced with lower frequency dynamics, corresponding to the insertion of the gearbox model. The displacement in the negative direction is a result of a negative unit pulse velocity command.

As shown in the above three examples, the zeroes are left unchanged by the boundary conditions, while the poles shift. In the time domain the effects of these base constraints are shown to lower the frequency of the fundamental mode, and to alter the steady state behavior of the system. The time response of Figure 2.3.7 highlights the typical behavior of non-minimum phase systems. Notice the response is initially upward even though the quasi steady state value is negative. This is not the typical behavior of minimum phase systems. These results are shown to gain more understanding of the mathematical model used to design the control system, and to demonstrate the insensitivity of the zeroes of the open loop model to the base boundary conditions.

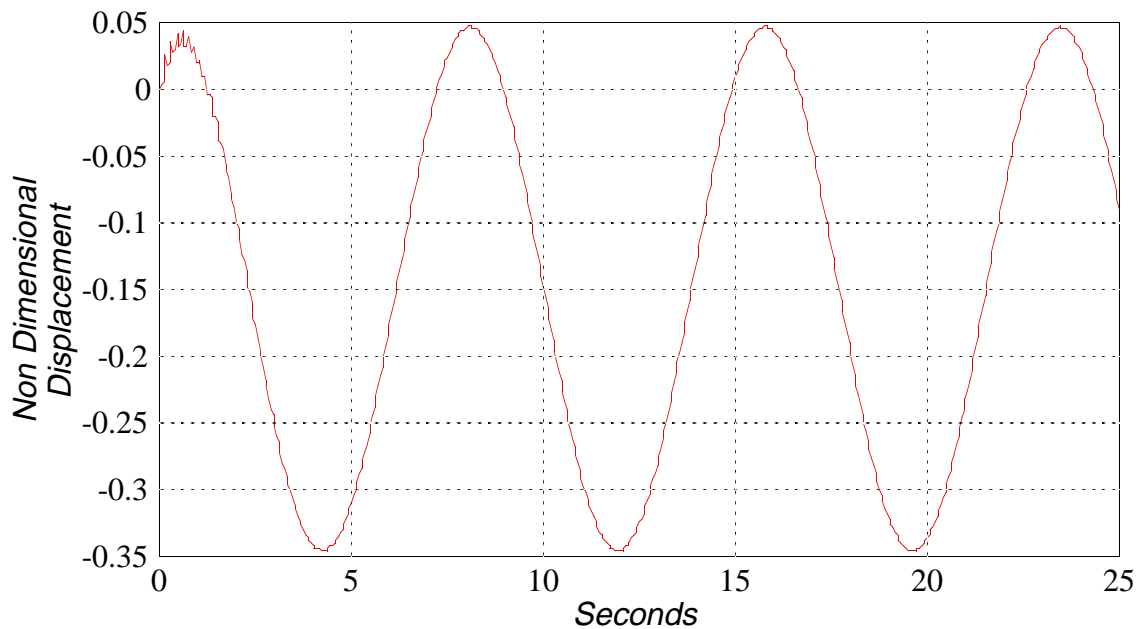


Figure 2.3.7 Pulse Time History with Gearbox Model and Rate Command

## 2.4 Frequency Dependence on Payload Mass

In developing the two link model, Euler-Bernoulli beam theory was used for which the following assumptions are implicit (Graf, 1975). Rotary motion, longitudinal motion, and shear strain of the beam fibers are negligible; beam material properties and cross section are symmetric with respect to the neutral bending axis; and structural damping is small. A further assumption is that the material properties and cross section do not depend on  $x$ . The system is described by the Equation (2.4.1):

$$y^{iv}(x,t) + \frac{\rho A}{EI} \ddot{y}(x,t) = 0 \quad (2.4.1)$$

with boundary conditions:

$$\begin{aligned} y(0,t) &= 0 \\ y'(0,t) &= 0 \\ y''(L,t) &= 0 \\ EIy'''(L,t) &= m_p \ddot{y}(L,t) \end{aligned} \quad (2.4.2)$$

where  $\rho \equiv$  mass density,  $A \equiv$  cross-sectional area,  $E \equiv$  Young's Modulus,  $I \equiv$  area moment of inertia.

The solution to the boundary value problem (2.4.1) and (2.4.2) is expressed as an infinite product which is then truncated to provide a finite order approximation of the plant with exact transfer function poles and zeroes (Wie, 1981; Spector, 1988, 1989; and Goodson, 1970) By applying separation of variables and by taking the Laplace transform with respect to time, the solution to Equation (2.4.1) has the form:

$$y(x,t) = q(t)\phi(x) \quad (2.4.3)$$

inserting this into (2.4.1) yields

$$\phi^{(iv)}(x)q(t) + \frac{\rho A}{EI} \ddot{q}(t)\phi(x) = 0 \quad (2.4.4)$$

solving yields:

$$\phi(x) = C_1 \sin(\beta x) + C_2 \cos(\beta x) + C_3 \sinh(\beta x) + C_4 \cosh(\beta x) \quad (2.4.5)$$

where

$$S^2 = \pm i \sqrt{\frac{\rho A}{EI}} \beta^2 \quad (2.4.6)$$

where  $S$  is the transformed variable and  $i = \sqrt{-1}$ . Transforming the boundary conditions to the  $\beta$  domain results in:

$$C_2 + C_4 = 0 \quad (2.4.7)$$

$$C_1 + C_3 = 0 \quad (2.4.8)$$

and

$$C_1[\sin(\beta L) + \sinh(\beta L)] + C_2[\cos(\beta L) + \cosh(\beta L)] = 0 \quad (2.4.9)$$

$$\begin{aligned} EI\beta^3 [C_1(-\cos(\beta L) - \cosh(\beta L)) + C_2(\sin(\beta L) - \sinh(\beta L))] = \\ \omega^2 m_p [C_1(\sin(\beta L) - \sinh(\beta L)) + C_2(\cos(\beta L) - \cosh(\beta L))] \end{aligned} \quad (2.4.10)$$

Solving the boundary value problem of the Wronskian yields the following matrix.

$$\begin{bmatrix} \sin(\bar{\beta}) + \sinh(\bar{\beta}) & \cos(\bar{\beta}) + \cosh(\bar{\beta}) \\ \bar{\beta}\bar{M}[\sinh(\bar{\beta}) - \sin(\bar{\beta})] + \cos(\bar{\beta}) + \cosh(\bar{\beta}) & \bar{\beta}\bar{M}[\cosh(\bar{\beta}) - \cos(\bar{\beta})] + \sin(\bar{\beta}) + \sinh(\bar{\beta}) \end{bmatrix} = \begin{bmatrix} 0 \\ 0 \end{bmatrix} \quad (2.4.11)$$

where

$$\bar{M} = \frac{m_p}{\rho AL}, \text{ and } \bar{\beta} = \frac{\beta}{L}.$$

Solving for the determinant of Equation (2.4.11) and simplifying yields the following characteristic equation:

$$\bar{\beta}\bar{M} \sin(\bar{\beta}) \cosh(\bar{\beta}) - 1 - \bar{\beta}\bar{M} \sinh(\bar{\beta}) \cos(\bar{\beta}) - \cos(\bar{\beta}) \cosh(\bar{\beta}) = 0 \quad (2.4.12)$$

As the payload mass ratio  $\bar{M} \Rightarrow \infty$ , the characteristic equation (2.4.12) reduces to that of the hinged problem as shown in Figure 2.4.1 and is given by (2.4.13).

$$\sin(\bar{\beta}) \cosh(\bar{\beta}) - \sinh(\bar{\beta}) \cos(\bar{\beta}) = 0 \quad (2.4.13)$$

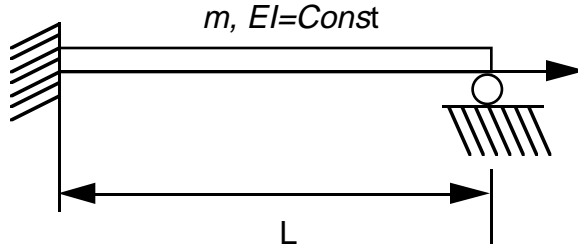


Figure 2.4.1 Cantilever Hinged Problem

### Frequency separation between sequential modes

A characteristic of this structure is that *the frequency separation between the first and second modal frequency for the manipulator model increases as the payload mass is increased*. Figure 2.4.2 shows the modal frequencies with no payload tip mass (Meirovitch, 1975). The frequency separation is larger as the payload mass is increased. Table 2.4.1 shows the frequency separation for various payload to arm mass ratios,  $\bar{M}$ .

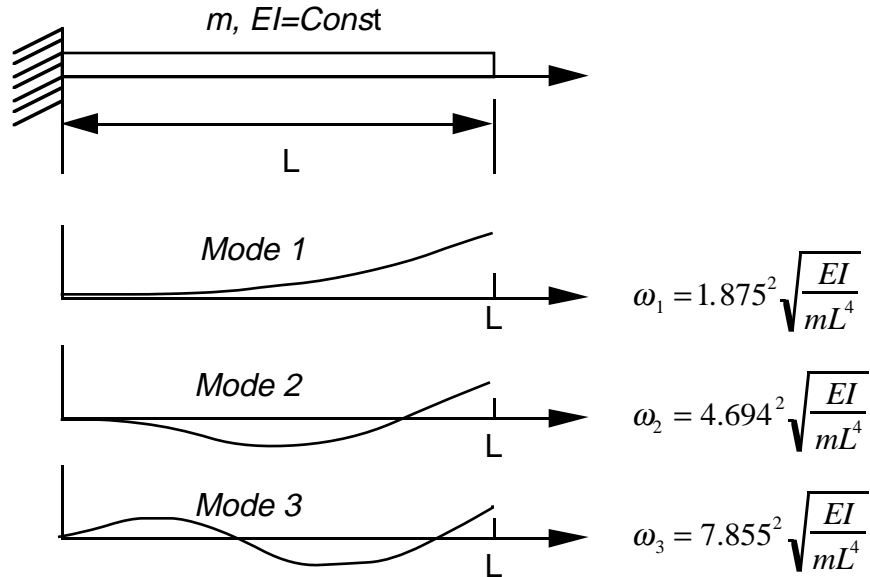


Figure 2.4.2 Theoretical Frequency Separation for Cantilever Free Boundary Condition

<p style="text-align: center;"><i>Table 2.4.1</i> Frequency Versus Non-Dimensional Payload Mass Ratio</p>			
$\bar{M} = \frac{m_p}{\rho AL}$	Non-Dimensional Frequency		
	mode 1 $f_1$	mode 2 $f_2$	mode 3 $f_3$
0.1	18.82	124.6	350.3
0.316	14.76	112.4	331.7
1	9.89	104.2	321.7
3.16	5.97	100.6	317.9
10	3.44	99.3	316.5
31.6	1.95	98.9	316.1
100	1.10	98.7	315.9

Figure 2.4.3 shows the frequency ratio versus payload mass ratios for various modes. Each frequency depicted in the graph is divided by the first modal frequency for the given payload mass ratio  $\frac{M_p}{M}$ , where  $M_p$  is the payload mass and  $M$  is the total arm weight. For the non-dimensional manipulator as shown in Figure 2.3.2, with no payload, and  $\theta_2=0$ , the 2nd modal frequency is 6 times the frequency of the 1st mode. In addition, the 3rd modal frequency is 18 times the frequency of the 1st mode, etc. If a payload 100 times the mass of the arm is considered, the 2nd modal frequency is 98 times the frequency of the 1st mode. The 3rd modal frequency is 316 times the frequency of the 1st mode, etc. It is worth noting that for the SRMS, a payload to arm mass ratio of 100 is considered a small to medium class in terms of payload size.

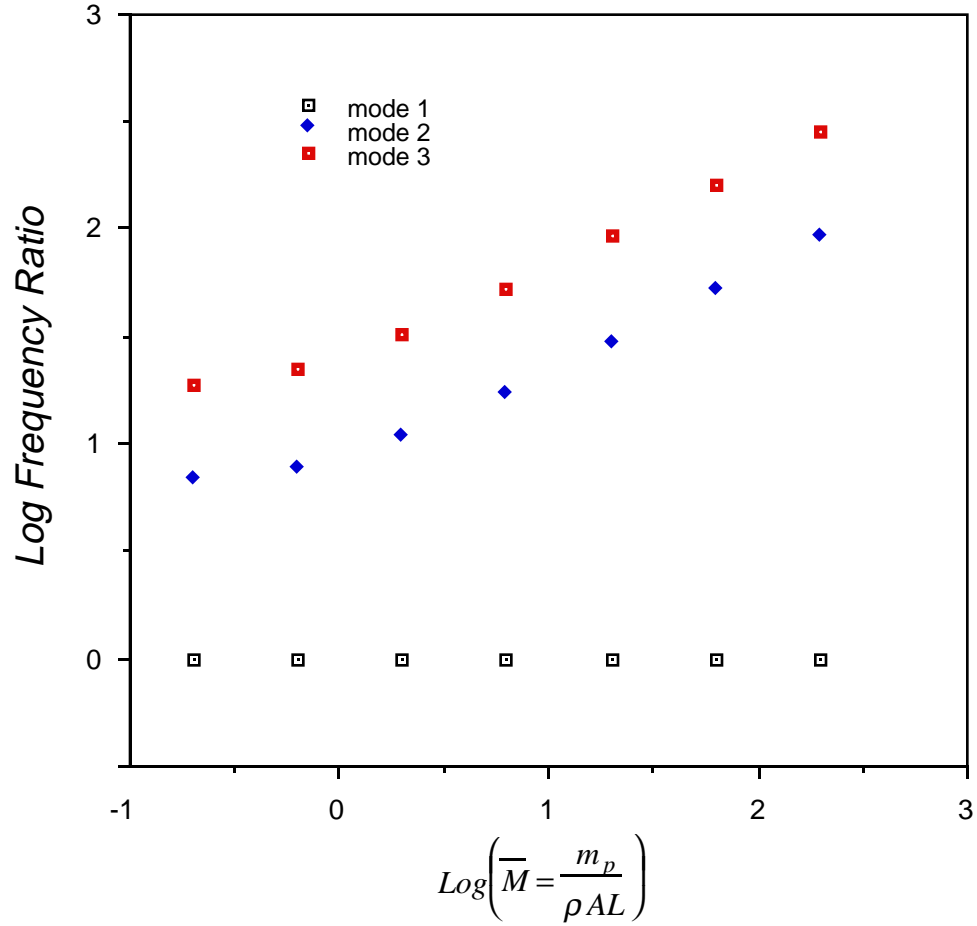


Figure 2.4.3 Frequency Ratio Versus Payload Mass Ratios for Various Modes

## 2.5 Root Locus of Open Loop System as Theta Varies

The root loci of the characteristic equation for the first two modes are shown below (Table 2.5.1) for theta varying between zero and 90 degrees. Figure 2.5.1 and 2.5.2 display the roots of the characteristic equation as a function of the elbow joint angle  $\theta_2$  in the root locus domains for the first and second mode respectively. In Figure 2.5.1 the first mode poles shift upward and to the left in the root locus domain as theta is increased, corresponding to the frequency increasing as theta increases.

<p style="text-align: center;"><i>Table 2.5.1</i> Root location for 1st and 2nd Modes as Theta Varies</p>		
Theta (Degrees)	Root Location	
	Mode 1	Mode 2
0	$-7.8896\text{e-}03 \pm 7.8896\text{e-}01i$	$-7.1338\text{e-}01 \pm 7.1338\text{e+}01i$
10	$-7.9160\text{e-}03 \pm 7.9160\text{e-}01i$	$-2.6507\text{e-}01 \pm 2.6507\text{e+}01i$
20	$-7.9957\text{e-}03 \pm 7.9957\text{e-}01i$	$-1.4049\text{e-}01 \pm 1.4049\text{e+}01i$
30	$-8.1310\text{e-}03 \pm 8.1310\text{e-}01i$	$-9.5490\text{e-}02 \pm 9.5490\text{e+}00i$
40	$-8.3259\text{e-}03 \pm 8.3259\text{e-}01i$	$-7.2809\text{e-}02 \pm 7.2809\text{e+}00i$
50	$-8.5858\text{e-}03 \pm 8.5858\text{e-}01i$	$-5.9347\text{e-}02 \pm 5.9347\text{e+}00i$
60	$-8.9183\text{e-}03 \pm 8.9183\text{e-}01i$	$-5.0585\text{e-}02 \pm 5.0585\text{e+}00i$
70	$-9.3330\text{e-}03 \pm 9.3330\text{e-}01i$	$-4.4573\text{e-}02 \pm 4.4573\text{e+}00i$
80	$-9.8410\text{e-}03 \pm 9.8410\text{e-}01i$	$-4.0349\text{e-}02 \pm 4.0349\text{e+}00i$
90	$-1.0455\text{e-}02 \pm 1.0455\text{e+}00i$	$-3.7411\text{e-}02 \pm 3.7411\text{e+}00i$

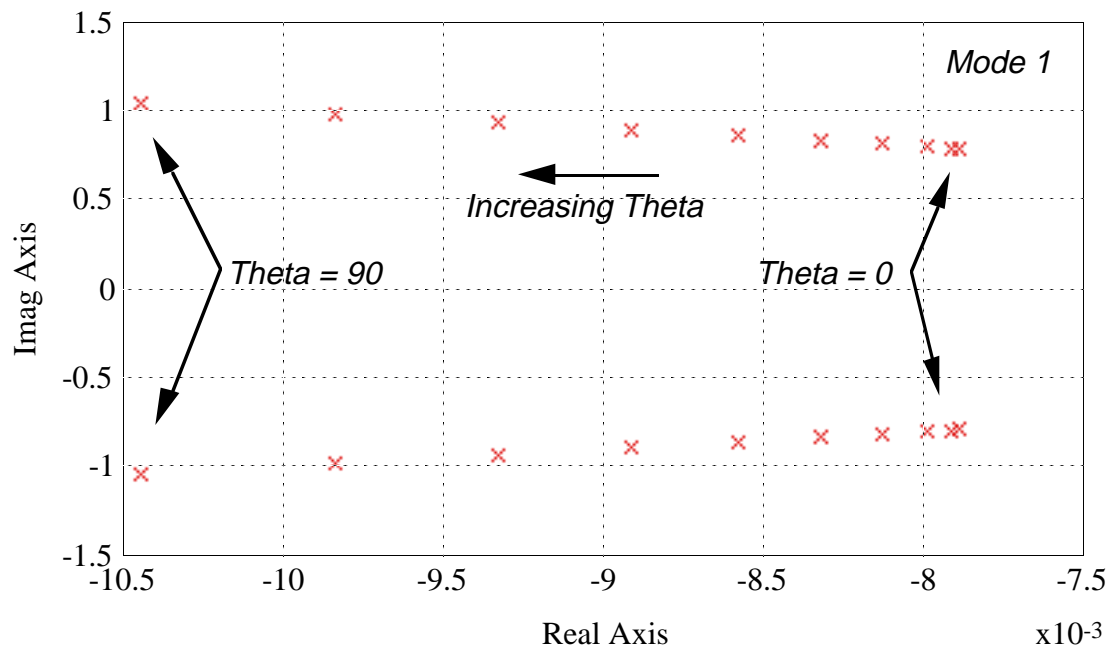


Figure 2.5.1 First Mode Poles as a Function of Theta

In Figure 2.5.2 the second mode poles shift downward and to the right in the root locus domain as theta is increased, corresponding to the frequency decreasing as theta increases. This is in contrast to the first mode in which the frequency increased. However, over the entire range of theta there is considerable frequency separation between the first and successive modes.

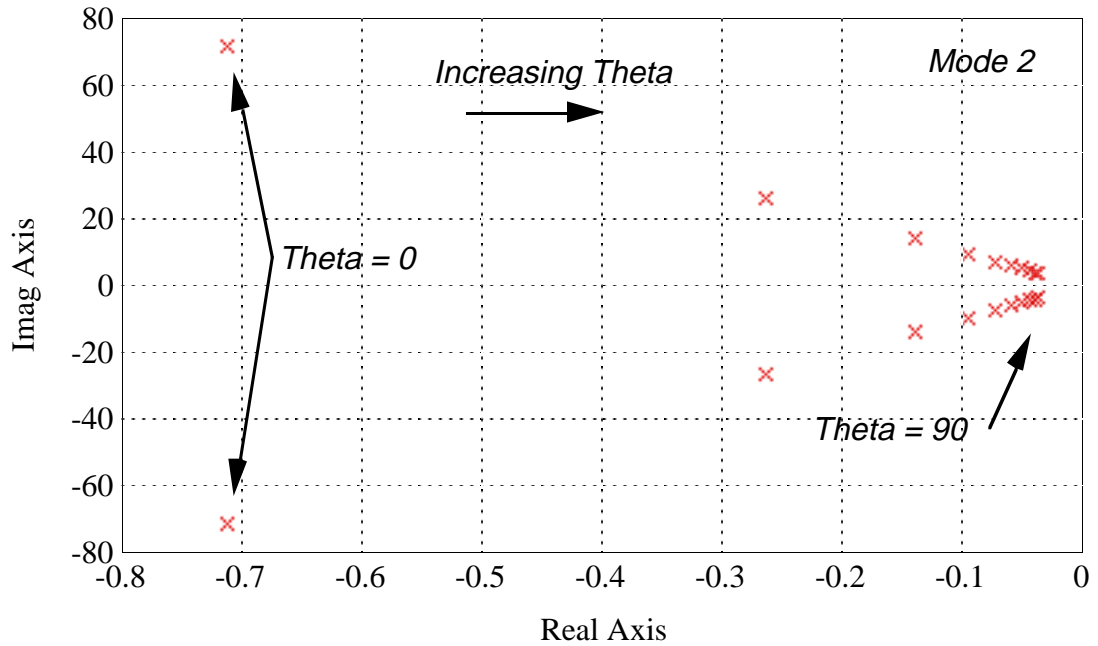


Figure 2.5.2 Second Mode poles as Function of Theta

## 2.6 Modal Open Loop Infinity Norm

The cost associated with the first mode versus the residual modes is shown in Figure 2.6.1 as a function of the elbow joint angle  $\theta_2$ . Each point on this surface plot is the infinity norm of the Bode plot for the individual modes as  $\theta_2$  is varied. Where

$$\text{Infinity Norm} \equiv \sup_{0 < \omega < \infty} \left\| \frac{H(j\omega)}{u(j\omega)} \right\| \quad (2.6.1)$$

The input/output pair is the torque actuator at the hub and the tip displacement sensor respectively. This surface plot reflects the fact that the tip motion is largely dominated by the first mode. The absolute value on the plot is not as important as the relative dominance of the first versus the respective modes. The parameters used for this heavy payload simulation are shown in Table 2.4.1.

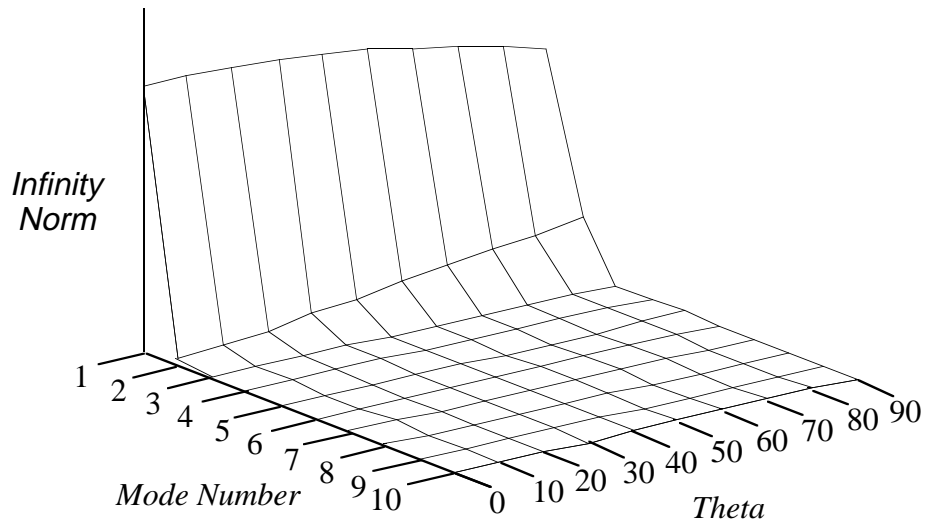


Figure 2.6.1 Infinity Norm of Mode Response as a Function of Mode Number and Theta - Heavy Payload

The exact amplitude ratio of the first mode versus second mode is shown in Figure 2.6.2. The log plot indicates that for heavy payloads the response is largely dominated by the first mode. For example, the infinity norm ratio of the 1st versus the 2nd mode is 40:1 and the infinity norm ratio of the 1st versus the 3rd mode is 600:1.

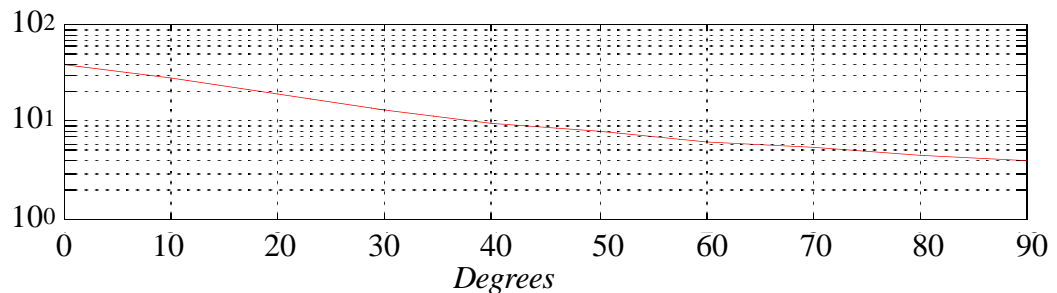


Figure 2.6.2 Infinity Norm Ratio of 2nd Versus 1st Mode as a Function of Theta

For higher order modes the infinity norm ratio is still larger. Figure 2.6.3 indicates the infinity norm ratio of 3rd versus 1st mode as a function of theta.

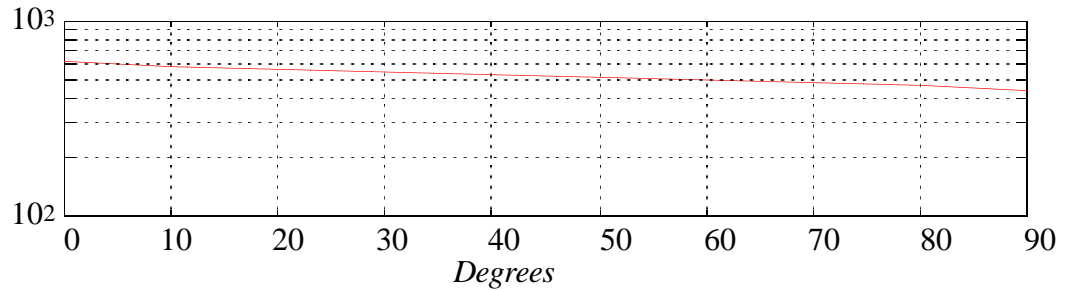


Figure 2.6.3 Infinity Norm Ratio of 3rd Versus 1st Mode as a Function of Theta

For comparison to a zero payload case, Figure 2.6.4 shows the maximum value of the Bode plot for various values of theta, and mode number for the non-dimensional parameters shown in Table 2.6.1

Table 2.6.1 Non-Dimensional Parameters used in Zero Payload Experiment	
$\eta_1 = \frac{m_1}{M_1} = 0$	Mass ratio of link 1; end mass to link 1 mass
$\eta_2 = \frac{m_2}{M_2} = 0$	Mass ratio of link 2; tip mass to link 2 mass
$\eta_L = \frac{M_2}{M_1} = 1$	Link mass ratio: mass of link 2 relative to link 1
$r_L = \frac{L_2}{L_1} = 1$	Link length ratio: length of link 2 to link 1
$\mu_i = \left( \frac{E_i I_i}{M_i L_i^3} \right) = 18$	Non-dimensional stiffness properties of link i

When comparing Figure 2.6.4 with 2.6.1, notice that the heavier the payload, the larger the infinity norm amplitude ratio between the fundamental and the higher modes. These figures represent the relative dominance of the successive modes as predicted by the

infinity norm of the Bode response. Thus the plots are associated with inputs that have broad spectral energy. In actual systems where safety monitoring functions are included, such as slew rate limitations, the input has a higher spectral energy at the low end of the frequency spectrum. Thus the open loop response will be *further* dominated by the lower frequency modes than those depicted in Figure 2.6.4. In chapter five the slew rate limits mandated by the Shuttle Remote Manipulator safety monitoring system will be discussed in greater detail.

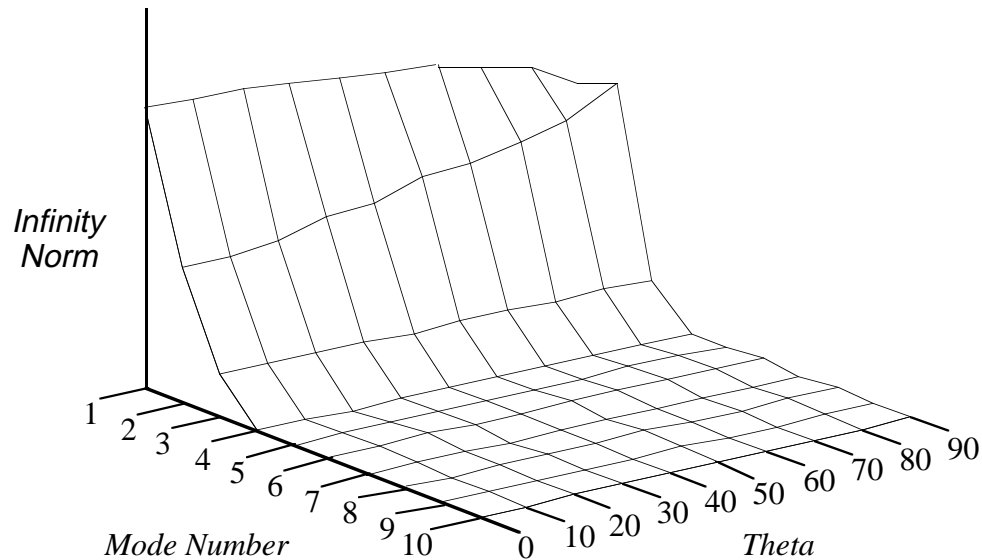


Figure 2.6.4 Infinity Norm of Bode Response as a Function of Mode Number and Theta - Zero Tip Mass

## 2.7 Summary

This chapter has laid the groundwork for the mathematical modeling of the reconfigurable system. The non-dimensionalized second order dynamics have been decomposed into parameter independent and parameter dependent block matrices. The equivalent first order state-space form is introduced. The overall transfer function sensitivity to the variations in the shoulder yaw, elbow pitch, and wrist roll, yaw and pitch arm orientations are discussed. A method is introduced which models the reverse

dynamics of the gearbox. The non-minimum phase zeroes are explored in light of the base boundary conditions. It is shown that the zeroes do not change when base boundary conditions are changed, although the poles move considerably. Light and heavy payloads have been explored and their effect on the modal frequencies are analyzed. For heavier payloads it is shown that the frequency separation between successive modal frequencies increases. As the payload approaches infinity it is shown that the cantilever free problem approaches the cantilever fixed problem. The frequency separation as a function of  $\theta$  is examined. It is shown that the fundamental mode poles shift upward in the root locus domain as  $\theta$  is increased, corresponding to the frequency increasing as  $\theta$  increases. This is in contrast to the second mode in which the frequency decreases. However, over the entire range of  $\theta$ , there is considerable frequency separation between the first and successive modes. The open loop infinity norm of the Bode response is examined in modal form as a function of mode, arm orientation, and payload mass, to understand the relative dominance in the time and frequency domain of the successive modes. It is shown that the response is largely dominated by the first or fundamental mode.

These observations will be used to aid in the development of the system identification and controller design methodologies discussed in the following chapters.

## **CHAPTER 3**

### **SYSTEM IDENTIFICATION**

In the past decade many system identification techniques have been developed to identify state-space models of electro/mechanical space structures for modal analysis or controller design. Identifying a mathematical model from data eliminates the need to develop accurate models of operational safety functions, sensor, and actuator transfer functions of the system under control. As the system complexity increases, accurate analytical models increase the time to develop a controller. Large analytical model based controllers require a large order compensator and may not be as accurate as identified reduced order mathematical models. Before 1970 a great majority of modal tests were performed by tuned-dwell techniques (Stroud, 1987). In modal analysis the parameters include frequencies, damping and mode shapes. For control system design, accurate actuator influence coefficients are required as well. System identification in most techniques is accomplished using MIMO time histories to create sampled pulse response histories. The usual practice uses the Fast Fourier Transforms (FFT)s of the input and output histories to compute the Frequency Response Functions (FRF)s, and then use the Inverse Discrete Fourier Transform (IDFT) to compute the sampled pulse response histories. Another approach is to solve for the Markov parameters directly in the time domain. This approach obviates the need to compute and store FFTs, FRFs, and IDFTs, although it is necessary to invert an input matrix which becomes large for lightly damped systems. An approach by Juang (1993), uses an asymptotically stable observer to form a stable discrete state-space model, rather than identifying the system

Markov parameters, which may exhibit very slow decay. The purpose of introducing an observer is to compress the data and improve system identification results.

In this chapter the Markov parameters are introduced and their relationship to the state space model is discussed. In practice, if the system is lightly damped, a large number of system Markov parameters is needed. The observer is introduced in the state space model and it is shown to decrease the number of estimated parameters to a unique set of observer Markov parameters. The relationship of the observer state space models on linear and recurrent networks is shown. The identification of time varying systems is presented as the observer Markov parameters are identified for various “set points” of the time varying plant shown in Figure 3.1. Finally a simply connected observer is constructed using the observer Markov parameters in an example problem. Various size observers were identified from the time varying plant and results are discussed. The observer Markov parameters are then used to construct time varying observer canonical state space models. In the following theoretical and numerical experimental results, to simplify the mathematics, the angle  $\theta$  (without the subscript) will refer to the elbow joint angle  $\theta_2$ .

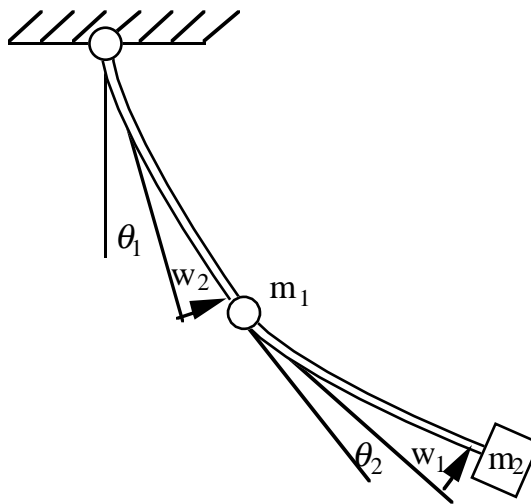


Figure 3.1 Two Link Model used for System Identification

### 3.1 Markov Parameters and the State Space Model

This section describes the relationship between the feed forward linear network and the state space model, which is a common form of representing linear systems (Phan, 1993). The discrete time state space model of an  $N$ -th order,  $m$ -input,  $q$ -output system is a set of  $N$  simultaneous first order difference equations of the form

$$\begin{aligned} x(k+1) &= Ax(k) + Bu(k) \\ y(k) &= Cx(k) + Du(k) \end{aligned} \quad (3.1.1)$$

where the dimensions of  $A$ ,  $B$ ,  $C$ , and  $D$  are  $n \times n$ ,  $n \times m$ ,  $q \times n$ , and  $q \times m$ , respectively. Solving for the output  $y(k)$  in terms of the previous inputs yields

$$y(k) = \sum_{i=0}^k h_i u(k-i) \quad (3.1.2)$$

where the parameters

$$h_0 = D, \quad h_k = CA^{k-1}B, \quad k = 1, 2, 3, \dots \quad (3.1.3)$$

are the *Markov parameters* (Phan, 1992) of the system described by Equation (3.1.1), which are also the system pulse response samples. The Markov parameters are expressed in terms of the system discrete state space matrices  $A$ ,  $B$ ,  $C$ , and  $D$ .

For an asymptotically stable system, the pulse response can be neglected after a finite number of time steps, say  $p_s$ . The input-output description in Equation (3.1.2) can be approximated by a finite number of Markov parameters

$$y(k) \approx h_0 u(k) + h_1 u(k-1) + h_2 u(k-2) + \dots + h_{p_s} u(k-p_s) \quad (3.1.4)$$

where  $p_s$  is sufficiently large so that  $CA^k B \approx 0$ ,  $k \geq p_s$ . Note that the elements of the Markov parameters are simply the weights of a single-layer linear network, where

inputs to the network include both current and past values of the input signal and  $z^{-1}$  denotes the time delay operator (see Figure 3.1.1).

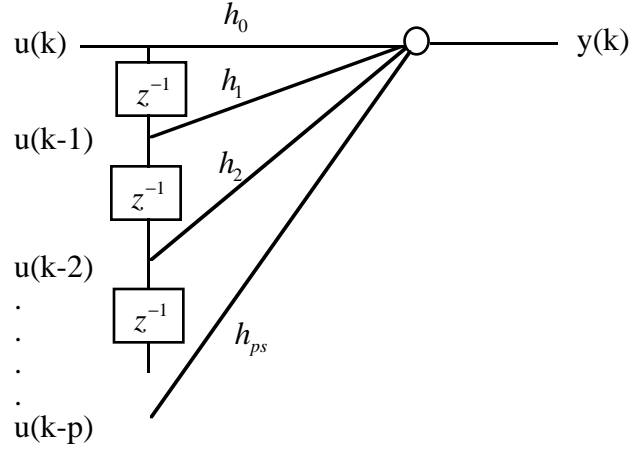


Figure 3.1.1 Markov Parameters as Weights in a Linear Network

In practice, if the system is lightly damped, a large number of system Markov parameters is needed to maintain (3.1.4) as a valid approximation. The fact that a large number of system Markov parameters is required to represent a lightly damped system of the form in Equation (3.1.4) is a major weakness of the representation.

### 3.2 Observer Markov Parameters

To reduce the number of Markov parameters needed to adequately model the system, an observer model is introduced. Adding and subtracting the term  $Ky(k)$  to the right hand side of the state equation in Equation (3.1.1) yields

$$\begin{aligned} x(k+1) &= Ax(k) + Bu(k) + Ky(k) - Ky(k) \\ &= (A + KC)x(k) + (B + KD)u(k) - Ky(k) \end{aligned} \quad (3.2.1)$$

If  $K$  is a matrix so that  $A + KC$  is deadbeat of order  $p$ , i.e.,

$$(A + KC)^k \equiv 0, \quad k \geq p \quad (3.2.2)$$

then for  $k \geq p$  the output  $y(k)$  can be expressed as a finite difference equation

$$y(k) = \alpha_1 y(k-1) + \dots + \alpha_p y(k-p) + \beta_0 u(k) + \beta_1 u(k-1) + \dots + \beta_p u(k-p) \quad (3.2.3)$$

where

$$\begin{aligned} \alpha_k &= -C(A + KC)^{k-1} K \\ \beta_k &= C(A + KC)^{k-1} (B + KD), \quad \beta_0 = h_0 = D \end{aligned} \quad (3.2.4)$$

The matrix  $K$  in the above development can be interpreted as an observer gain. The system considered in Equation (3.1.4) has an observer of the form (Phan, 1992)

$$\begin{aligned} \hat{x}(k+1) &= A\hat{x}(k) + Bu(k) - K[y(k) - \hat{y}(k)] \\ \hat{y}(k) &= C\hat{x}(k) + Du(k) \end{aligned} \quad (3.2.5)$$

Defining the state estimation error  $e(k) = x(k) - \hat{x}(k)$ , the equation that governs  $e(k)$  is

$$e(k+1) = (A + KC)e(k) \quad (3.2.6)$$

For an observable system, the matrix  $K$  exists such that the eigenvalues of  $A + KC$  may be placed in any desired symmetric configuration. If the matrix  $K$  is such that  $A + KC$  is asymptotically stable, then the estimated state  $\hat{x}(k)$  tends to the true state  $x(k)$  as  $k$  tends to infinity for any initial difference between the assumed observer state and the actual system state. The matrix  $K$  can therefore be interpreted as an observer gain. The parameters defined as

$$\begin{aligned} \bar{Y}(k) &= C(A + KC)^{k-1} [B + KD, \quad -K] \\ &= [\beta_k, \quad \alpha_k] \end{aligned} \quad (3.2.7)$$

are the Markov parameters of an observer system, hence they are referred to as *observer Markov parameters* (Juang, 1991).

Notice that in Equation (3.2.3), the output  $y(k)$  is the open loop response of the system, yet the coefficients  $\alpha_k$ ,  $\beta_k$  are related to an observer gain. Consider the special case where  $K$  is a deadbeat observer gain such that all eigenvalues of  $A + KC$  are zero, the observer Markov parameters will become identically zero after a finite number of terms. For lightly damped structures this means that the system can be described by a reduced number of observer Markov parameters  $\bar{Y}(k)$ , instead of an otherwise large number of the usual system Markov parameters  $h_k$ . For this reason, the observer Markov parameters are important in linear system identification.

Equation (3.2.3) can be represented by a single layer of a recurrent network (Phan, 1993) in Figure 3.2.1.

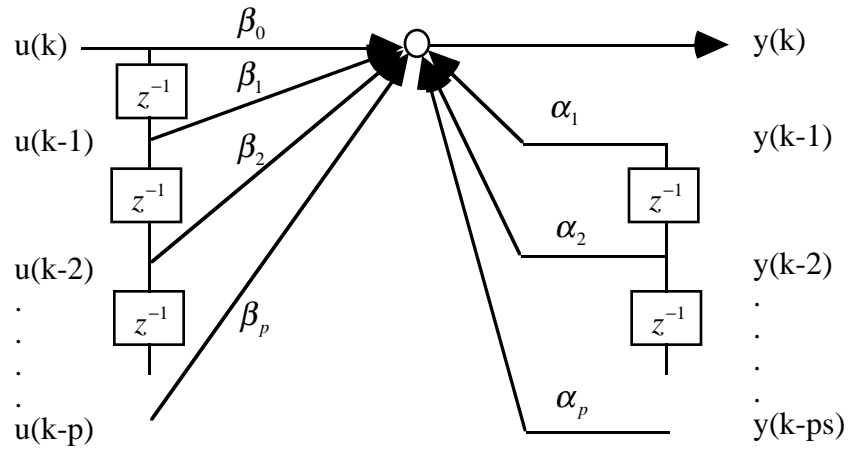


Figure 3.2.1 A Single Layer of a Recurrent Network

The system Markov parameters or the feed forward network weights are related to the recurrent network weights by

$$h_k = \beta_k + \sum_{i=1}^k \alpha_i h_{k-i} \quad (3.2.8)$$

Where  $\alpha_k \equiv 0$ ,  $\beta_k \equiv 0$  for  $k > p$ . To describe a system of order  $N$ , the number of observer Markov parameters  $p$  must be such that  $qp \geq N$ , where  $q$  is the number of outputs. The implication of this result to the network configuration is that a recurrent network requires fewer number of parameters or weights than are required by an equivalent feed forward network. Furthermore, it is not possible to represent a marginally stable or unstable system by a feed forward network. However, it is possible to represent such a system by a recurrent network.

### 3.3 Identification of Linear Systems

The problem of linear system identification using linear networks is reduced to finding these network weights from input-output data. The computation may be done off-line or on-line. In off-line computation the input-output data is already available and a network representing the system is to be determined. On-line computation refers to the case where the network weights are continually updated as data is made available.

The weights of the network represented by Equation (3.2.3) can be computed using a feed forward model (Phan, 1993). For linear systems it is sufficient to use a one layer network having as many nodes as the number of outputs. This is a simple linear parameter estimation problem. The off-line computation is shown first, followed by an equivalent on-line computation. Equation (3.2.3) can be written as

$$y(k) = \sum_{i=1}^p [\beta_i, \alpha_i] \begin{bmatrix} u(k-i) \\ y(k-i) \end{bmatrix} + \beta_0 u(k) \quad (3.3.1)$$

where network weight parameters  $\alpha_k$ ,  $\beta_k$  are defined by Equation (3.2.4). Writing Equation (3.3.1) in matrix form for a set of input-output data  $N+1$  samples long yields:

$$\mathbf{y} = \bar{\mathbf{Y}}\mathbf{V} \quad (3.3.2)$$

where

$$\mathbf{y} = [y(0) \quad y(1) \quad \cdots \quad y(p) \quad y(p+1) \quad \cdots \quad y(N)] \quad (3.3.3)$$

and

$$\bar{\mathbf{Y}} = [\beta_0, \quad \beta_1, \quad \alpha_1, \quad \beta_2, \quad \alpha_2, \quad \dots \quad \beta_p, \quad \alpha_p] \quad (3.3.4)$$

and

$$\mathbf{V} = \begin{bmatrix} u(0) & u(1) & \cdots & u(p) & u(p+1) & \cdots & u(N) \\ & \begin{bmatrix} u(0) \\ y(0) \end{bmatrix} & \cdots & \begin{bmatrix} u(p-1) \\ y(p-1) \end{bmatrix} & \begin{bmatrix} u(p) \\ y(p) \end{bmatrix} & \cdots & \begin{bmatrix} u(N-1) \\ y(N-1) \end{bmatrix} \\ & & \ddots & \vdots & \vdots & \ddots & \vdots \\ & & & \begin{bmatrix} u(0) \\ y(0) \end{bmatrix} & \begin{bmatrix} u(1) \\ y(1) \end{bmatrix} & \cdots & \begin{bmatrix} u(N-p) \\ y(N-p) \end{bmatrix} \end{bmatrix} \quad (3.3.5)$$

The network weight matrices are estimated using the equation

$$\hat{\bar{\mathbf{Y}}} = \mathbf{y}\mathbf{V}^+ \quad (3.3.6)$$

or

$$\hat{\bar{\mathbf{Y}}} = \mathbf{y}\mathbf{V}^T[\mathbf{V}\mathbf{V}^T]^{-1} \quad (3.3.7)$$

where  $(.)^+$  denotes the pseudo-inverse of the quantity in the parentheses. And

$$\hat{\bar{\mathbf{Y}}} = [\hat{\beta}_0, \quad \hat{\beta}_1, \quad \hat{\alpha}_1, \quad \hat{\beta}_2, \quad \hat{\alpha}_2, \quad \dots \quad \hat{\beta}_p, \quad \hat{\alpha}_p] \quad (3.3.8)$$

Note that the least squares solution  $\hat{\bar{\mathbf{Y}}}$  is the same as the true Markov parameters  $\bar{\mathbf{Y}}$  in (3.3.4) only when there is no noise present and (3.3.5) is of sufficient rank. The least squares solution of Equation (3.3.7) can be obtained by an on-line parameter estimation scheme (Phan, 1993). First write each column in  $\mathbf{V}$  as

$$\mathbf{V} = [\Gamma(0), \quad \Gamma(1), \quad \Gamma(2), \quad \cdots] \quad (3.3.9)$$

so that at each time step  $k$ , Equation (3.3.2) can be written as

$$y(k) = \bar{\mathbf{Y}}\Gamma(k) \quad (3.3.10)$$

The recursive least squares equation for the network weights is simply,

$$\hat{\mathbf{Y}}(k) = \hat{\mathbf{Y}}(k-1) + \left[ y(k) - \hat{\mathbf{Y}}(k-1)\Gamma(k) \right] \left\{ \frac{\Gamma(k)^T R(k-1)}{1 + \Gamma(k)^T R(k-1)\Gamma(k)} \right\} \quad (3.3.11)$$

where

$$R(k) = R(k-1) - \frac{R(k-1)\Gamma(k)\Gamma(k)^T R(k-1)}{1 + \Gamma(k)^T R(k-1)\Gamma(k)} \quad (3.3.12)$$

with an arbitrary initial guess  $\hat{\mathbf{Y}}(0)$ , and  $R(0)$  is any arbitrary positive definite matrix. Other recursive parameter estimation algorithms may be used to replace the standard least squares at this step, e.g., the projection or instrumental variable methods (Goodwin, 1984) and (Ljung, 1983).

### 3.4 Identification of Time Varying Systems

The observer Markov parameters are identified using (3.3.7) which accurately model the mathematics at each “*set point*” of the system. In this way, linear identification techniques can be used to develop the time varying model. Thus the observer Markov parameters will depend on the kinematic elbow pitch angle. The time varying system can be modeled at each set point using the single layer time varying recurrent network shown in Figure 3.4.1.

The objective, then is to use data from several arm orientations to derive estimates of the observer Markov parameters as a function of the elbow joint angle.

$$\hat{\mathbf{Y}}(\theta) = [\hat{\beta}_0(\theta), \hat{\beta}_1(\theta), \hat{\alpha}_1(\theta), \hat{\beta}_2(\theta), \hat{\alpha}_2(\theta), \dots, \hat{\beta}_p(\theta), \hat{\alpha}_p(\theta)] \quad (3.4.1)$$

using the batch method

$$\hat{\mathbf{Y}}(\theta) = \mathbf{y}(\theta) \mathbf{V}(\theta)^T [\mathbf{V}(\theta) \mathbf{V}(\theta)^T]^{-1} \quad (3.4.2)$$

where

$$\mathbf{y}(\theta) = [y(0) \quad y(1) \quad \dots \quad y(p) \quad y(p+1) \quad \dots \quad y(N)] \quad (3.4.3)$$

and

$$\mathbf{V}(\theta) = \begin{bmatrix} u(0) & u(1) & \dots & u(p) & u(p+1) & \dots & u(N) \\ & \begin{bmatrix} u(0) \\ y(0) \end{bmatrix} & \dots & \begin{bmatrix} u(p-1) \\ y(p-1) \end{bmatrix} & \begin{bmatrix} u(p) \\ y(p) \end{bmatrix} & \dots & \begin{bmatrix} u(N-1) \\ y(N-1) \end{bmatrix} \\ & & \ddots & \vdots & \vdots & \vdots & \vdots \\ & & & \begin{bmatrix} u(0) \\ y(0) \end{bmatrix} & \begin{bmatrix} u(1) \\ y(1) \end{bmatrix} & \dots & \begin{bmatrix} u(N-p) \\ y(N-p) \end{bmatrix} \end{bmatrix} \quad (3.4.4)$$

The vector  $\mathbf{y}(\theta)$  and matrix  $\mathbf{V}(\theta)$  consist of data gathered from system identification experiments as outlined in the following section.

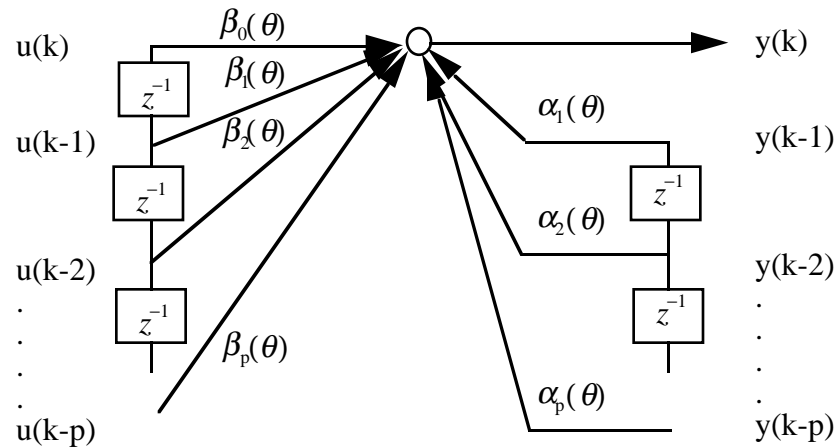


Figure 3.4.1 A Single Layer Time Varying Recurrent Network

### 3.5 Numerical Experimental Results

In this section the batch method (3.4.2) is used to identify the observer Markov parameters of the system shown in Table 3.5.1 for ten different arm orientations. Ten arm orientations were chosen here to show that the third order polynomial, or spline function approximates the observer Markov parameters. The observer Markov parameters will be put into the observer canonical form for control system development. Data gathering numerical experiments for the ten arm orientations were used to derive input and output data for use in the batch method. A broad input spectrum consisting of a random dither was applied. For the following numerical results, these non-dimensional parameters were used (Table 3.5.1).

<p style="text-align: center;"><i>Table 3.5.1</i> Non-Dimensional Parameters used in Numerical Experiment</p>	
$\eta_1 = \frac{m_1}{M_1} = 0$	Mass ratio of link 1; end mass to link 1 mass
$\eta_2 = \frac{m_2}{M_2} = 200$	Mass ratio of link 2; tip mass to link 2 mass
$\eta_L = \frac{M_2}{M_1} = 1$	Link mass ratio: mass of link 2 relative to link 1
$r_L = \frac{L_2}{L_1} = 1$	Link length ratio: length of link 2 to link 1
$\mu_i = \left( \frac{E_i I_i}{M_i L_i^3} \right) = 18$	Non-dimensional stiffness properties of link i

The first results in Table 3.5.2 show the identified time varying system for  $p = 2$  corresponding to a system of order 2. As was shown in Chapter 2, the response is largely dominated by the first system mode (see Figure 2.6.1).

Using the batch method the observer Markov parameters were identified. Table 3.5.2 shows the identified observer for  $p = 2$ .

$$\hat{\mathbf{Y}}(\theta) = [\hat{\beta}_0(\theta) \quad \hat{\beta}_1(\theta) \quad \hat{\alpha}_1(\theta) \quad \hat{\beta}_2(\theta) \quad \hat{\alpha}_2(\theta)] \quad (3.5.1)$$

<p style="text-align: center;"><i>Table 3.5.2</i> Identified Observer Markov Parameters - <math>p = 2</math></p>					
Theta (Degrees)	$\hat{\beta}_0(\theta)$	$\hat{\beta}_1(\theta)$	$\hat{\alpha}_1(\theta)$	$\hat{\beta}_2(\theta)$	$\hat{\alpha}_2(\theta)$
0	-3.7379e-16	2.7522e-04	1.7132	1.2007e-04	-0.9521
10	-1.9967e-16	2.7676e-04	1.7116	1.2158e-04	-0.9522
20	3.4113e-16	2.8147e-04	1.7069	1.2620e-04	-0.9524
30	1.1819e-16	2.8961e-04	1.6987	1.3422e-04	-0.9528
40	-1.0406e-17	3.0163e-04	1.6866	1.4620e-04	-0.9533
50	9.7203e-17	3.1826e-04	1.6700	1.6297e-04	-0.9540
60	2.2409e-16	3.4051e-04	1.6480	1.8579e-04	-0.9551
70	-2.2244e-16	3.6978e-04	1.6191	2.1651e-04	-0.9564
80	-9.6469e-17	4.0792e-04	1.5816	2.5772e-04	-0.9582
90	-4.4990e-16	4.5712e-04	1.5329	3.1299e-04	-0.9607

In Figure 3.5.1 - 3.5.4 the observer elements shown in Table 3.5.2 are plotted and a spline function approximation is fit to the data as  $\theta_2$  is varied from 0 degrees to 90 degrees. Note the first column is the D matrix which should be zero, since there is no feed through term in the system. In all cases, except for the  $\hat{\beta}_0(\theta)$  term, which is zero, a third order polynomial fit the data exactly. The third order approximation, requires four constants for each polynomial. Thus, these four constants can be identified using four system identification experiments.

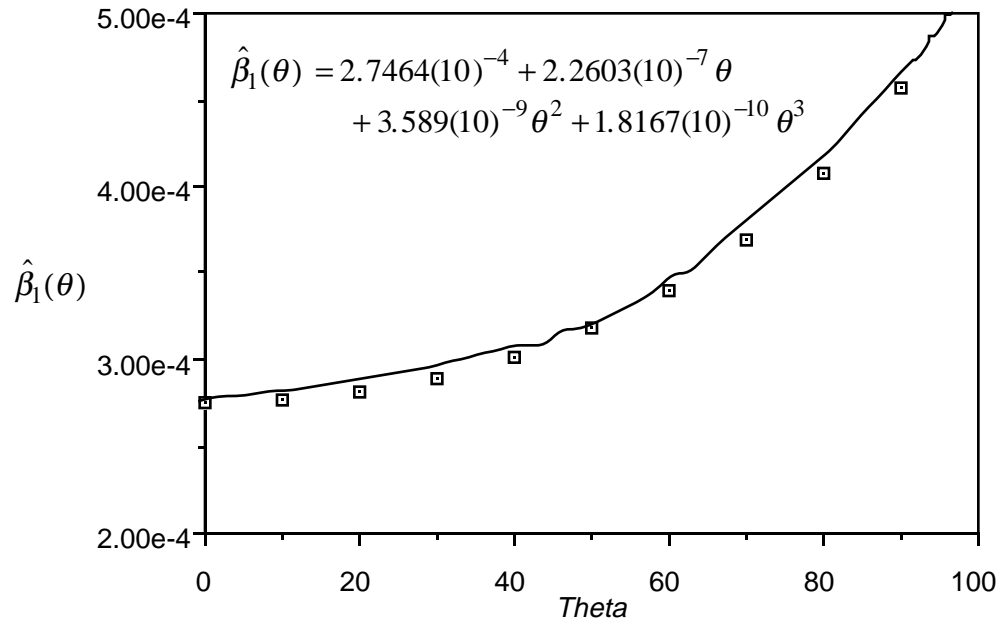


Figure 3.5.1 Identified Polynomial  $\hat{\beta}_1(\theta)$  as Function of Theta

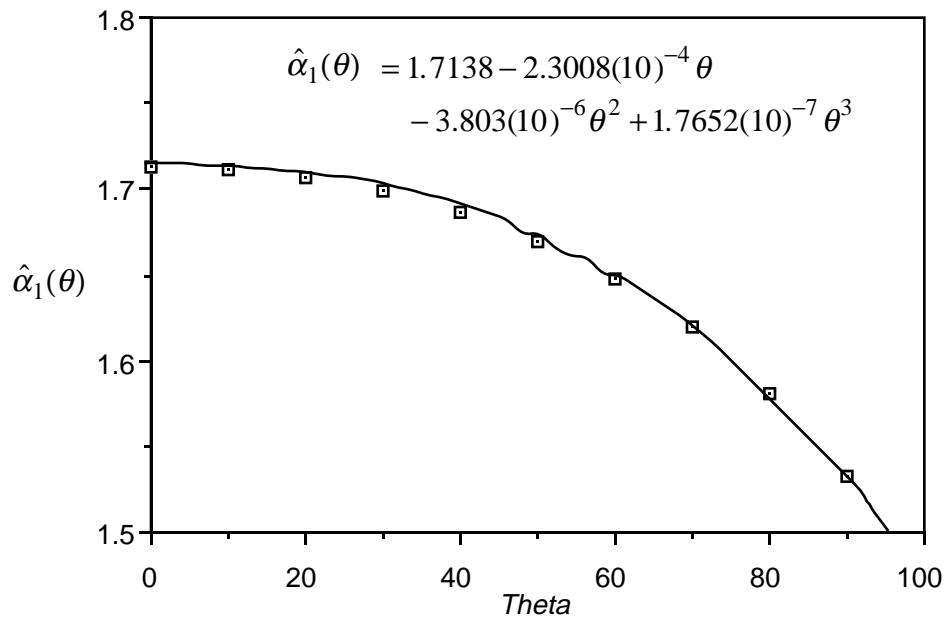


Figure 3.5.2 Identified Polynomial  $\hat{\alpha}_1(\theta)$  as Function of Theta

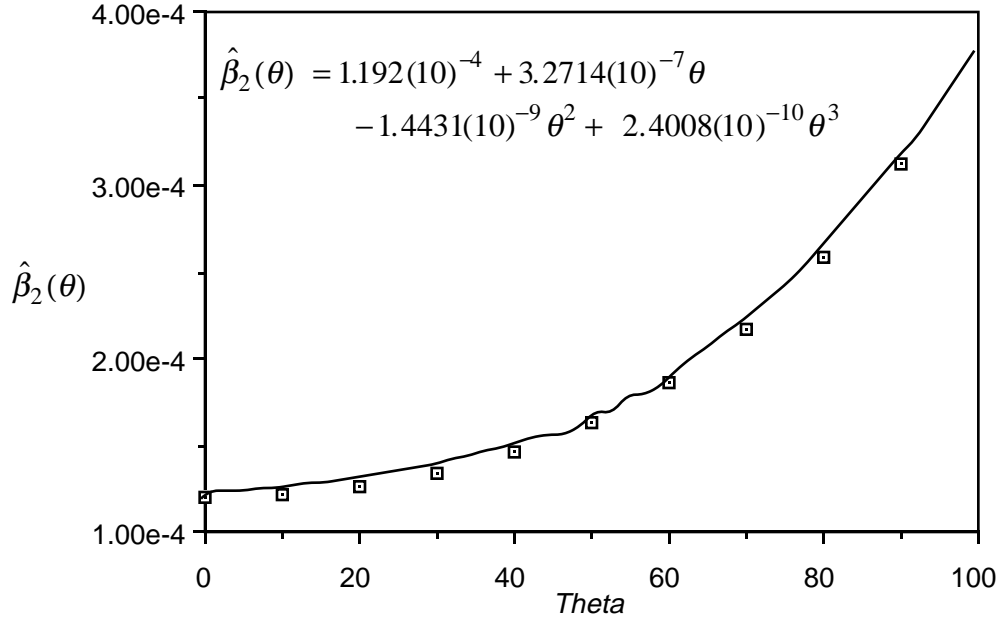


Figure 3.5.3 Identified Polynomial  $\hat{\beta}_2(\theta)$

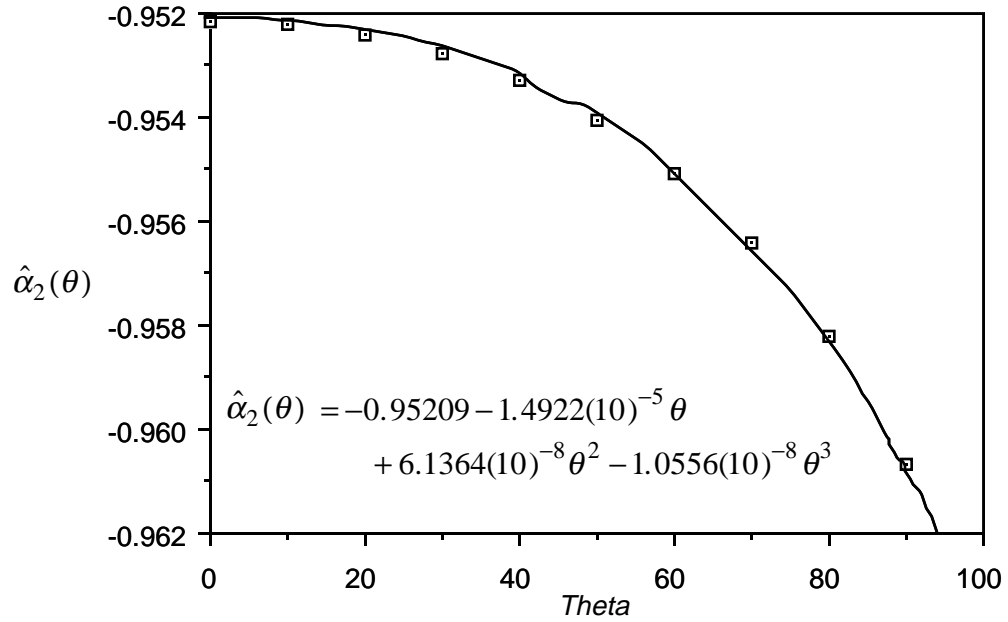


Figure 3.5.4 Identified Polynomial  $\hat{\alpha}_2(\theta)$

The observer Markov parameters reduced the complex mathematical model to a simply connected spline function. This has not been previously reported in the literature. This observation will be used later to design controllers for this system. The observer Markov parameters are the key to reducing the highly heterogeneous parameters in

observer based models to one simply connected observer. Understanding how the essential kernel of the mathematical problem is changing with a measurable state, such as the elbow joint angle, is fundamental to designing low order high performance time varying controllers.

In Table 3.5.3 the results of the identified Markov parameters is shown for  $p = 4$  corresponding to a system of order 4. The purpose of this experiment is to identify an appropriate curve fit for the higher order system. Using the batch method, the observer Markov parameters were identified.

$$\hat{\mathbf{Y}}(\theta) = \begin{bmatrix} \hat{\beta}_0(\theta) & \hat{\beta}_1(\theta) & \hat{\alpha}_1(\theta) & \hat{\beta}_2(\theta) & \hat{\alpha}_2(\theta) & \hat{\beta}_3(\theta) & \hat{\alpha}_3(\theta) & \hat{\beta}_4(\theta) & \hat{\alpha}_4(\theta) \end{bmatrix} \quad (3.5.2)$$

Notice that after about 30 degrees (for  $p=4$ ) there is not much change in the observer Markov parameters. The first Markov parameter is essentially zero, and no attempt is made to fit the data to the exponential function. However, the rest of the Markov parameters are approximated by the exponential function and are shown in Figures 3.5.5-12. In each graph the identified Markov parameters are shown by a “+” and the exponential function is represented by an “x”. Each exponential function curve fit is of the form:

$$f(\theta) = C_1 + C_2 e^{\frac{\theta}{C_3}} \quad (3.5.3)$$

The curve fit for  $p = 4$  is not as accurate as for  $p = 2$ . Since the canonical forms are numerically sensitive to the Markov parameters, the exponential curve fit is not as accurate as the identified Markov parameters. The eigenvalues and eigenvectors associated with the observer Markov parameters are found to be very sensitive to the exponential function. When controlling the higher order dynamics, it was found that a higher order curve fit is required to more accurately fit the data. However, if an accurate curve fit function is not available one can simply use the identified parameters

<p style="text-align: center;"><i>Table 3.5.3</i> Identified Observer Markov Parameters - <math>p = 4</math></p>					
Theta (Degrees)	$\hat{\beta}_0(\theta)$	$\hat{\beta}_1(\theta)$	$\hat{\alpha}_1(\theta)$	$\hat{\beta}_2(\theta)$	$\hat{\alpha}_2(\theta)$
0	2.0861e-15	7.1658e-05	1.1835	-3.0718e-03	-.32979
10	-1.4219e-13	1.1920e-03	3.5036	-4.0705e-03	-4.9931
20	-3.8531e-13	1.3309e-03	3.8531	-4.1363e-03	-5.6984
30	8.8561e-13	1.3609e-03	3.9297	-4.1504e-03	-5.8539
40	2.8695e-12	1.3719e-03	3.9577	-4.1560e-03	-5.9112
50	-1.2457e-12	1.3771e-03	3.9710	-4.1589e-03	-5.9384
60	-3.0983e-12	1.3800e-03	3.9782	-4.1605e-03	-5.9533
70	1.9590e-13	1.3818e-03	3.9825	-4.1615e-03	-5.9622
80	4.6381e-12	1.3830e-03	3.9852	-4.1621e-03	-5.9678
90	-2.3083e-11	1.3838e-03	3.9869	-4.1625e-03	-5.9713

<p style="text-align: center;"><i>Table 3.5.3 Continued</i> Identified Observer Markov Parameters - <math>p = 4</math></p>				
Theta (Degrees)	$\hat{\beta}_3(\theta)$	$\hat{\alpha}_3(\theta)$	$\hat{\beta}_4(\theta)$	$\hat{\alpha}_4(\theta)$
0	3.0900e-03	1.1055	-8.7649e-05	-9.6040e-01
10	4.0734e-03	3.4747	-1.1944e-03	-9.8547e-01
20	4.1388e-03	3.8374	-1.3333e-03	-9.9211e-01
30	4.1530e-03	3.9187	-1.3634e-03	-9.9450e-01
40	4.1587e-03	3.9491	-1.3745e-03	-9.9569e-01
50	4.1615e-03	3.9638	-1.3798e-03	-9.9640e-01
60	4.1631e-03	3.9719	-1.3826e-03	-9.9685e-01
70	4.1640e-03	3.9768	-1.3843e-03	-9.9715e-01
80	4.1644e-03	3.9799	-1.3853e-03	-9.9735e-01
90	4.1645e-03	3.9818	-1.3859e-03	-9.9748e-01

in a gain scheduled controller. Perhaps if more data were used and a higher order curve fit yielded more accurate results, a function could be used to represent this nonlinear system.

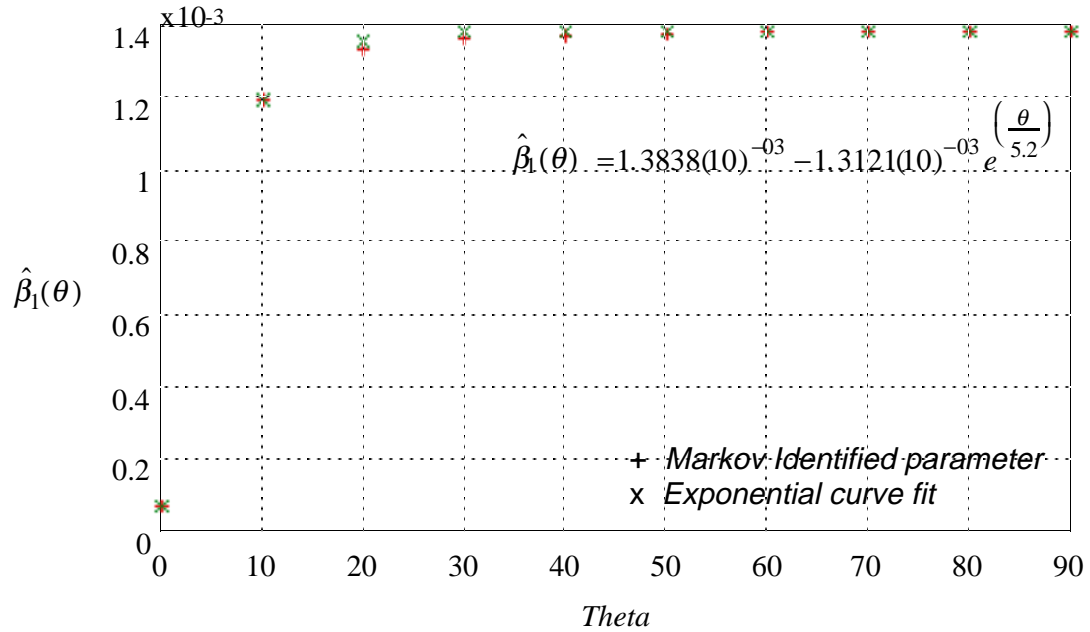


Figure 3.5.5 Identified Exponential Function  $\hat{\beta}_1(\theta)$  -  $p = 4$

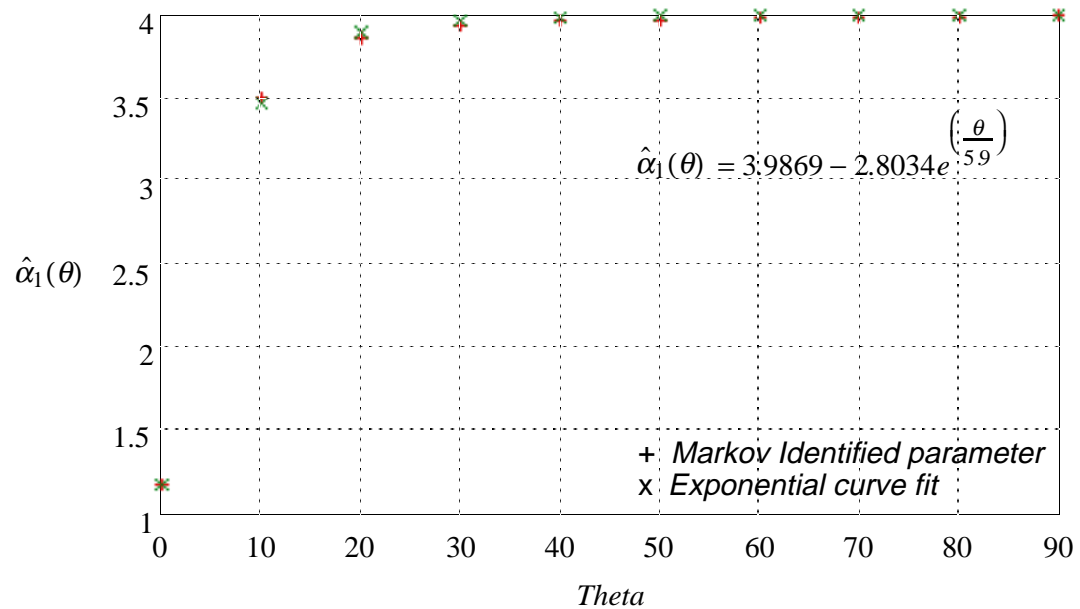


Figure 3.5.6 Identified Exponential Function  $\hat{\alpha}_1(\theta)$  -  $p = 4$

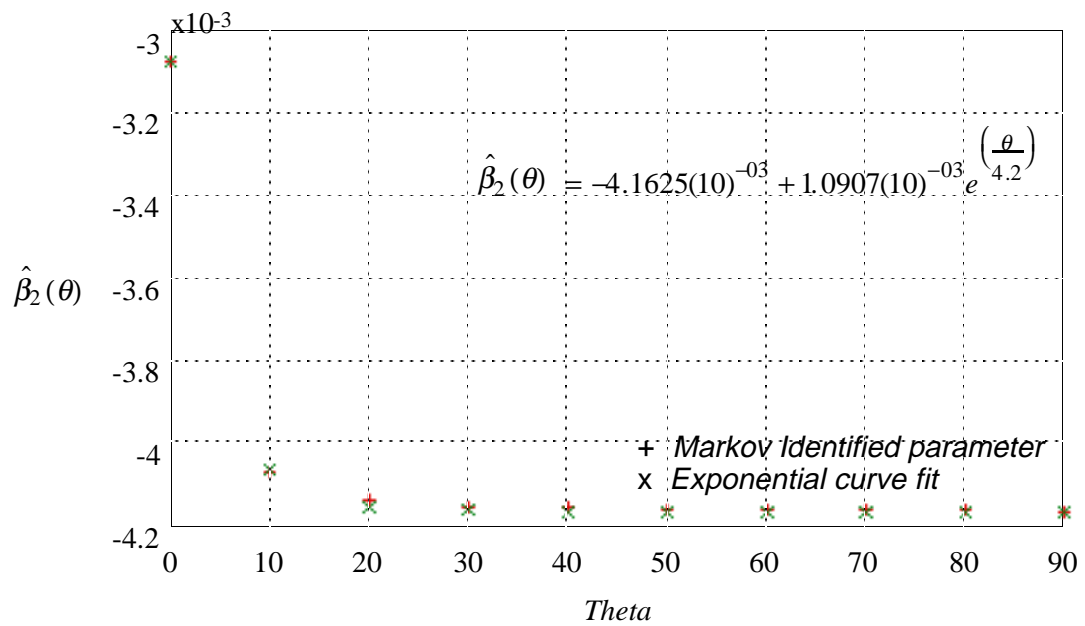


Figure 3.5.7 Identified Exponential Function  $\hat{\beta}_2(\theta)$  -  $p = 4$

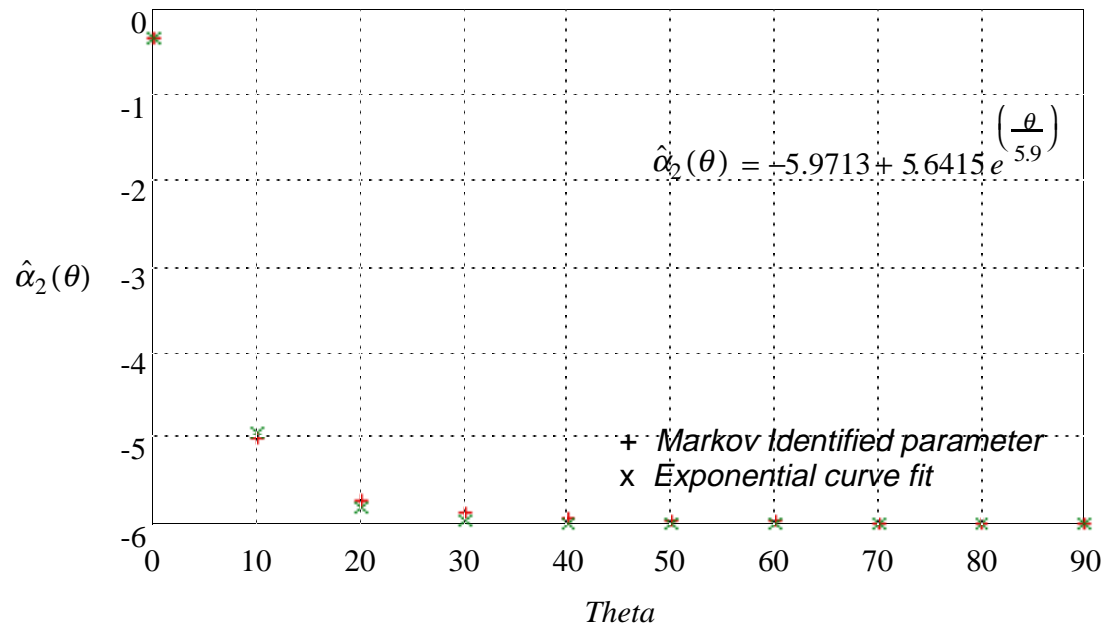


Figure 3.5.8 Identified Exponential Function  $\hat{\alpha}_2(\theta)$  -  $p = 4$

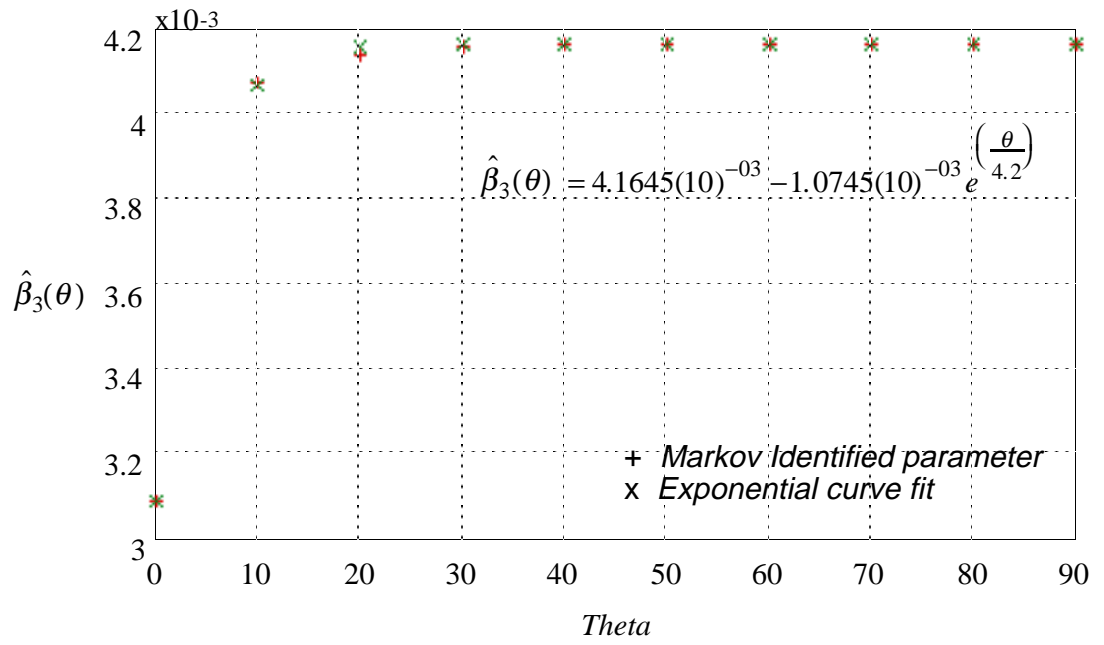


Figure 3.5.9 Identified Exponential Function  $\hat{\beta}_3(\theta)$  -  $p = 4$

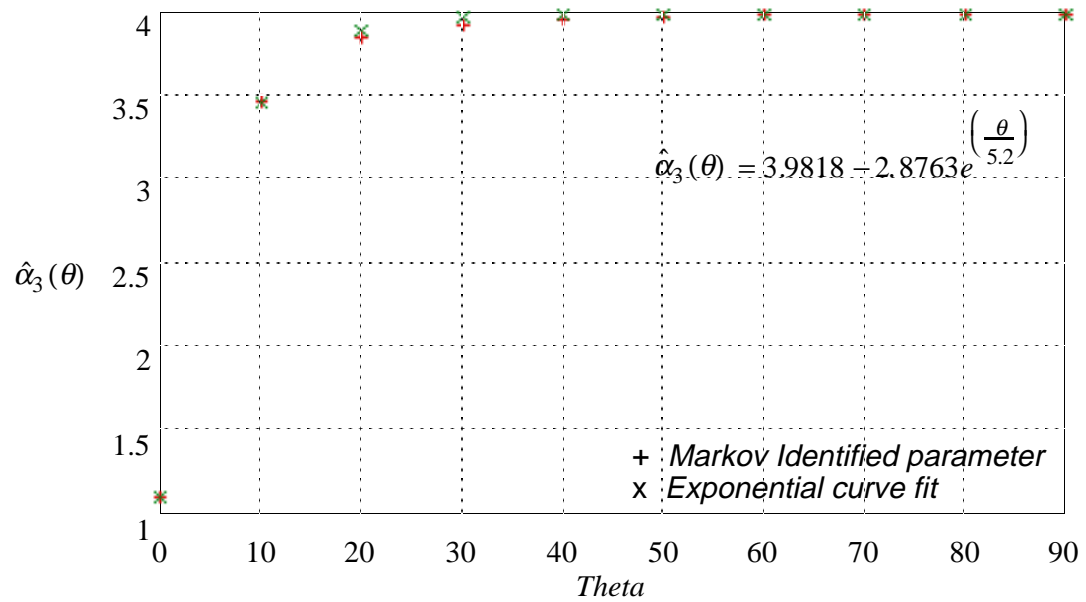


Figure 3.5.10 Identified Exponential Function  $\hat{\alpha}_3(\theta)$ -  $p = 4$

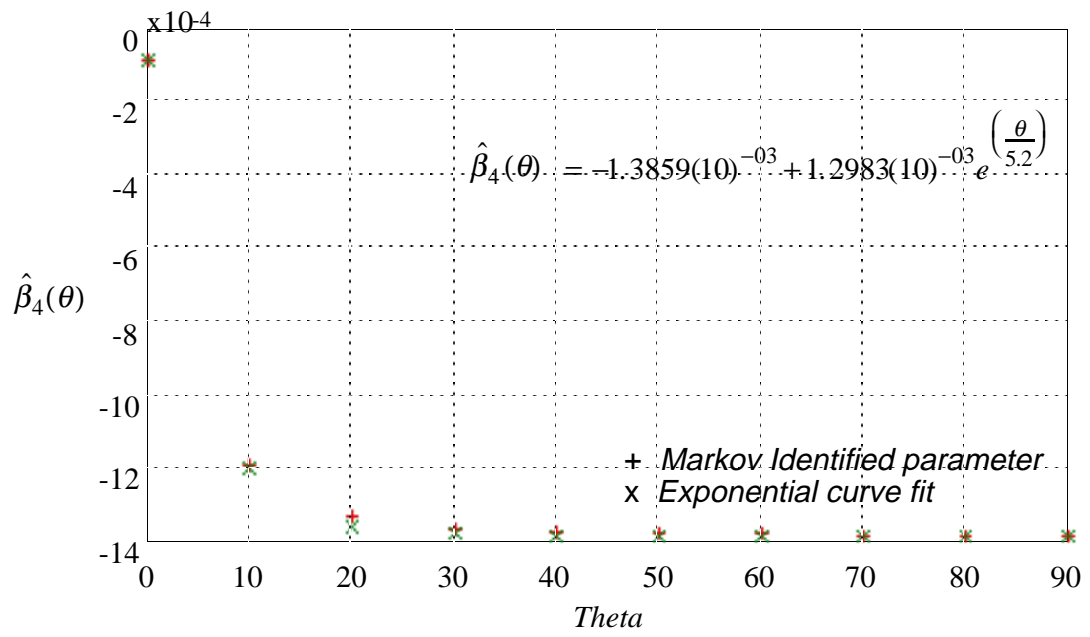


Figure 3.5.11 Identified Exponential Function  $\hat{\beta}_4(\theta)$  -  $p = 4$

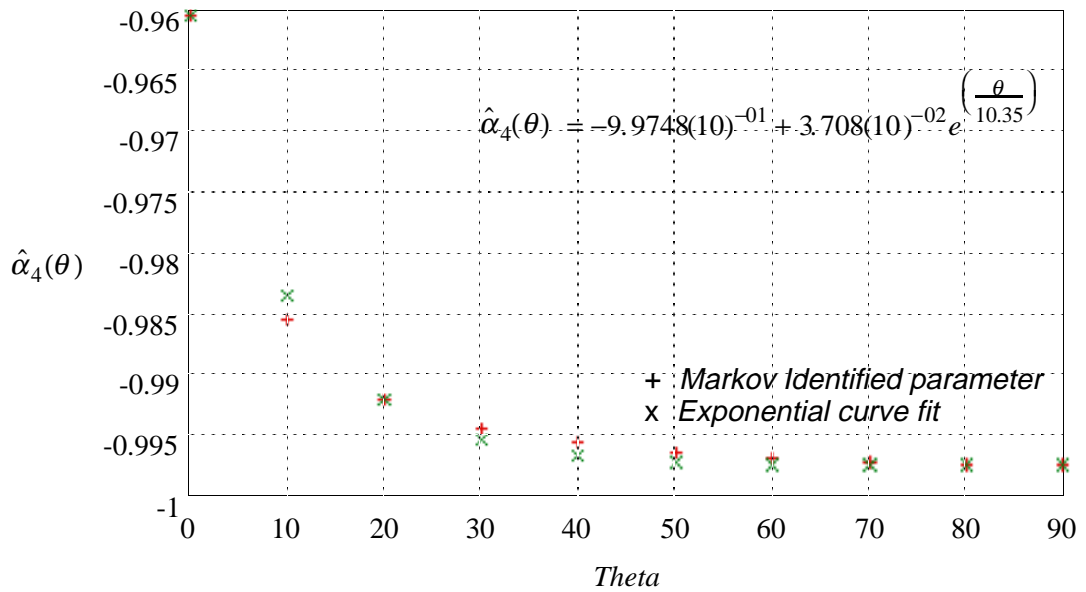


Figure 3.5.12 Identified Exponential Function  $\hat{\alpha}_4(\theta)$  -  $p = 4$

### 3.6 Observer Canonical State Space Model

In this section the observer Markov parameters are used to derive a discrete observer canonical state space model. There is a direct way of determining the system matrices  $A(\theta)$ ,  $B(\theta)$ ,  $C$ , and  $D(\theta)$  without first computing the system Markov parameters. In this similarity transformation the time varying state space model is derived quickly for control system design. Note that there is no need for induction (3.2.8), which unnecessarily increases control design development time. Using the state space model, the optimal regulator is then designed in the following chapter.

The finite difference equation for  $y(k)$  is

$$y(k) = \alpha_1(\theta)y(k-1) + \alpha_2(\theta)y(k-2) + \cdots + \alpha_p(\theta)y(k-p) + \beta_0(\theta)u(k) + \beta_1(\theta)u(k-1) + \cdots + \beta_p(\theta)u(k-p) \quad (3.6.1)$$

Choose the state variables as

$$\begin{aligned} x_p(k) &= y(k) - \beta_0(\theta)u(k) \\ x_{p-1}(k) &= y(k+1) - \beta_0(\theta)u(k+1) \\ &\quad - \alpha_1(\theta)y(k) - \beta_1(\theta)u(k) \\ x_{p-2}(k) &= y(k+2) - \beta_0(\theta)u(k+2) \\ &\quad - \alpha_1(\theta)y(k+1) - \beta_1(\theta)u(k+1) \\ &\quad - \alpha_2(\theta)y(k) - \beta_2(\theta)u(k) \\ &\quad \vdots \\ x_1(k) &= y(k+p-1) - \beta_0(\theta)u(k+p-1) \\ &\quad - \alpha_1(\theta)y(k+p-2) - \beta_1(\theta)u(k+p-2) \\ &\quad - \alpha_2(\theta)y(k+p-3) - \beta_2(\theta)u(k+p-3) \\ &\quad \vdots \\ &\quad - \alpha_{p-1}(\theta)y(k) - \beta_{p-1}(\theta)u(k) \end{aligned} \quad (3.6.2)$$

This set of equations yields

$$\begin{aligned}
y(k) &= x_p(k) + \beta_0(\theta)u(k) \\
x_{p-1}(k) &= x(k+1) - \alpha_1(\theta)y(k) - \beta_1(\theta)u(k) \\
x_{p-2}(k) &= x_{p-1}(k+1) - \alpha_2(\theta)y(k) - \beta_2(\theta)u(k) \\
&\vdots \\
x_1(k) &= x_2(k+1) - \alpha_{p-1}(\theta)y(k) - \beta_{p-1}(\theta)u(k) \\
x_1(k+1) &= \alpha_p(\theta)y(k) + \beta_{p-1}(\theta)u(k)
\end{aligned} \tag{3.6.3}$$

Equation (3.6.3) can be arranged in matrix form as

$$\begin{aligned}
x(k+1) &= A(\theta)x(k) + B(\theta)u(k) \\
y(k) &= Cx(k) + D(\theta)u(k)
\end{aligned} \tag{3.6.4}$$

where

$$x(k) = \begin{bmatrix} x_1(k) \\ x_2(k) \\ x_3(k) \\ \vdots \\ x_p(k) \end{bmatrix} \tag{3.6.5}$$

$$A(\theta) = \begin{bmatrix} 0 & 0 & 0 & 0 & \alpha_p(\theta) \\ 1 & 0 & 0 & 0 & \alpha_{p-1}(\theta) \\ 0 & 1 & 0 & 0 & \alpha_{p-2}(\theta) \\ \vdots & \vdots & \vdots & \ddots & \vdots \\ 0 & 0 & 0 & 1 & \alpha_1(\theta) \end{bmatrix} \tag{3.6.6}$$

$$B(\theta) = \begin{bmatrix} \beta_p(\theta) - \alpha_p(\theta)\beta_0(\theta) \\ \beta_{p-1}(\theta) - \alpha_{p-1}(\theta)\beta_0(\theta) \\ \beta_{p-2}(\theta) - \alpha_{p-2}(\theta)\beta_0(\theta) \\ \vdots \\ \beta_1(\theta) - \alpha_1(\theta)\beta_0(\theta) \end{bmatrix} \tag{3.6.7}$$

$$C = [0 \quad 0 \quad 0 \quad \dots \quad 1] \tag{3.6.8}$$

$$D(\theta) = \beta_0(\theta) \tag{3.6.9}$$

When using a deadbeat observer it is interesting to see the relationship between the observer gain and the Markov parameters. For example, consider the observer form above for a 2nd order system. The eigenvalues of the estimator dynamics are zero for a deadbeat observer, thus,

$$\left| -\lambda I + [A(\theta) + K(\theta)C]^2 \right| = \lambda^2 = 0 \quad (3.6.10)$$

or

$$\left| -\begin{bmatrix} \lambda & 0 \\ 0 & \lambda \end{bmatrix} + \left[ \begin{bmatrix} 0 & \alpha_2(\theta) \\ 1 & \alpha_1(\theta) \end{bmatrix} + \begin{bmatrix} K_1(\theta) \\ K_2(\theta) \end{bmatrix} \begin{bmatrix} 0 & 1 \end{bmatrix} \right]^2 \right| = 0 \quad (3.6.11)$$

Solving for the determinant gives

$$\begin{aligned} & \left[ \begin{array}{cc} -\lambda + \alpha_2(\theta) + K_1(\theta) & (\alpha_2(\theta) + K_1(\theta))(\alpha_1(\theta) + K_2(\theta)) \\ \alpha_1(\theta) + K_2(\theta) & -\lambda + \alpha_2(\theta) + K_2(\theta) + \alpha_1^2(\theta) + 2\alpha_1(\theta)K_2(\theta) + K_2^2(\theta) \end{array} \right] \\ & = \lambda^2 - 2\lambda\alpha_2(\theta) - 2\lambda K_1(\theta) - \lambda\alpha_1^2(\theta) - 2\lambda\alpha_1(\theta)K_2(\theta) - \lambda K_2^2(\theta) \\ & \quad + \alpha_2^2(\theta) - 2\alpha_2(\theta)K_1(\theta) + K_1^2(\theta) = 0 \end{aligned} \quad (3.6.12)$$

Factoring the expression (3.6.12) gives

$$\begin{aligned} & \lambda^2 + \left( -2\alpha_2(\theta) - 2\alpha_1(\theta)K_2(\theta) - K_2^2(\theta) - 2K_1(\theta) - \alpha_1^2(\theta) \right) \lambda \\ & \quad + \left( \alpha_2^2(\theta) + 2\alpha_2(\theta)K_1(\theta) + K_1^2(\theta) \right) = 0 \end{aligned} \quad (3.6.13)$$

Setting Equation (3.6.13) to zero yields the two following equations:

$$-2\alpha_2(\theta) - 2\alpha_1(\theta)K_2(\theta) - K_2^2(\theta) - 2K_1(\theta) - \alpha_1^2(\theta) = 0 \quad (3.6.14)$$

and

$$\alpha_2^2(\theta) + 2\alpha_2(\theta)K_1(\theta) + K_1^2(\theta) = 0 \quad (3.6.15)$$

Solving (3.6.15) for  $K_1(\theta)$  yields

$$K_1(\theta) = -\alpha_2(\theta) \quad (3.6.16)$$

Inserting (3.6.16) into (3.6.14) and solving yields

$$K_2(\theta) = -\alpha_1(\theta) \quad (3.6.17)$$

The significance of (3.6.16) and (3.6.17) is that the estimator gains are identified directly from the data. This fact will be used later during the control system design in Chapter 4.

### 3.7 Summary

This chapter presents the basic concepts of the time varying network as related to the problem of modeling a time varying system. Two basic forms of the network, the feed forward and the recurrent network, are discussed. Emphasis is placed on the interpretation of the time varying networks in terms of time varying state space systems. The relationship between the feed forward time varying network and the time varying observer model is explained.

The main contribution of this chapter is the fact that the performance or fundamental mode observer Markov parameters, which are unique, satisfy a third order approximation, or spline function as a function of the elbow joint angle ( $\theta_2$ ) when  $p = 2$ . This has not been previously reported in the literature. The third order approximation, or spline function, requires four constants for each polynomial. These four constants can be identified using four system identification experiments. Thus, if an accurate physical model is not available, identification can be accomplished for the optimal controller via the observer Markov parameters, using data gathering experiments of four arm orientations. This observation will be used later to design controllers for this system.

In addition, it was observed that when the size of the observer was increased, the Markov parameter fit an exponential function of the elbow joint angle ( $\theta_2$ ). However, the eigenvalues and eigenvectors associated with the observer Markov parameters were found to be very sensitive to the exponential function. There may be other more accurate high order functions which would yield more accurate eigenvalues and eigenvectors. In conclusion, when controlling the fundamental mode, the spline function approximation is an exact approximation of the fundamental dynamics. The higher modes can still be controlled, although a higher order curve fit is required. If an accurate curve fit is not attainable a standard look up table in a gain scheduled controller could be assembled using the identified Markov parameters.

There is a direct way of determining the system matrices  $A(\theta)$ ,  $B(\theta)$ ,  $C$ , and  $D(\theta)$  without first computing the system Markov parameters by using the observer canonical state space model form. In this similarity transformation, the time varying state space model is derived quickly for control system design. Note that there is no need for induction which unnecessarily increases control design development time.

## **CHAPTER 4**

### **COMPENSATOR DESIGN**

The identification results of Chapter 3 will be used in this chapter to design the compensator. This chapter is organized as follows. First, two characteristics of reconfigurable structures are used to develop the controller implementation strategy. The two characteristics shown in Chapter 2 are: There is an attenuation of the infinity norm of the amplitude of the higher frequency modes in the response; and there is a considerable frequency separation between consecutive modes for the cantilevered two link manipulator which represents the fundamental dynamics of the system. The overall controller implementation strategy is introduced. The overall strategy is to design the compensator for performance and then adjust for stability. The compensator design section describes four different types of compensator designs. The first section derives a fixed gain dynamic compensator. This section provides insight of the stability of the compensator when large variations of the plant exist. The second section derives the equations necessary for a robust fixed compensator to a time varying plant. The third section derives the equations necessary to obtain an optimal gain scheduled compensator where the dynamics matrix remains fixed and the output gain matrix is allowed to vary. Also in this section an adaptive frequency domain compensator is described which requires no a-priori knowledge of the changing plant dynamics. The fourth section develops a Spline Varying Optimal (SVO) Controller in which a time varying observer/controller is derived. The SVO controller developed in this chapter is the first simply connected time varying compensator shown in the literature. The SVO controller includes elements whose parameters change in time. The elements of the

dynamic matrices change according to a polynomial which fits the linear quadratic regulator optimal gain designed at each arm configuration. In this way minimal on board computing is required. Following the theoretical development, an example problem is introduced and the performance of each controller is compared. Each controller design is evaluated using a consistent cost function. . With the SVO controller there is an improvement of 20:1 over the open loop manipulator dynamics along the range of motion. Finally, the stability of the SVO compensator is examined by evaluating the minimum singular value of the return difference matrix. In the development that follows, the angle  $\theta$  refers to the elbow pitch joint angle.

#### **4.1 Controller Implementation Strategy**

One feature of the implementation of the compensator is important to discuss prior to investigating the stability of the closed loop system. The fundamental assumption is *the system dynamics do not change while the compensator is operational*. This is an important assumption since there presently are no theorems to address the stability issues associated with allowing the implementation of the SVO *during* an arm maneuver. The SVO controller will reduce the tip vibratory response *after* the operator has maneuvered the arm. Since the joints on the reconfigurable structure have gearbox elements, the flexible energy of the structure does not back drive the joints, as described in section 2.3. In the proposed controller the shoulder joint of the manipulator is the most effective actuator to improve the damping level of the first mode. Thus the elbow joint will remain fixed and the shoulder actuator will remain active after the operator finishes the maneuver.

## 4.2 Fixed Optimal Compensator

One approach to improving the performance of the manipulator is to design a compensator for a linearized state space model about a nominal arm orientation, and then see how well the compensator performs while the kinematics are allowed to vary. Although this is not a recommended approach, it does provide some useful insights and answers some basic questions, such as “Are the dynamics changing significantly enough to warrant a more sophisticated time varying or robust controller?” The approach taken in this section is to design one fixed controller which is “optimized” about a nominal arm orientation. A heuristic method is applied to “identify” this nominal model. The nominal model is identified by the following procedure:

- (1) Design an optimal controller for a “set point” or arm orientation.
- (2) Evaluate the performance of this controller as the open loop system dynamics are varied by using an additive cost function (described later).
- (3) Design an optimal controller for successive arm orientations and repeat step two until all “set point” controllers have been evaluated.

In this manner the controller that has the lowest additive cost function, and hence the nominal arm orientation is “identified.” The optimal fixed compensator designed about the nominal arm orientation will use standard observer based state feedback, where assumptions are made concerning the process and measurement noise covariance's. Since the controller is operating over a dynamically changing system, these assumptions are at best dubious. However, as stated earlier, this is an exercise to examine how well one controller could perform, and whether more sophisticated controllers are warranted. In Section 4.3, a more rigorous approach is applied to ensure stability for the closed loop time varying system. In either case, since the

observer is meaningless for the time varying system, the controller state is labeled  $z$ , as opposed to the state estimate  $\hat{x}$ , and the controller will be referred to as a dynamic compensator, as opposed to the traditional state feedback controller.

The time varying plant model as outlined in Chapter 2 is given by,

$$\begin{aligned}\dot{x} &= A(\theta_i)x + B(\theta_i)u + Gw \\ y &= C(\theta_i)x + D(\theta_i)u + v\end{aligned}\tag{4.2.1}$$

with process noise and measurement noise covariance's:

$$E\{w\} = E\{v\} = 0, \quad E\{ww'\} = Q_w, \quad E\{vv'\} = R_v, \quad E\{wv'\} = 0$$

Where  $x$  is the state,  $A(\theta_i)$  the dynamic matrix at  $\theta_i$ ,  $B(\theta_i)$  the control influence matrix,  $C(\theta_i)$  is the system output matrix,  $D(\theta_i)$  the direct transmission matrix, and  $y$  is the plant output. Using a fixed dynamic compensator of the form:

$$\begin{aligned}\dot{z} &= A_i z + B_i u + K_i[y - \hat{y}] \\ \hat{y} &= C_i z + D_i u\end{aligned}\tag{4.2.2}$$

where  $z$  is the controller state, and  $K_i$  is the steady state Kalman filter gain solved for a nominal arm configuration described below. Substituting yields:

$$\dot{z} = (A_i - K_i C_i)z + (B_i - K_i D_i)u + K_i y\tag{4.2.3}$$

Using a state feedback gain  $C_c$ , the control input is given by:

$$u = C_c z\tag{4.2.4}$$

To minimize the Linear Quadratic Regulator (LQR) cost function:

$$J = \int_0^{\infty} [y^T Q y + u^T R u] dt\tag{4.2.5}$$

The control gain matrix  $C_c$  is given by

$$C_c = -R^{-1} B_i^T P\tag{4.2.6}$$

The matrix  $P = P^T \geq 0$  is computed from the solution of the following algebraic Riccati equation:

$$A_i^T P + P A_i - P B_i R^{-1} B_i^T P + Q = 0 \quad (4.2.7)$$

Inserting (4.2.4) into (4.2.2) yields:

$$\dot{z} = (A_i - K_i C_i + B_i C_c - K_i D_i C_c) z + K_i y \quad (4.2.8)$$

Substituting

$$\begin{aligned} A_c &= A_i - K_i C_i + B_i C_c - K_i D_i C_c \\ B_c &= K_i \end{aligned} \quad (4.2.9)$$

into (4.2.8) yields the *fixed* compensator equations:

$$\begin{aligned} \dot{z} &= A_c z + B_c y \\ u &= C_c z \end{aligned} \quad (4.2.10)$$

Thus, the fixed dynamic compensator is given by the following transfer function:

$$G_c(s) = C_c (sI - A_c)^{-1} B_c + D_c \quad (4.2.11)$$

A control block diagram of the fixed optimal compensator is shown in Figure 4.2.1.

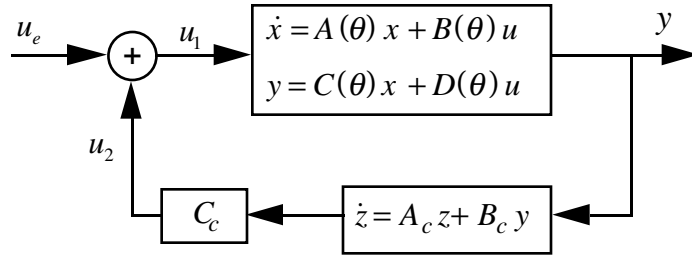


Figure 4.2.1 Fixed Dynamic Compensator

The plant dynamic equations for the time varying system is  $u_e = 0$ , and  $u = u_1 = u_2$ :

$$\begin{aligned} \dot{x} &= A(\theta_i)x + B(\theta_i)u \\ y &= C(\theta_i)x + D(\theta_i)u \end{aligned} \quad (4.2.12)$$

The state equations for zero exogenous inputs are:

$$\begin{aligned}
\dot{x} &= A(\theta_i)x + B(\theta_i)C_c z \\
\dot{z} &= (A_c C(\theta_i) + B_c D(\theta_i)C_c)z + B_c C(\theta_i)x \\
y &= C(\theta_i)x + D(\theta_i)u \\
&= C(\theta_i)x + D(\theta_i)C_c z
\end{aligned} \tag{4.2.13}$$

These equations (4.2.13) written in block matrix form are:

$$\begin{aligned}
\begin{bmatrix} \dot{x} \\ \dot{z} \end{bmatrix} &= \begin{bmatrix} A(\theta_i) & B(\theta_i)C_c \\ B_c C(\theta_i) & A_c + B_c D(\theta_i)C_c \end{bmatrix} \begin{bmatrix} x \\ z \end{bmatrix} \\
\begin{bmatrix} y \\ u \end{bmatrix} &= \begin{bmatrix} C(\theta_i) & D(\theta_i)C_c \\ 0 & C_c \end{bmatrix} \begin{bmatrix} x \\ z \end{bmatrix}
\end{aligned} \tag{4.2.14}$$

The Linear Quadratic Regulator (LQR) cost function is given by

$$J(\theta_i) = \int_0^{\infty} [y^T Q y + u^T R u] dt \tag{4.2.15}$$

inserting

$$\begin{aligned}
u^T &= z^T C_c^T \\
y^T &= x^T C(\theta_i)^T + z^T C_c^T D(\theta_i)^T
\end{aligned} \tag{4.2.16}$$

into (4.2.15) yields

$$J(\theta_i) = \int_0^{\infty} \left[ \begin{bmatrix} x^T C(\theta_i)^T + z^T C_c^T D(\theta_i)^T \\ + z^T C_c^T R C_c z \end{bmatrix} Q \begin{bmatrix} C(\theta_i)x + D(\theta_i)C_c z \end{bmatrix} \right] dt \tag{4.2.16}$$

rewriting (4.2.16)

$$J(\theta_i) = \int_0^{\infty} \left[ \begin{bmatrix} x^T C(\theta_i)^T Q C(\theta_i)x + x^T C(\theta_i)^T Q D(\theta_i)C_c z \\ + z^T C_c^T D(\theta_i)^T Q C(\theta_i)x + z^T C_c^T D(\theta_i)^T Q D(\theta_i)C_c z \\ + z^T C_c^T R C_c z \end{bmatrix} \right] dt \tag{4.2.17}$$

which can be written in matrix block form

$$J(\theta_i) = \int_0^\infty \begin{bmatrix} \bar{x}^T & z^T \end{bmatrix} \begin{bmatrix} C(\theta_i)^T Q C(\theta_i) & C(\theta_i)^T Q D(\theta_i) C_c \\ C_c^T D(\theta_i)^T Q C(\theta_i) & C_c^T (D(\theta_i)^T Q D(\theta_i) + R) C_c \end{bmatrix} \begin{bmatrix} x \\ z \end{bmatrix} dt \quad (4.2.18)$$

let  $\bar{x}$  be an augmented vector of the plant state and compensator state

$$\bar{x} = \begin{bmatrix} x \\ z \end{bmatrix} \quad (4.2.19)$$

Then the cost can be rewritten as

$$J(\theta_i) = \int_0^\infty \bar{x}^T \bar{Q}(\theta_i) \bar{x} dt \quad (4.2.20)$$

where

$$\bar{Q}(\theta_i) = \begin{bmatrix} C(\theta_i)^T Q C(\theta_i) & C(\theta_i)^T Q D(\theta_i) C_c \\ C_c^T D(\theta_i)^T Q C(\theta_i) & C_c^T (D(\theta_i)^T Q D(\theta_i) + R) C_c \end{bmatrix} \quad (4.2.21)$$

and the augmented state vector satisfies the equation

$$\dot{\bar{x}} = \bar{A}(\theta_i) \bar{x} \quad (4.2.22)$$

where

$$\bar{A}(\theta_i) = \begin{bmatrix} A(\theta_i) & B(\theta_i) C_c \\ B_c C(\theta_i) & A_c + B_c D(\theta_i) C_c \end{bmatrix} \quad (4.2.23)$$

If  $\bar{A}(\theta_i)$  is stable, there exists a symmetric positive definite matrix  $P$  which satisfies the Lyapunov equation:

$$\bar{A}(\theta_i)^T \bar{P}(\theta_i) + \bar{P}(\theta_i) \bar{A}(\theta_i) + \bar{Q}(\theta_i) = 0 \quad (4.2.24)$$

the cost can be rewritten as

$$J(\theta_i) = - \int_0^\infty \bar{x}^T (\bar{A}(\theta_i)^T \bar{P}(\theta_i) + \bar{P}(\theta_i) \bar{A}(\theta_i)) \bar{x} dt \quad (4.2.25)$$

but

$$\frac{d}{dt}[\bar{x}^T \bar{P}(\theta_i) \bar{x}] = \dot{\bar{x}}^T \bar{P}(\theta_i) \bar{x} + \bar{x}^T \bar{P}(\theta_i) \dot{\bar{x}} \quad (4.2.26)$$

using

$$\dot{\bar{x}} = \bar{A}(\theta_i) \bar{x} \quad (4.2.27)$$

yields

$$\frac{d}{dt}[\bar{x}^T \bar{P}(\theta_i) \bar{x}] = \bar{x}^T (\bar{A}(\theta_i)^T \bar{P}(\theta_i) + \bar{P}(\theta_i) \bar{A}(\theta_i)) \bar{x} \quad (4.2.28)$$

The cost is rewritten using (4.2.28) and (4.2.25)

$$\begin{aligned} J(\theta_i) &= - \int_0^\infty \frac{d}{dt} [\bar{x}^T \bar{P}(\theta_i) \bar{x}] dt \\ &= - [\bar{x}^T \bar{P}(\theta_i) \bar{x}]_0^\infty \\ &= -(\bar{x}_\infty^T \bar{P}(\theta_i) \bar{x}_\infty - \bar{x}_0^T \bar{P}(\theta_i) \bar{x}_0) \end{aligned} \quad (4.2.29)$$

If  $\bar{A}(\theta_i)$  stable then  $\bar{x}_\infty = 0$ , and the cost is:

$$J(\theta_i) = \bar{x}_0^T \bar{P}(\theta_i) \bar{x}_0 \quad (4.2.30)$$

Thus, the infinite time total cost of the control effort for the fixed compensator

$G_c(s) = C_c(sI - A_c)^{-1} B_c + D_c$  over the workspace is the sum of each cost at the

respective values of theta. The total cost varies for the nominal compensator  $G_c$  which

is optimal only for a fixed arm orientation  $\theta_i$

$$T_J(G_c) = \sum_{i=0}^n J(\theta_i) \quad (4.2.31)$$

where the fixed compensator state matrices are given by:

$$\begin{aligned} A_c &= A_i - K_i C_i + B_i C_c - K_i D_i C_c \\ B_c &= K_i \end{aligned} \quad (4.2.32)$$

Thus by finding the minimum value of

$$T_J(G_c) \tag{4.2.33}$$

for various nominal compensators, the ‘optimal’ nominal fixed gain compensator is found. An example is shown in Section 4.6.

### 4.3 Fixed Robust Dynamic Compensator

The main focus of the discussion in this section is the stability of feedback control systems. There is a difference between *nominal* stability and *stability-robustness*. Nominal stability relates to the stability of the feedback loop that employs the mathematical model of the nominal plant. Stability-robustness refers to the stability of the feedback loop that contains the *actual plant*. The fact that model errors cannot be precisely defined presents a significant challenge in ensuring closed-loop stability. Indeed, model errors may not correspond to a finite-dimensional dynamic system (a very small but unknown time-delay is a good example), so that a state-space representation for modeling errors is inappropriate. Thus, checking the eigenvalues of a particular matrix is not sufficient for stability-robustness, unlike the eigenvalue based tests which are available for deducing nominal stability using state-space models. This state of affairs forces the examination of stability-robustness using frequency domain ideas and tests.

To derive these frequency domain stability-robustness tests for SISO feedback loops, one can use the familiar Nyquist stability criterion. However, to develop stability-robustness tests for multivariable feedback systems, it is necessary to develop a MIMO

Nyquist stability criterion. MIMO Nyquist tests using the singular value concept can also be used to arrive at stability for MIMO systems.

### Nominal Stability and Stability-Robustness

The nominal compensator  $G_c(s)$  developed for the plant  $G_i(s)$  that was discussed in the preceding section will be used in this section as the initial compensator. The nominal compensator  $G_c(s)$  is modified by changing the output gain  $C_c$  such that the nominal feedback loop shown in Figure 4.3.1 is robust. Thus the nominal feedback loop addresses the nominal stability issue.

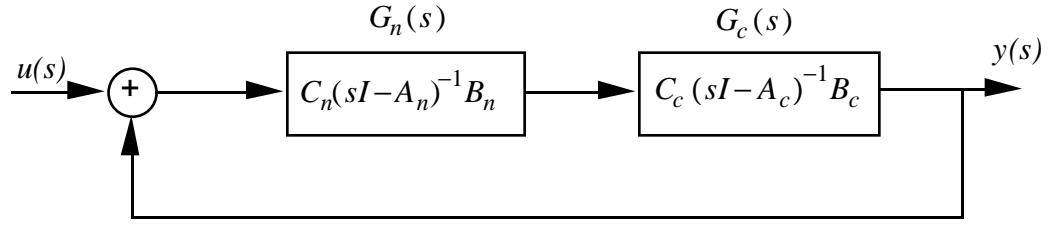


Figure 4.3.1 Fixed Robust Compensator - Nominal Stability

Alternatively the nominal or average model could have been computed in the state space domain by the following procedure (Anderson, 1989).

Step 1: Compute the Average Model

$$G(\theta_i, s) = C(\theta_i)(sI - A(\theta_i))^{-1}B(\theta_i) + D(\theta_i) \quad (\text{Plant Models}) \quad (4.3.1)$$

$$A_{ave} = \text{diag}[A(\theta_1), A(\theta_2), \dots, A(\theta_p)], \quad B_{ave} = \begin{bmatrix} B(\theta_1) \\ B(\theta_2) \\ \vdots \\ B(\theta_p) \end{bmatrix} \quad (4.3.2)$$

$$C_{ave} = \frac{1}{p} [C(\theta_1), C(\theta_2), \dots, C(\theta_p)], D_{ave} = \frac{1}{p} \sum_{i=1}^p D(\theta_i) \quad (4.3.3)$$

$$G_{ave}(s) = C_{ave} (sI - A_{ave})^{-1} B_{ave} + D_{ave} \quad (\text{Average Model}) \quad (4.3.4)$$

The order of  $G_{ave}(s)$  is 'np', where 'n' is the number of states in each model. Since the average system order can be quite large, the chosen nominal model will be  $G_i(s)$  developed in the preceding section.

To address the stability robustness issue, the nominal compensator will be used with the actual feedback loop, where the elbow joint angle  $\theta$  is changing with time as shown in Figure 4.3.2.

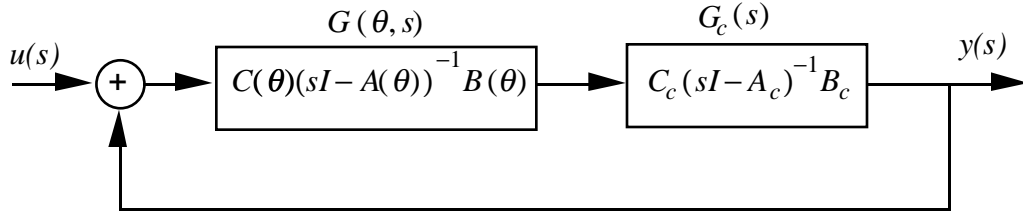


Figure 4.3.2 Fixed Robust Compensator with Large Plant Variations

### Structured and Unstructured Uncertainty

Since the late seventies, the words *structured uncertainty* and *unstructured uncertainty* have been used to distinguish between two types of plant uncertainty and model errors. A brief overview of these two types of uncertainties is given below.

Plant *structured uncertainty* refers to model errors caused by the assumption that the *actual plant* is linear, time-invariant and with the same order as the nominal plant model, except that the numerical values of the matrices that define the state space representation are different. Additional information may be available with respect to the

range of the numerical values. Such structured uncertainty gives rise to model errors that leave the number of poles and zeroes invariant, but they influence the location of the actual poles and zeroes (and their directions) as compared to the nominal values.

*Unstructured uncertainty* is quite different. Assume that the actual plant is still linear and time-variant. However, plead total ignorance regarding the order of the plant and its phase characteristics. In particular, the key assumption of unstructured uncertainty is that model errors are characterized by  $\pm 180^\circ$  phase uncertainty. Such complete phase uncertainty due to modeling errors, can “flip” the sign of the nominal feedback loop(s) and perhaps lead to instability.

Modeling errors due to unstructured uncertainty cannot be captured by a finite dimensional state space model. Thus one can adopt an input-output model and use frequency domain methods to “bound” the size of the model error.

The design philosophy for meeting the stability-robustness specification hinges on the assumption that the maximum bound for all elbow joint angles, or plant perturbation, is known. The maximum bound satisfies the following equation:

$$E_a(j\omega) = \max_{i=1..p} (G(\theta_i, j\omega) - G_n(j\omega)) \quad \forall \theta \in [0^\circ, 90^\circ] \quad (4.3.5)$$

Using the phase information from the additive uncertainty vector  $E_a(j\omega)$  enables the use of structured uncertainty stability robustness properties, which are less conservative than unstructured uncertainty. In unstructured uncertainty the phase would have been completely arbitrary.

With the definition above,  $E_a(j\omega)$  reflects the largest variation between any of the ‘p’ plant models and the design model  $G_n(j\omega)$ .

The control block diagram representing the additive model error is shown below.

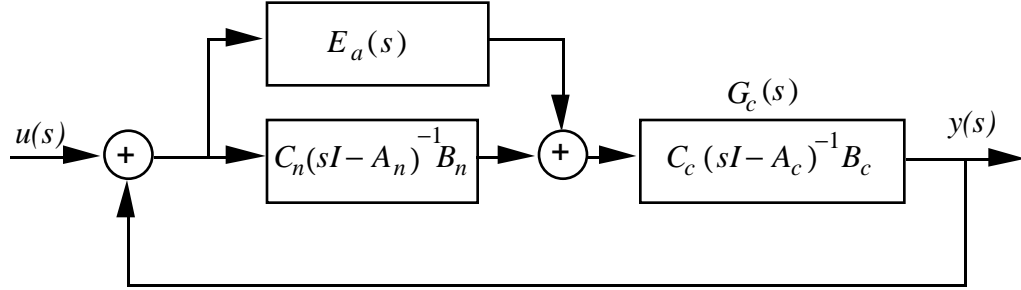


Figure 4.3.3 Additive Model Errors

### Return Difference Transfer Function Matrix

Since frequency-domain representation are used, and the concern is about stability, one must be sure that the transfer functions do not hide any right-half plane pole-zero cancellations, thus the standing assumption is made that  $G_c(s)G_n(s)$  does not have any right half plane pole-zero cancellations. Define the loop transfer function matrix  $T_n(s)$  by  $T_n(s) = G_c(s)[G_n(s) + E_a(s)]$ . The following relationship holds for the system of Figure 4.3.3.

$$y(s) = C(s)u(s) \quad (4.3.6)$$

where  $C(s)$  is the closed-loop transfer matrix given by

$$C(s) = T_n(s)(I + T_n(s))^{-1} = (I + T_n(s))^{-1}T_n(s) \quad (4.3.7)$$

and  $I + T(s)$  is the *return difference* transfer function matrix. The magnitude of the return difference matrix  $|I + T_n(j\omega)|$  represents the distance of the nominal Nyquist

locus,  $T_n(j\omega)$ , to the “critical point”, -1. The basic idea of the stability-robustness tests relies on the following interpretation: If at each frequency, the “size” of the modeling error  $E_a(j\omega)$  is less than  $|I + T_n(j\omega)|$ , then the number of encirclements cannot change and closed-loop stability is retained. More specifically, if

$$\bar{\sigma}(L^{-1} - I) < \underline{\sigma}[I + G_c(j\omega)G_n(j\omega) + G_c(j\omega)E_a(j\omega)], \quad \forall \omega \in [0, \infty] \quad (4.3.8)$$

where

$$L = \text{Diag}[k_n e^{j\phi_n}] \quad (4.3.9)$$

then the actual feedback loop is closed-loop stable. Thus the stability-robustness test is a *sufficient* condition for the stability of the feedback system in the presence of the structured modeling errors.

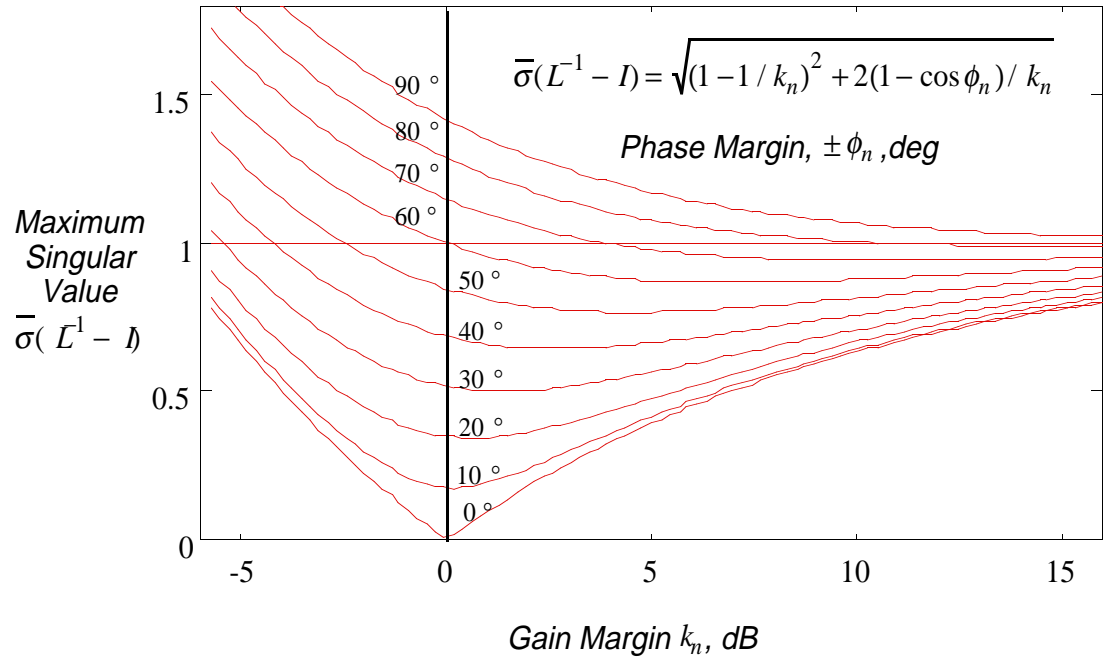


Figure 4.3.4 Universal Diagram for Gain-Phase Margin Evaluation

Equation 4.3.8 can be visualized by examining the diagram for gain-phase margin evaluation. Figure 4.3.4 can be used to determine the gain margins for a particular

phase margin for simultaneous changes of both gain and phase in all input channels (Mukhopadhyay, 1982).

#### 4.4 Gain Scheduled Compensator

The nominal arm configuration is now perturbed about the nominal “*set point*”. By allowing the controller gain vector  $C_c$  to be a free parameter, the quadratic performance cost function is evaluated over the surface of the gain space. The minimum of this surface is found. This process is continued for various arm configurations. Once the ‘optimal’ gains and the respective surfaces are known, questions such as, “are the ‘optimal’ gains simply connected?” can be explored. If such gains are simply connected, an ‘optimal’ polynomial expression of the gain versus the robot joint angle could be derived using optimization approaches. If the gains are not simply connected, a look-up table will be used to adjust the output gain vector.

By adjusting the elbow joint angle, the system matrices are a function of  $\theta$ . The new state estimator is now a dynamic compensator which will remain fixed. The compensator state gain  $C_c$  will vary with the parameter  $\theta$  to minimize some performance function. The gain scheduled compensator is shown in Figure 4.4.1

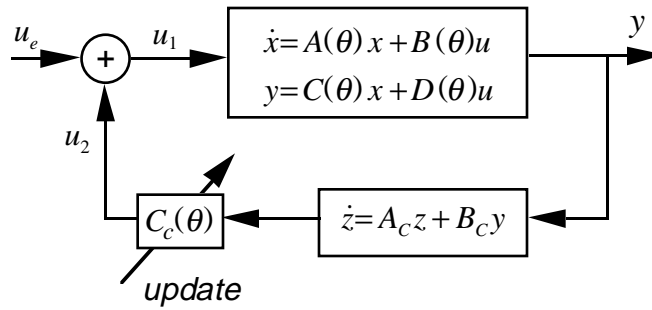


Figure 4.4.1 Gain Scheduled Compensator

The plant dynamic equations for the time varying system is  $u_e = 0$ , and  $u = u_1 = u_2$ :

$$\begin{aligned}\dot{x} &= A(\theta)x + B(\theta)u \\ y &= C(\theta)x + D(\theta)u\end{aligned}\tag{4.4.1}$$

The state compensator feedback gain will be allowed to change with  $\theta$ .

$$\begin{aligned}\dot{z} &= A_c z + B_c y \\ u &= C_c(\theta)z\end{aligned}\tag{4.4.2}$$

The state equations for zero exogenous inputs are:

$$\begin{aligned}\dot{x} &= A(\theta)x + B(\theta)C_c(\theta)z \\ \dot{z} &= (A_c C(\theta) + B_c D(\theta)C_c(\theta))z + B_c C(\theta)x \\ y &= C(\theta)x + D(\theta)u \\ &= C(\theta)x + D(\theta)C_c(\theta)z\end{aligned}\tag{4.4.3}$$

Written in block matrix form:

$$\begin{aligned}\begin{bmatrix} \dot{x} \\ \dot{z} \end{bmatrix} &= \begin{bmatrix} A(\theta) & B(\theta)C_c(\theta) \\ B_c C(\theta) & A_c + B_c D(\theta)C_c(\theta) \end{bmatrix} \begin{bmatrix} x \\ z \end{bmatrix} \\ \begin{bmatrix} y \\ u \end{bmatrix} &= \begin{bmatrix} C(\theta) & D(\theta)C_c(\theta) \\ 0 & C_c(\theta) \end{bmatrix} \begin{bmatrix} x \\ z \end{bmatrix}\end{aligned}\tag{4.4.4}$$

The Linear Quadratic Regulator (LQR) cost function is given by

$$J = \int_0^{\infty} [y^T Q y + u^T R u] dt\tag{4.4.5}$$

inserting

$$\begin{aligned}u^T &= z^T C_c(\theta)^T \\ y^T &= x^T C(\theta)^T + z^T C_c(\theta)^T D(\theta)^T\end{aligned}\tag{4.4.6}$$

into (4.4.5), yields:

$$J = \int_0^{\infty} \left[ \begin{bmatrix} x^T C(\theta)^T + z^T C_c(\theta)^T D(\theta)^T \\ + z^T C_c(\theta)^T R C_c(\theta) z \end{bmatrix} Q \begin{bmatrix} C(\theta)x + D(\theta)C_c(\theta)z \end{bmatrix} \right] dt\tag{4.4.7}$$

rewriting,

$$J = \int_0^{\infty} \begin{bmatrix} x^T C(\theta)^T Q C(\theta) x + x^T C(\theta)^T Q D(\theta) C_c(\theta) z \\ + z^T C_c(\theta)^T D(\theta)^T Q C(\theta) x + z^T C_c(\theta)^T D(\theta)^T Q D(\theta) C_c(\theta) z \\ + z^T C_c(\theta)^T R C_c(\theta) z \end{bmatrix} dt \quad (4.4.8)$$

Which can be written in matrix block form

$$J = \int_0^{\infty} \begin{bmatrix} x^T & z^T \end{bmatrix} \begin{bmatrix} C(\theta)^T Q C(\theta) & C(\theta)^T Q D(\theta) C_c(\theta) \\ C_c(\theta)^T D(\theta)^T Q C(\theta) & C_c(\theta)^T (D(\theta)^T Q D(\theta) + R) C_c(\theta) \end{bmatrix} \begin{bmatrix} x \\ z \end{bmatrix} dt \quad (4.4.9)$$

Let  $\bar{x}$  be an augmented vector of the plant state and compensator state

$$\bar{x} = \begin{bmatrix} x \\ z \end{bmatrix} \quad (4.4.10)$$

Then the cost can be rewritten as

$$J = \int_0^{\infty} \bar{x}^T \bar{Q}(\theta) \bar{x} dt \quad (4.4.11)$$

where

$$\bar{Q}(\theta) = \begin{bmatrix} C(\theta)^T Q C(\theta) & C(\theta)^T Q D(\theta) C_c(\theta) \\ C_c(\theta)^T D(\theta)^T Q C(\theta) & C_c(\theta)^T (D(\theta)^T Q D(\theta) + R) C_c(\theta) \end{bmatrix} \quad (4.4.12)$$

and the augmented state vector satisfies the equation

$$\dot{\bar{x}} = \bar{A}(\theta) \bar{x} \quad (4.4.13)$$

where

$$\bar{A}(\theta) = \begin{bmatrix} A(\theta) & B(\theta) C_c(\theta) \\ B_c C(\theta) & A_c + B_c D(\theta) C_c(\theta) \end{bmatrix} \quad (4.4.14)$$

If  $\bar{A}(\theta)$  is stable, there exist a symmetric positive definite matrix  $P$  which satisfies the Lyapunov equation:

$$\bar{A}(\theta)^T \bar{P}(\theta) + \bar{P}(\theta) \bar{A}(\theta) + \bar{Q}(\theta) = 0 \quad (4.4.15)$$

The cost can be rewritten as

$$J = - \int_0^{\infty} \bar{x}^T (\bar{A}(\theta)^T \bar{P}(\theta) + \bar{P}(\theta) \bar{A}(\theta)) \bar{x} dt \quad (4.4.16)$$

but

$$\frac{d}{dt} [\bar{x}^T \bar{P}(\theta) \bar{x}] = \dot{\bar{x}}^T \bar{P}(\theta) \bar{x} + \bar{x}^T \bar{P}(\theta) \dot{\bar{x}} \quad (4.4.17)$$

using

$$\dot{\bar{x}} = \bar{A}(\theta) \bar{x} \quad (4.4.18)$$

yields

$$\frac{d}{dt} [\bar{x}^T \bar{P}(\theta) \bar{x}] = \bar{x}^T (\bar{A}(\theta)^T \bar{P}(\theta) + \bar{P}(\theta) \bar{A}(\theta)) \bar{x} \quad (4.4.19)$$

The cost is rewritten using (4.4.19) and (4.4.16)

$$\begin{aligned} J &= - \int_0^{\infty} \frac{d}{dt} [\bar{x}^T \bar{P}(\theta) \bar{x}] dt \\ &= - [\bar{x}^T \bar{P}(\theta) \bar{x}]_0^{\infty} \\ &= -(\bar{x}_{\infty}^T \bar{P}(\theta) \bar{x}_{\infty} - \bar{x}_0^T \bar{P}(\theta) \bar{x}_0) \end{aligned} \quad (4.4.20)$$

If  $\bar{A}(\theta)$  is stable then  $\bar{x}_{\infty} = 0$ , and the cost is

$$J = \bar{x}_0^T \bar{P}(\theta) \bar{x}_0 \quad (4.4.21)$$

The objective of the gain schedule control law is to find  $J_*$  such that

$$J_* = \min_{C_c(\theta)} J \quad (4.4.22)$$

This minimum cost can be easily determined for each value of  $\theta$ . By plotting  $J$  as a function of  $C_{c1}(\theta)$  and  $C_{c2}(\theta)$  and minimizing the variance of the error between  $J$  and a polynomial function of  $\theta$ , a polynomial for the optimum gain scheduled control law can be found. In terms of real time control this analysis could be performed off line to reduce real time computational burden of the onboard computers. This gain scheduled compensator or the following adaptive frequency domain compensator were not further developed in this thesis due to the computational burden of the method. However an interesting adaptive control scheme will result if sufficient onboard computation is available.

### **Adaptive Frequency Domain Compensator**

A new adaptive control design method which does not require:

- The plant Strictly Positive Real (SPR) property;
- An adaptive realization of the plant;
- The design of a performance (or reference) model;

is described in this section. This MIMO design method updates the compensator gains directly based on new information gained from a measurement of Frequency Response Function (FRF) from available sensor data. Using gradient based optimization techniques, this method updates the compensator gains based on performance and stability objectives when the plant is slowly time varying or if the plant has pole, zero, or influence coefficient uncertainties or perturbations which are represented in the error bars of a multiple FRF measurement. The performance objective is based on a linear combination of a frequency weighted Linear Quadratic Regulator (LQR), combined

with a stability criterion derived from the minimum singular value of the return difference matrix.

The Frequency domain Performance/Stability optimization for adaptive control method is similar to a digital Robust Control Law Synthesis using constrained optimization (Mukhopadhyay, 1989). With Mukhopadhyay's method, a linear quadratic Gaussian cost function is minimized by updating the free parameters of the control law, while satisfying a set of constraints on the design loads, responses, and stability margins. Analytical expressions for gradients of the cost function and the constraints, with respect to the digital control law design variables, are used to facilitate numerical convergence. One difficulty with this technique is that the steady-state mean square responses are computed by solving the steady-state condition of the discrete Lyapunov function. Thus this Lyapunov function cannot be solved if the closed loop system is unstable. The algorithm in its present form would fail to attenuate appropriate loop gains when a new plant realization renders an unstable closed loop system. Thus the controller may not adapt to a time varying linear plant. This method also requires knowledge of the expected value of the plant and output discrete covariance matrices. Measurement noise covariance's are easily derived from experimental data, while the plant noise covariance determination is considerably less tractable. The method also requires a realization of the plant system matrices.

The frequency domain performance/stability optimization method proposed herein does not require the solution of the steady-state condition of the discrete Lyapunov function. Hence the optimization space may resolve unstable closed loop systems by attenuation of the respective loops while minimizing the performance indices. The MIMO FRF plots are also a more accurate indicator of the plant response than are realizations from the FRF. A distinctive property of this method is that no plant realization is required

for the update of control parameters. The method is applicable to non-minimum phase systems as well as when plant dimension is of larger order than the controller.

A nominal compensator is first designed as discussed in Section 4.2. While the system is under control, a closed loop Frequency Response Function (FRF)  $G_{cl}^*(j\omega)$  can be determined. It can also be derived from open loop data with knowledge of the nominal compensator  $K(j\omega)$  by using (4.4.23).

$$G_{cl}^*(\theta, j\omega) = (1 + G_{op}(\theta, j\omega)K(\theta, j\omega))^{-1} G_{op}(\theta, j\omega) \quad (4.4.23)$$

where

$$K(\theta, j\omega) = C_c(\theta, j\omega)(j\omega I - A_c)^{-1} B_c \quad (4.4.24)$$

Notice the compensator  $A_c$  and  $B_c$  matrices are constant. The FRF of the control input  $u_{cl}(j\omega)$  is also available. However, it is important to note that since these equations are in the frequency domain, the input used during the data gathering experiment is periodic. In addition, one has to assume that aliasing is appropriately handled. The two FRF's can be used to determine the cost of the closed loop system with a known nominal compensator  $K(\theta, j\omega)$ . This closed loop cost is thus determined using open or closed loop data.

$$J(\theta) = \int_{-\infty}^{\infty} tr \left[ G_{cl}^{*T}(\theta, j\omega) Q G_{cl}^*(\theta, j\omega) + u_{cl}^T(\theta, j\omega) R u_{cl}(\theta, j\omega) \right] d\omega \quad (4.4.25)$$

Since an observer is not utilized in the controller, the compensator represents a generalized dynamic feedback controller. By allowing only the gain matrix  $C_c(\theta, j\omega)$  to change, the cost is minimized using open or closed loop data. If this were an observer/controller system there would be one global minimizing controller which would simultaneously guarantee the well known LQR robustness properties.

However, minimizing the above integral does not guarantee robust closed loop system behavior. Thus while minimizing the above integral, an additional cost or constraint, which reflects the stability of the return difference matrix is added.

$$J(\theta) = \int_{-\infty}^{\infty} \text{tr} \left[ G_{cl}^{*T}(\theta, j\omega) Q G_{cl}^*(\theta, j\omega) + u_{cl}^T(\theta, j\omega) R u_{cl}(\theta, j\omega) \right] d\omega \quad (4.4.26)$$

$$+ k_s f \left( \underline{\sigma} \left[ I + K(\theta, j\omega) G_{op}(\theta, j\omega) \right], \eta \right)$$

where  $k_s \equiv$  gain of stability cost and

$$f(\cdot) \equiv \begin{cases} \eta - \underline{\sigma} \left[ I + K(\theta, j\omega) G_{op}(\theta, j\omega) \right] & \text{when } \underline{\sigma}(\cdot) \leq \eta \\ 0 & \text{when } \underline{\sigma}(\cdot) > \eta \end{cases} \quad (4.4.27)$$

and  $\underline{\sigma}$  is the minimum experimental singular value. Assuming the closed-loop system is stable, the robustness of the nominal system at the plant input can be examined by computing  $\underline{\sigma} \left[ I + K(\theta, j\omega) G_{op}(\theta, j\omega) \right]$  as a function of frequency ( $s = j\omega$ ) and using the guaranteed stability criterion

$$\bar{\sigma}(L^{-1} - I) < \underline{\sigma} \left[ I + K(\theta, j\omega) G_{op}(\theta, j\omega) \right] \quad (4.4.28)$$

at all frequencies. The matrix  $L$  is a diagonal gain and phase change matrix at the input of the plant as shown in Figure 4.4.2, and  $\bar{\sigma}$  is the maximum singular value.

$$L = \text{Diag} \left[ k_n e^{j\phi_n} \right] \quad (4.4.29)$$

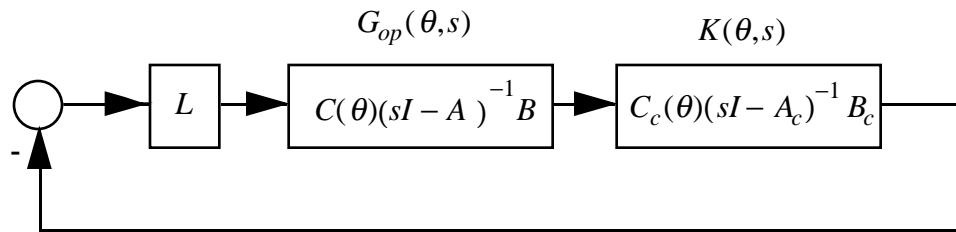


Figure 4.4.2 Diagonal Gain and Phase Change Matrix at Plant Input

The value of  $\eta$  is chosen based on desired gain and phase perturbation robustness properties. The matrix  $L$  is the identity matrix for the nominal system and it can be shown that

$$\overline{\sigma}(L^{-1} - I) = \sqrt{(1 - 1/k_n)^2 + 2(1 - \cos \phi_n)/k_n} \quad (4.4.30)$$

Equation (4.4.30) is plotted in Figure 4.3.4 (Newsom, 1983). By examining the universal diagram for gain-phase margin, the designer chooses the desired stability properties and the corresponding value of  $\eta$ . This figure can be used to determine the gain margins for a particular phase margin for simultaneous changes of both gain and phase in all input channels (Mukhopadhyay, 1982). For example, if a simultaneous gain and phase perturbation robustness of (-3,6) dB and  $\pm 20^\circ$  phase margin were desired, then a value of  $\eta = 0.4$  would be utilized. Since the minimum singular value is determined directly from test data as opposed to realizations of the data, it is a very accurate indicator of the actual gain and phase margins which exist in the loop.

#### 4.5 Spline Varying Optimal (SVO) Compensator

The plant dynamic equations for the time varying system is

$$\begin{aligned} \dot{x} &= A(\theta)x + B(\theta)u \\ y &= C(\theta)x + D(\theta)u \end{aligned} \quad (4.5.1)$$

The equivalent plant dynamics can be described by an  $N$ -th order transfer function

$$G(s) = \frac{\beta_1(\theta)s^{n-1} + \beta_2(\theta)s^{n-2} + \dots + \beta_n(\theta)}{s^n + \alpha_1(\theta)s^{n-1} + \dots + \alpha_n(\theta)} \quad (4.5.2)$$

by using the change of state matrix

$$T_{ob} = \begin{bmatrix} C \\ CA \\ \vdots \\ CA^{n-1} \end{bmatrix}^{-1} \quad (4.5.3)$$

where the new state variable and state matrices are given by  $\hat{x}_{ob} = T_{ob}^{-1}x$ ,  
 $\hat{A}_{ob} = T_{ob}^{-1}AT_{ob}$ ,  $\hat{B}_{ob} = T_{ob}^{-1}B$ ,  $\hat{C}_{ob} = CT_{ob}$

The time varying observer can be described in an observable canonical state-space equation by:

$$\begin{aligned} \dot{\hat{x}}_{ob} &= \hat{A}_{ob}(\theta)\hat{x}_{ob} + \hat{B}_{ob}(\theta)u + K_y(\hat{y} - y) \\ \hat{y} &= \hat{C}_{ob}\hat{x}_{ob} + \hat{D}_{ob}(\theta)u \end{aligned} \quad (4.5.4)$$

where the observer state matrix, influence matrix and output matrices are given by

$$\hat{A}_{ob}(\theta) = \begin{bmatrix} 0 & 1 & 0 & \cdots & 0 \\ 0 & 0 & 1 & \cdots & 0 \\ 0 & 0 & 0 & \cdots & \vdots \\ \vdots & \vdots & \vdots & \ddots & 1 \\ -\alpha_n(\theta) & -\alpha_{n-1}(\theta) & -\alpha_{n-2}(\theta) & \cdots & -\alpha_1(\theta) \end{bmatrix} \quad (4.5.5)$$

$$\begin{aligned} \hat{B}_{ob}(\theta) &= \begin{bmatrix} \beta_1(\theta) \\ \beta_2(\theta) - \alpha_1(\theta)\beta_1(\theta) \\ \beta_3(\theta) - \alpha_1(\theta)\beta_1(\theta) - \alpha_2(\theta)\beta_2(\theta) + \alpha_1^2(\theta)\beta_1(\theta) \\ \vdots \end{bmatrix} \\ \hat{C}_{ob} &= [1 \quad 0 \quad \cdots \quad 0] \end{aligned} \quad (4.5.6)$$

The optimal control can be implemented by full-state feedback and is given by

$$u^* = C_c(\theta)\hat{x}(t) \quad (4.5.7)$$

The control gain matrix  $C_c(\theta)$  is given by

$$C_c(\theta) = -R^{-1}\hat{B}_{ob}(\theta)^T P(\theta) \quad (4.5.8)$$

The matrix  $P(\theta) = P(\theta)^T \geq 0$  is computed from the solution of the following algebraic Riccati equation:

$$\hat{A}_{ob}(\theta)^T P(\theta) + P(\theta) \hat{A}_{ob}(\theta) - P(\theta) \hat{B}_{ob}(\theta) R^{-1} \hat{B}_{ob}(\theta)^T P(\theta) + Q = 0 \quad (4.5.9)$$

The SVO compensator block diagram is shown in Figure 4.5.1. An example problem will be shown in Section 4.6 which will demonstrate that the dependence on  $\theta$  is captured by the cubic spline function.

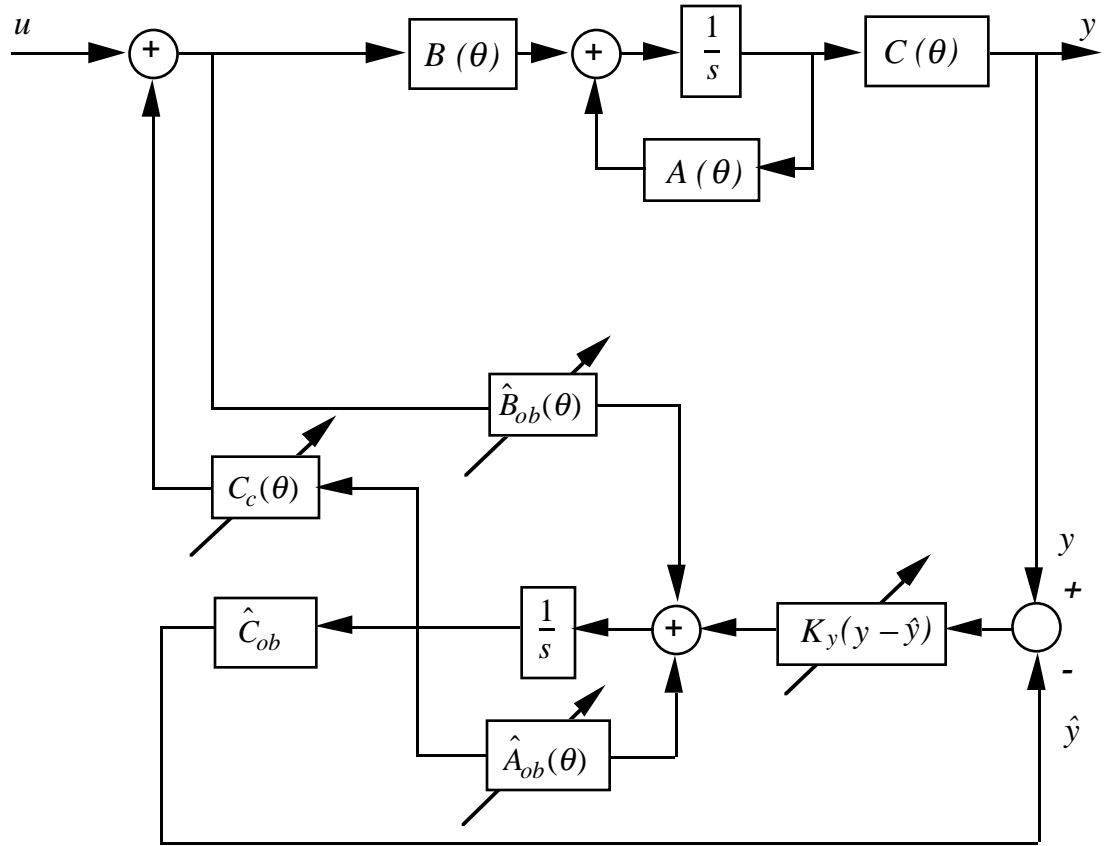


Figure 4.5.1 SVO Compensator Block Diagram

## 4.6 Performance Comparison

This section evaluates the various control law strategies based on a consistent cost function. The compensators are applied to the two link model and the open and closed loop performance for a wide variety of arm orientations are compared. Table 2.3.1 shows the non dimensional parameters used for the two link model. Ten modes were included in the truth model. Table 2.5.1 indicates the open loop eigenvalues as a function of theta. The infinity norm of the Bode response as a function of mode number and theta is shown in Figure 2.6.1.

### Fixed Dynamic Compensator Results

The fixed dynamic compensator design results show that the ‘optimal’ nominal arm orientation for the fixed compensator was at  $\theta_i = 50^\circ$ . Below is the cost as computed in Section 4.2 as a function of theta, where

$$J(\theta_i) = \bar{x}_0^T \bar{P}(\theta_i) \bar{x}_0 \quad (4.6.1)$$

where

$$\bar{Q}(\theta_i) = \begin{bmatrix} C(\theta_i)^T Q C(\theta_i) & C(\theta_i)^T Q D(\theta_i) C_c \\ C_c^T D(\theta_i)^T Q C(\theta_i) & C_c^T (D(\theta_i)^T Q D(\theta_i) + R) C_c \end{bmatrix} \quad (4.6.2)$$

and the augmented state vector satisfies the equation

$$\dot{\bar{x}} = \bar{A}(\theta_i) \bar{x} \quad (4.6.3)$$

where

$$\bar{A}(\theta_i) = \begin{bmatrix} A(\theta_i) & B(\theta_i) C_c \\ B_c C(\theta_i) & A_c + B_c D(\theta_i) C_c \end{bmatrix} \quad (4.6.4)$$

and the symmetric positive definite matrix  $\mathbf{P}$  satisfies the Lyapunov equation:

$$\bar{A}(\theta_i)^T \bar{P}(\theta_i) + \bar{P}(\theta_i) \bar{A}(\theta_i) + \bar{Q}(\theta_i) = 0 \quad (4.6.5)$$

Each initial state in  $\bar{x}_0$  was set equal to one for all performance comparisons. The Output weighting gain was  $Q = 0.1$ , the input weight was  $R = 0.001$ . The process noise and measurement noise covariance's were  $Q_w = 0.1$  and  $R_v = 0.1$  respectively for all performance comparisons. The fixed compensator performed well for most arm orientations (Figure 4.6.1).

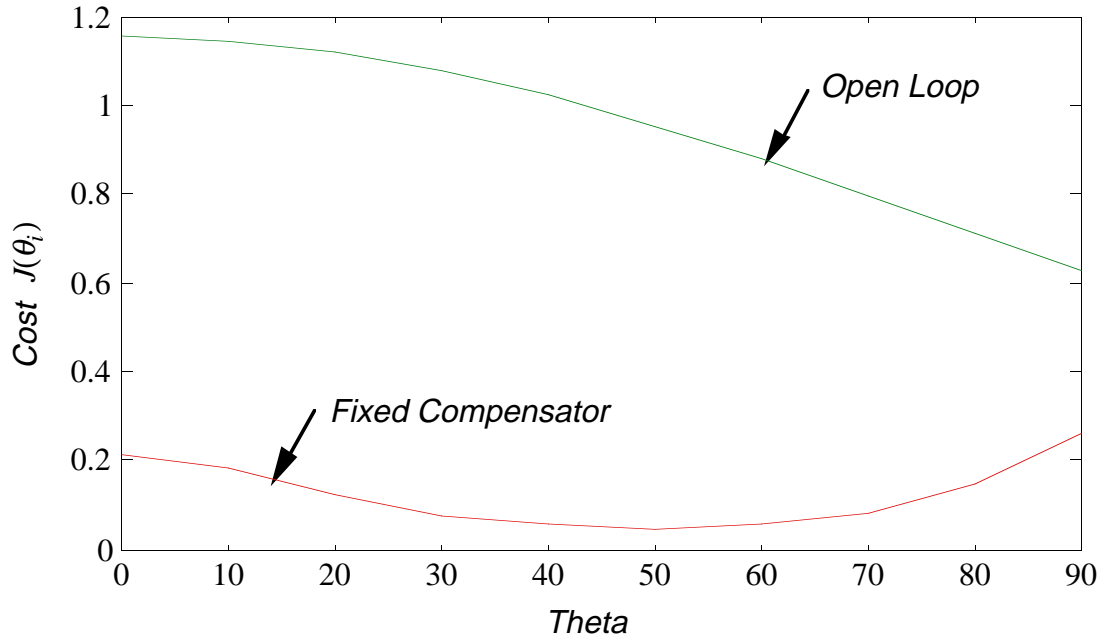


Figure 4.6.1 Open and Closed Loop Cost Comparison as a Function of Theta - Fixed Compensator

Although there were no instabilities induced by the fixed dynamic controller, the gain and phase margins were small. The minimum singular value of the return difference matrix evaluated over the workspace for the fixed controller reached

$$\underline{\sigma}[I + G_c(j\omega)G(\theta_i, j\omega)] = 0.16, \quad \forall \omega \in [0, \infty], \quad \forall \theta \in [0^\circ, 90^\circ] \quad (4.6.6)$$

indicating that there was only a  $10^\circ$  phase margin (See Figure 4.3.4). This low phase margin occurred for the  $\theta = 90^\circ$  arm orientation. The presence of no instabilities

reflects the fact that there is significant modal frequency separation between successive modes, and significant attenuation of the infinity norm of the residual modes.

The total cost is found by calculating the area under the above curves for the fixed dynamic compensator.

$$T_J(G_c = \text{Fixed Compensator}) = \sum_{i=0}^{10} J(\theta_i) = 1.268 \quad (4.6.7)$$

The 10 values in the summation correspond to values of theta in increments of  $10^\circ$  from  $[0^\circ, 90^\circ]$ . For comparison, the open loop total cost is evaluated by setting the fixed compensator to zero. Thus

$$T_J(G_c = 0) = \sum_{i=0}^{10} J(\theta_i) = 9.477 \quad (4.6.8)$$

### **Fixed Robust Dynamic Compensator results**

The fixed robust compensator results show an improved performance over all arm orientations. The mandated stability constraint was a  $40^\circ$  phase margin, or  $\overline{\sigma}(L^{-1} - I) = 0.75$ . Shown in Figure 4.6.2 is the Bode response of the nominal plant model  $G_n(s)$  at  $50^\circ$ .

The maximum bound on the additive model error over the entire workspace was calculated from

$$E_a(j\omega) = \max_{i=1..10} (G(\theta_i, j\omega) - G_n(j\omega)) \quad \forall \theta \in [0^\circ, 90^\circ] \quad (4.6.9)$$

and is shown in the frequency domain in Figure 4.6.3.

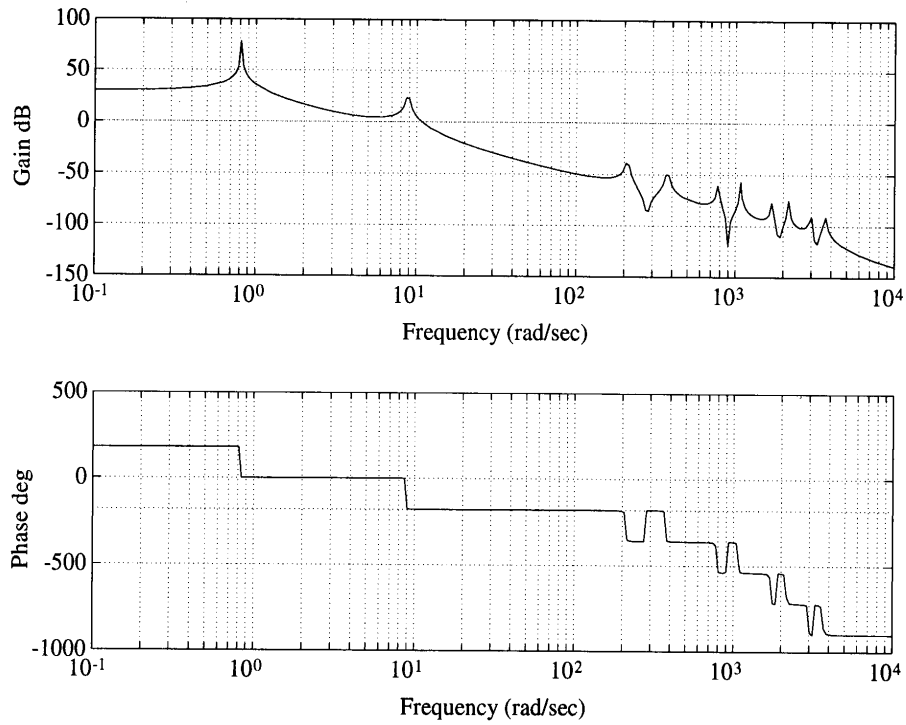


Figure 4.6.2 Bode Response of Nominal Plant Model  $G_n(s)$  at  $50^\circ$ .

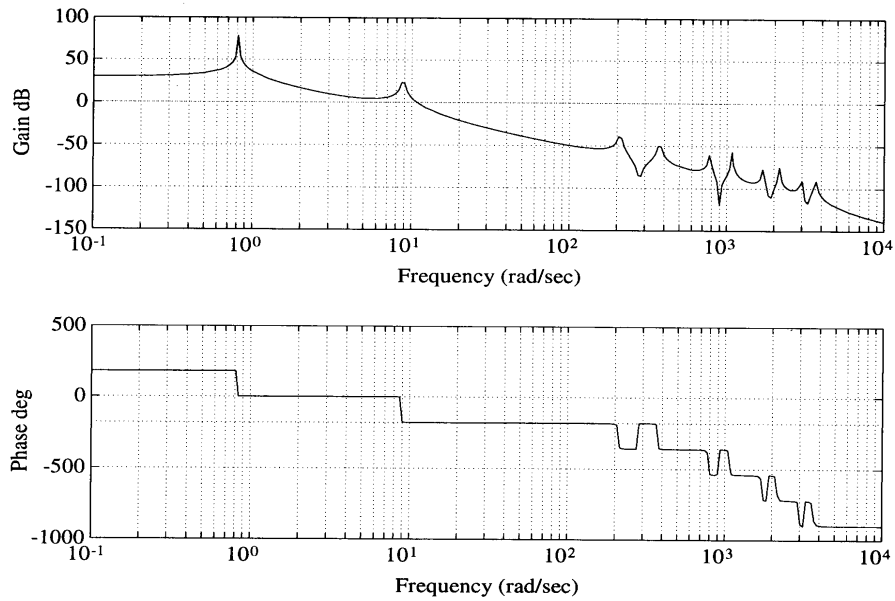


Figure 4.6.3 Maximum Bound on the Additive Model Error  $E_a(j\omega)$

Using the optimization tools in Matlab a constraint of

$$\underline{\sigma}[I + G_c(j\omega)G_n(j\omega) + G_c(j\omega)E_a(j\omega)] \geq 0.75 \quad (4.6.10)$$

was used to modify the *return difference* transfer function. The resultant fixed robust controller performance is depicted in Figure 4.6.4.

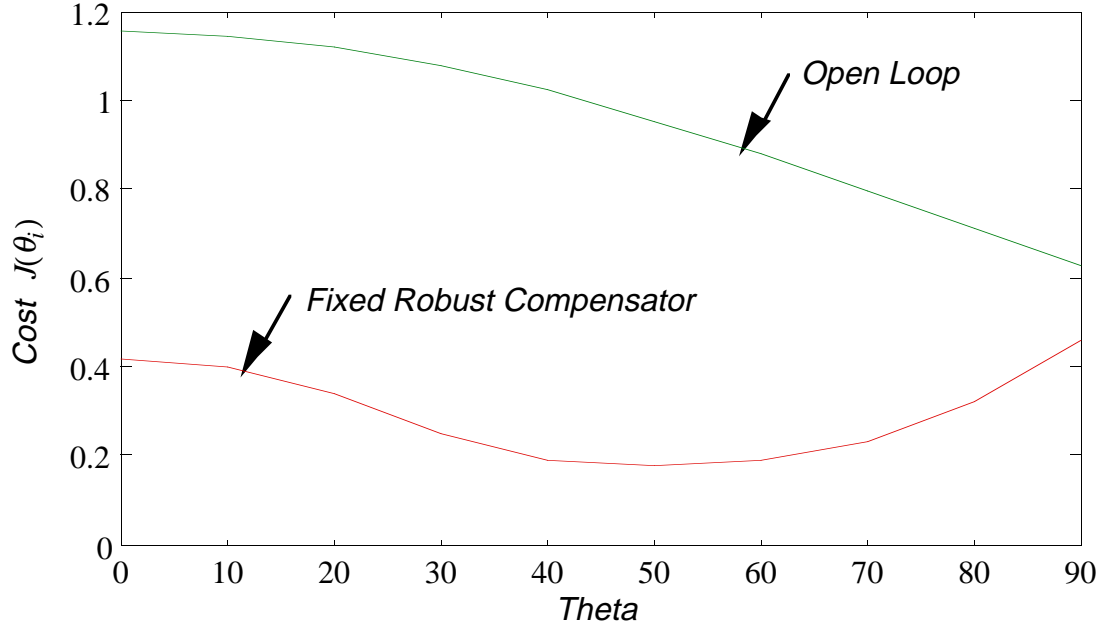


Figure 4.6.4 Open and Closed Loop Cost Comparison as a Function of Theta - Fixed Robust Compensator

$$T_J(G_c = \text{Robust Compensator}) = \sum_{i=0}^{10} J(\theta_i) = 3.022 \quad (4.6.11)$$

### Spline Varying Optimal Compensator Results

The observer  $\hat{A}_{ob}(\theta)$ ,  $\hat{B}_{ob}(\theta)$ ,  $\hat{C}_{ob}$ , and  $C_c(\theta)$  matrices were evaluated as a function of theta. These parameters were used in the observer equations to derive the state space matrices. Figures 4.6.5 and 4.6.6 show the non zero  $\hat{A}_{ob}(\theta)$  coefficients  $\alpha_1(\theta)$  and  $\alpha_2(\theta)$  in the observer dynamic equations.

$$\begin{aligned} \dot{\hat{x}}_{ob} &= \hat{A}_{ob}(\theta)\hat{x}_{ob} + \hat{B}_{ob}(\theta)u + K_y(\theta)(\hat{y} - y) \\ \hat{y} &= \hat{C}_{ob}\hat{x}_{ob} + \hat{D}_{ob}(\theta)u \end{aligned} \quad (4.6.12)$$

where

$$\hat{A}_{ob}(\theta) = \begin{bmatrix} 0 & 1 \\ -\alpha_2(\theta) & -\alpha_1(\theta) \end{bmatrix} \quad (4.6.13)$$

Figures 4.6.7 and 4.6.8 show the  $\hat{B}_{ob}(\theta)$  coefficients  $\beta_1(\theta)$  and  $\beta_2(\theta)$ ., where

$$\hat{B}_{ob}(\theta) = \begin{bmatrix} \beta_1(\theta) \\ \beta_2(\theta) - \alpha_1(\theta)\beta_1(\theta) \end{bmatrix} \quad (4.6.14)$$

Since the observer is the observer canonical form, the non zero elements of the  $\hat{C}_{ob}$  vector is simply one.

$$\hat{C}_{ob} = [1 \quad 0] \quad (4.6.15)$$

Figure 4.6.9 and 4.6.10 show  $C_{c1}(\theta)$  and  $C_{c2}(\theta)$ , which were found by solving the algebraic Riccati equation for each value of theta.

$$C_c(\theta) = -R^{-1}\hat{B}_{ob}(\theta)^T P(\theta) \quad (4.6.16)$$

The matrix  $P(\theta) = P(\theta)^T \geq 0$  is computed from the solution of the following algebraic Riccati equation:

$$\hat{A}_{ob}(\theta)^T P(\theta) + P(\theta)\hat{A}_{ob}(\theta) - P(\theta)\hat{B}_{ob}(\theta)R^{-1}\hat{B}_{ob}(\theta)^T P(\theta) + Q = 0 \quad (4.6.17)$$

The observer gain  $K_{y1}(\theta)$  and  $K_{y2}(\theta)$  were found using the process noise and measurement noise covariance's where  $Q_w = 0.1$  and  $R_v = 0.1$ . Table 4.6.1 shows the numerical Markov parameters and controller and observer gain for 10 successive values of theta starting at  $\theta_2=0$ .

For each graph 4.6.6 through 4.6.12, the observer and optimal gain were plotted as a function of  $\theta_2$ . Each of the curves were then fitted to a third order polynomial.

<p style="text-align: center;"><i>Table 4.6.1</i> SVO Compensator Parameters</p>				
Theta (Degrees)	$\alpha_1(\theta)$	$\alpha_2(\theta)$	$\beta_1(\theta)$	$\beta_2(\theta)$
0	1.6356e-02	0.6688	-8.3579e-06	-2.0611e+01
10	1.6412e-02	0.6734	-8.4277e-06	-2.0787e+01
20	1.6583e-02	0.6875	-8.6416e-06	-2.1328e+01
30	1.6874e-02	0.7118	-9.0135e-06	-2.2273e+01
40	1.7294e-02	0.7477	-9.5688e-06	-2.3690e+01
50	1.7857e-02	0.7972	-1.0347e-05	-2.5694e+01
60	1.8582e-02	0.8633	-1.1406e-05	-2.8459e+01
70	1.9495e-02	0.9501	-1.2829e-05	-3.2253e+01
80	2.0627e-02	1.0637	-1.4728e-05	-3.7486e+01
90	2.2020e-02	1.2122	-1.7240e-05	-4.4799e+01

<p style="text-align: center;"><i>Table 4.6.1 Continued</i> SVO Compensator Parameters</p>				
Theta (Degrees)	$C_{c1}(\theta)$	$C_{c2}(\theta)$	$K_{y1}(\theta)$	$K_{y2}(\theta)$
0	-3.0246e-01	-1.7053e-01	1.4220e+00	5.1111e-01
10	-3.0251e-01	-1.6982e-01	1.4206e+00	5.0900e-01
20	-3.0265e-01	-1.6769e-01	1.4161e+00	5.0267e-01
30	-3.0290e-01	-1.6417e-01	1.4085e+00	4.9200e-01
40	-3.0326e-01	-1.5928e-01	1.3978e+00	4.7686e-01
50	-3.0375e-01	-1.5307e-01	1.3835e+00	4.5709e-01
60	-3.0438e-01	-1.4560e-01	1.3657e+00	4.3256e-01
70	-3.0517e-01	-1.3696e-01	1.3440e+00	4.0321e-01
80	-3.0616e-01	-1.2726e-01	1.3185e+00	3.6920e-01
90	-3.0737e-01	-1.1665e-01	1.2892e+00	3.3102e-01

It should be noted that the third order polynomial is an approximation of the data. The actual optimal gain function will be of a higher order, at least sixth order in theta, although a third order polynomial is a very good approximation. Thus SVO controller

can be implemented easily on a computer in real time. The respective third order polynomial coefficients are shown in each graph.

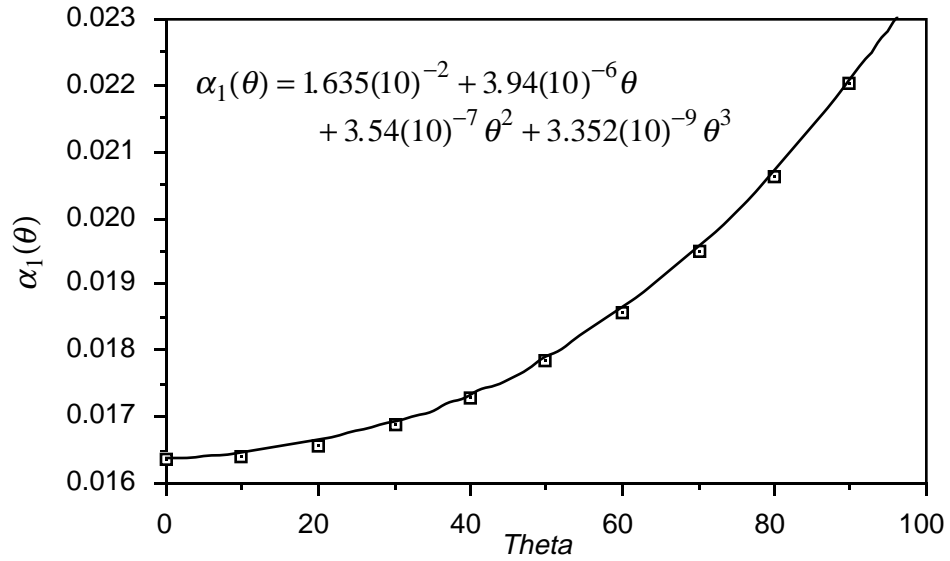


Figure 4.6.5 SVO Compensator Parameter  $\alpha_1(\theta)$

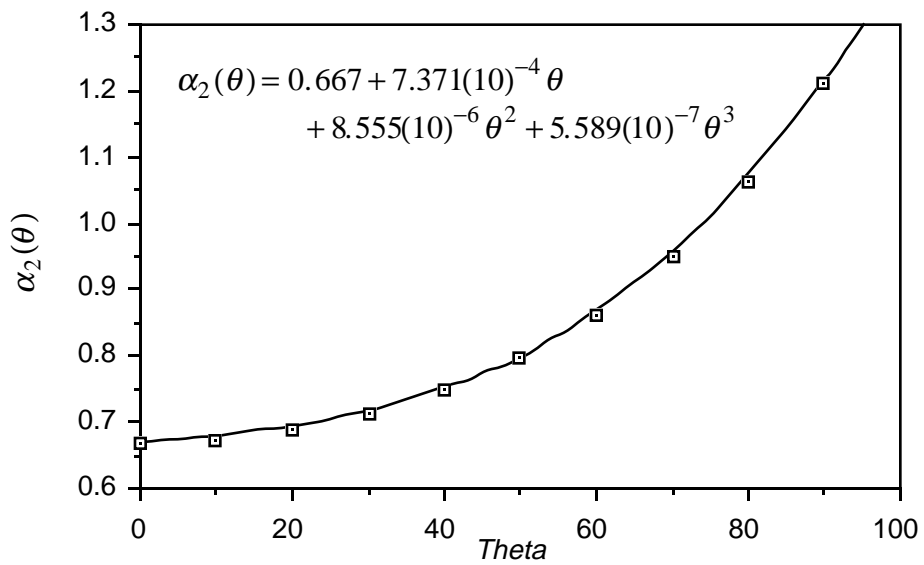


Figure 4.6.6 SVO Compensator Parameter  $\alpha_2(\theta)$

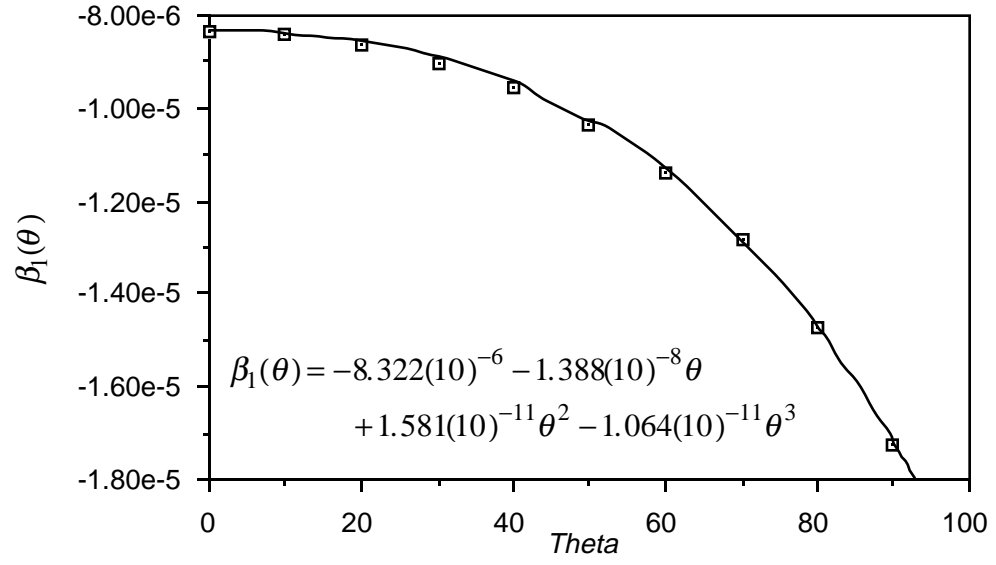


Figure 4.6.7 SVO Compensator Parameter  $\beta_1(\theta)$

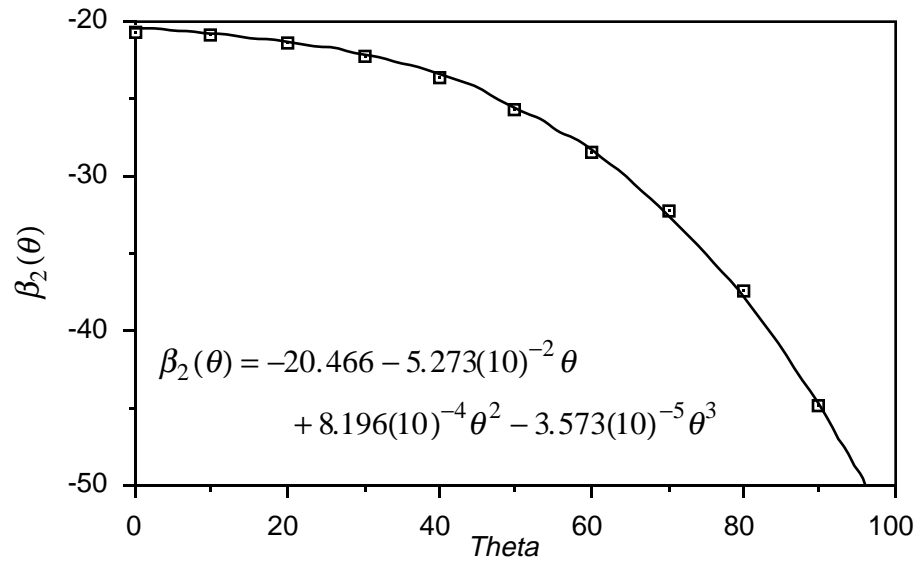


Figure 4.6.8 SVO Compensator Parameter  $\beta_2(\theta)$

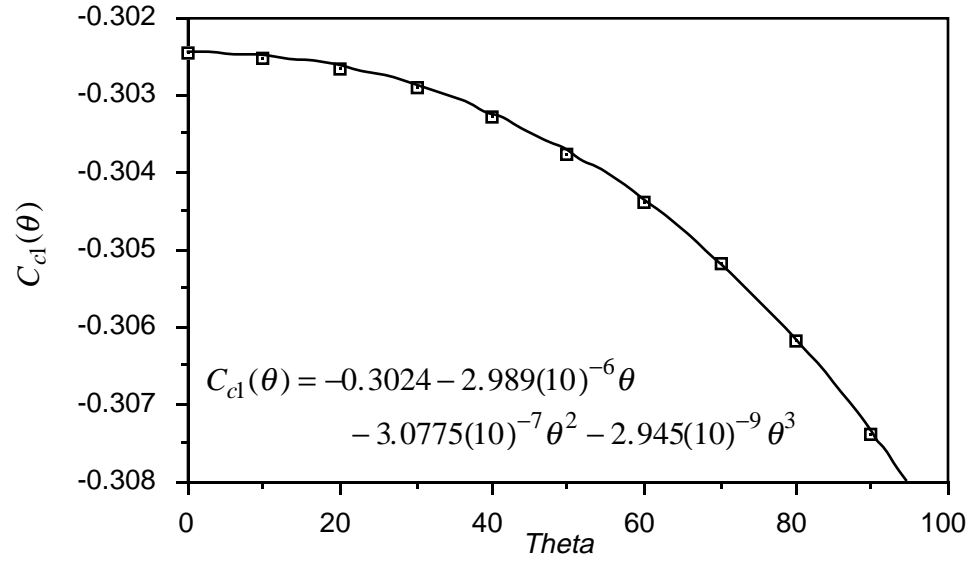


Figure 4.6.9 SVO Compensator Parameter  $C_{c1}(\theta)$

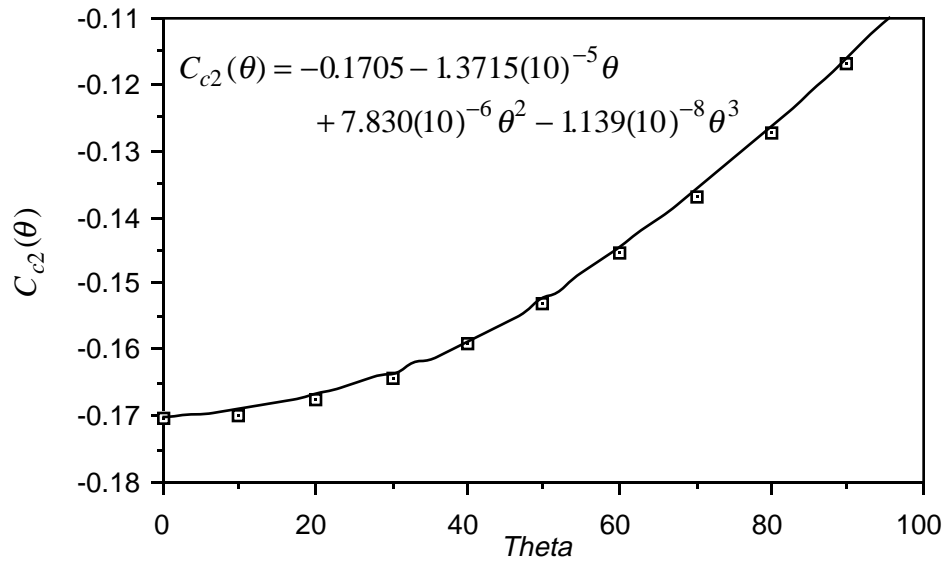


Figure 4.6.10 SVO Compensator Parameter  $C_{c2}(\theta)$

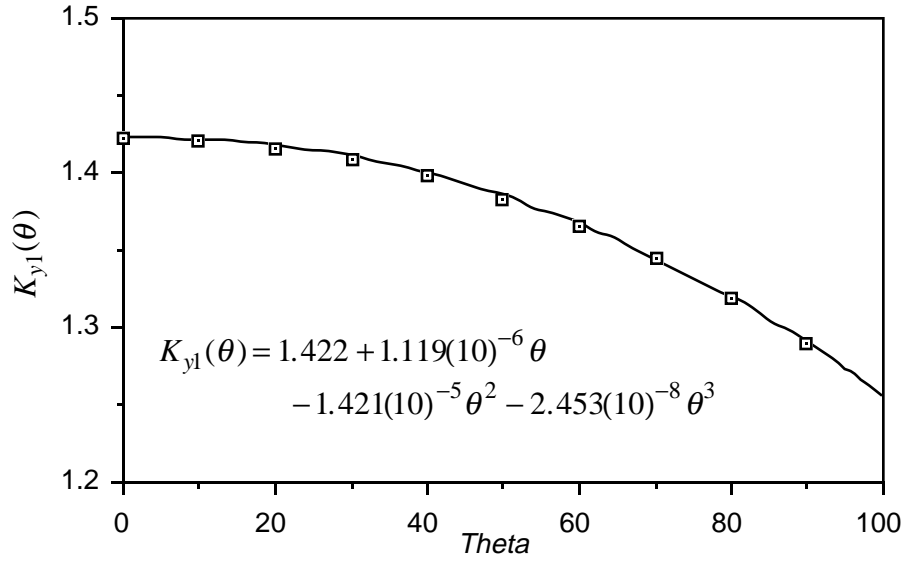


Figure 4.6.11 SVO Compensator Parameter  $K_{y1}(\theta)$

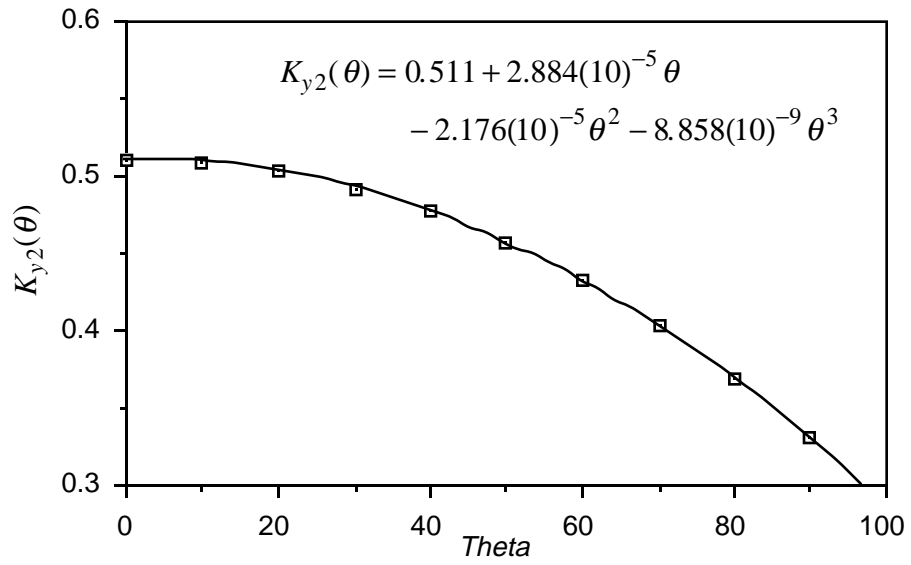


Figure 4.6.12 SVO Compensator Parameter  $K_{y2}(\theta)$

Figure 4.6.13 shows the open and closed loop (SVO) cost versus theta. There is an improvement of 20:1 over the open loop manipulator along the range of motion.

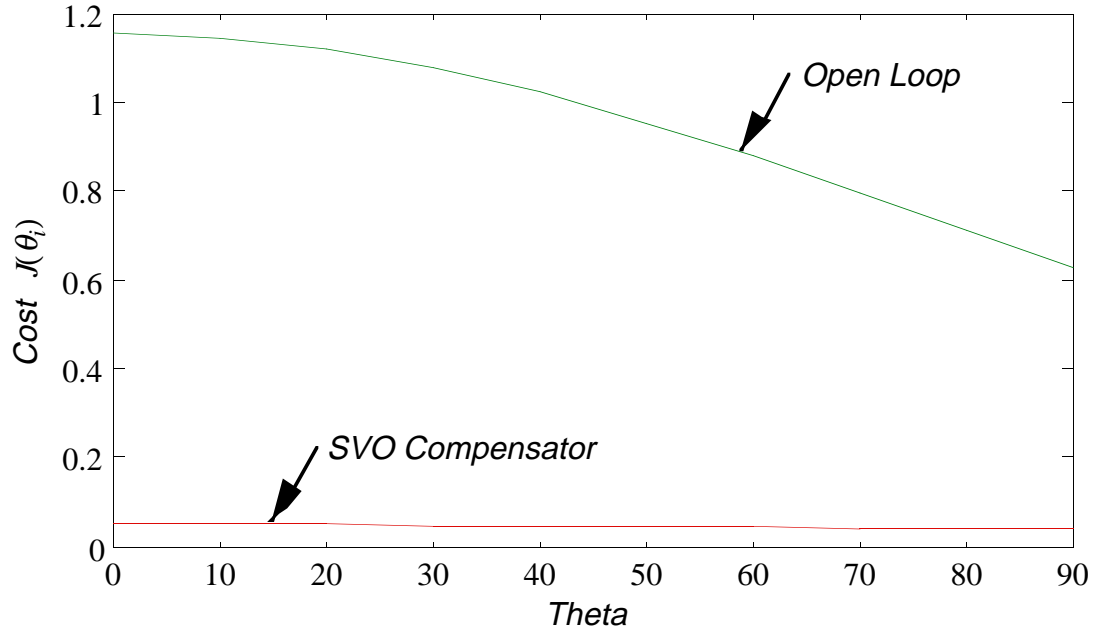


Figure 4.6.13 Open and Closed Loop Cost Comparison as a Function of Theta - SVO Compensator

A cost comparison of the controllers studied above is summarized in Table 4.6.2. All of the compensators improved the open loop performance over the workspace. For comparison purposes, the total cost of the open and closed loop systems is computed by integrating the area under the curves above. These results for the open loop, fixed robust compensator, fixed compensator SVO compensator are plotted in Figure 4.6.14. Figure 4.6.14 indicates the improvement of the SVO controller over the fixed gain and fixed robust controller. It is important to note that the fixed gain controller remains stable over a wide variety of elbow pitch arm angles, although its performance is significantly worse than that of the SVO controller. The overall improvement in performance is 7:1 for the fixed gain compensator, 3:1 for the fixed robust compensator, and 20:1 for the SVO compensator. Although the stability margin for the fixed gain controller was relatively low ( $10^\circ$  phase margin), its performance was about

<p style="text-align: center;"><i>Table 4.6.2</i> Cost Comparisons</p>				
Theta (Degrees)	Open Loop	Closed Loop		
	Cost	Cost Fixed Gain	Cost Fixed Robust	Cost SVO
0	1.153	0.217	0.420	0.0512
10	1.144	0.185	0.401	0.0510
20	1.118	0.128	0.346	0.0505
30	1.077	0.0792	0.253	0.0497
40	1.021	0.0567	0.198	0.0485
50	0.954	0.0471	0.182	0.0471
60	0.878	0.0585	0.194	0.0454
70	0.795	0.0852	0.235	0.0435
80	0.711	0.146	0.326	0.0413
90	0.626	0.265	0.467	0.0391
Total Cost $\sum_{i=0}^{10} J(\theta_i)$	9.477	1.268	3.022	0.467

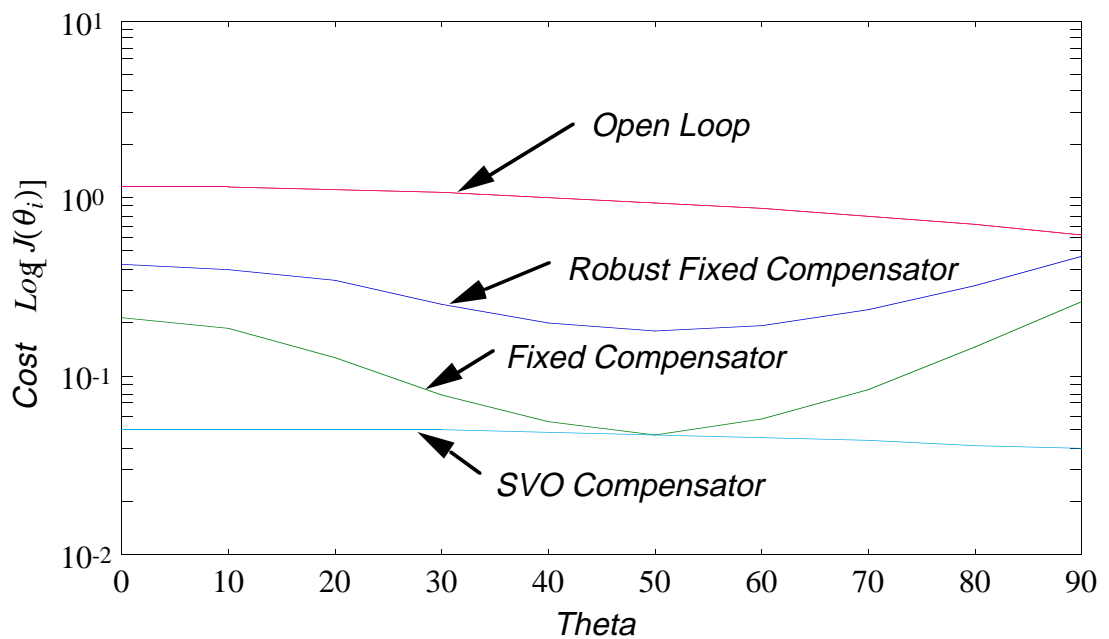


Figure 4.6.14 Open and Closed Loop Cost Comparison as a Function of Theta

two times better than the fixed robust compensator ( $40^\circ$  phase margin). Thus, by increasing the robustness of the closed loop system, the fixed robust compensator sacrificed on performance.

#### **4.7 Summary**

This chapter has developed and compared the theoretical and numerical results for several control strategies of a time varying flexible manipulator. The consistent cost functions for evaluation of the various controllers on the time varying system have been derived. An example problem was used to evaluate the performance of the various controllers for the time varying system. It was determined that a fixed robust controller can remain stable over the workspace limits, although its performance is sacrificed at the expense of stability margins. A novel SVO controller has been developed. There are several advantages of the SVO controller over traditional gain scheduling controllers. The four advantages of using the SVO controller where the spline function approximates the system model, observer, and controller gain are:

- (1) The spline function approximation is simply connected, thus the SVO controller is more continuous than traditional gain scheduled controllers when implemented on a time varying plant.
- (2) The SVO controller is easier for real time implementations in storage and computational effort, when compared to traditional gain scheduled compensators.
- (3) Where system identification is required, the spline function requires fewer experiments. Namely four experiments are required to identify the four

polynomials in each of the non zero elements in the controller (See Chapter 3).

- (4) Startup transients are reduced. When the estimator is determining the state at all times during the maneuver, initial estimator transients can be eliminated.

The SVO controller outperformed the fixed gain and fixed robust controller as determined by the consistent cost function. The SVO controller developed in this section is the first simply connected time varying compensator shown in the literature. As discussed in the previous chapter on system identification, the fundamental mode Markov parameters which are unique, satisfy a third order approximation, or spline function, as a function of the elbow joint angle ( $\theta_2$ ). In this chapter it was shown that in addition to the Markov parameters satisfying the spline function, both the observer gain and the time varying regulator gains satisfy this spline function approximation. The results of this observation allow the myriad of free parameters in a time varying optimal controller to be reduced to a fundamental set of time varying optimal parameters which are simply connected. With the SVO controller there is an improvement of 20:1 over the open loop manipulator dynamics along the range of motion.

## **CHAPTER 5**

### **ACTIVE VIBRATION DAMPING OF THE SPACE SHUTTLE REMOTE MANIPULATOR SYSTEM**

In this chapter the various control strategies described in Chapter 4 are applied to a high fidelity simulation code of the Shuttle Remote Manipulator System (SRMS). The code, which is used routinely for predicting arm dynamic motions for on-orbit RMS operations, was obtained from Charles Stark Draper Laboratory (CSDL) for this purpose. The simulation code includes models of the RMS structural dynamics, joint servos, motors, gearboxes, and the software modules loaded in the Shuttle computers for RMS control (Metzinger, 1988). To demonstrate that the Draper RMS simulation is a valid representation of the flight article, 22 specific maneuvers were performed in flight and reproduced via DRS simulation (Gray, 1985). The comparisons show excellent agreement between DRS and flight data. Various sensor/actuator pairs are evaluated including collocated control with the shoulder and elbow joints. For both joints, feedback of the tachometer measurement initially results in a small increase in RMS damping. However, feedback of the acceleration measurement to drive the shoulder joint show a large increase in damping. Linear models are derived for four arm orientations and are used to derive SVO controller.

The approach to the RMS active damping feasibility study is the following. First, a set of payloads and arm configuration combinations consistent with the types of payloads expected during Space Station Freedom assembly is defined. Second, RMS dynamics and operational characteristics were examined using the nonlinear Draper RMS

Simulator (DRS) code. The determination of active damping augmentation feasibility involved the design and simulation of candidate damping augmentation control laws. For this purpose, system identification methods were employed on output data from the DRS to identify time varying nonlinear models which closely match the DRS response. With the nonlinear control design models, various active control law design concepts described in Chapter 4 were evaluated, as were the requirements for feedback sensors to measure arm motions. The final step was the simulation of the SVO control law in a modified version of the DRS to determine the effects of system kinetic and kinematic nonlinearities and computer time delays.

## **5.1 Shuttle Remote Manipulator System**

Figure 5.1.1 illustrates the elements of the Space Shuttle RMS (JSC, 1988). The system is a six-joint telerobotic arm controlled from a panel located on the aft flight deck of the Space Shuttle. These six joints are directly analogous to the joints and freedom of a human arm, defined as shoulder-yaw and pitch, elbow-pitch, and wrist-pitch, yaw, and roll. An end effector for grappling payloads is mounted at the free end of the arm. From the control panel and translational and rotational hand controllers, commands to move the arm are processed by the Shuttle computers and an interface unit to provide electrical signals to drive the joint servo motors. The actual joint servo commands that are generated depend on the selected operational mode, which can be either direct drive, single joint mode, one of four manual augmented modes, or an automatic control mode. The manual augmented mode is normally used for payload operations on-orbit, although the single joint mode is used for RMS stowing and to avoid joint singularities. Joint angle position and motor shaft rate at each joint are measured by an encoder and tachometer, respectively.

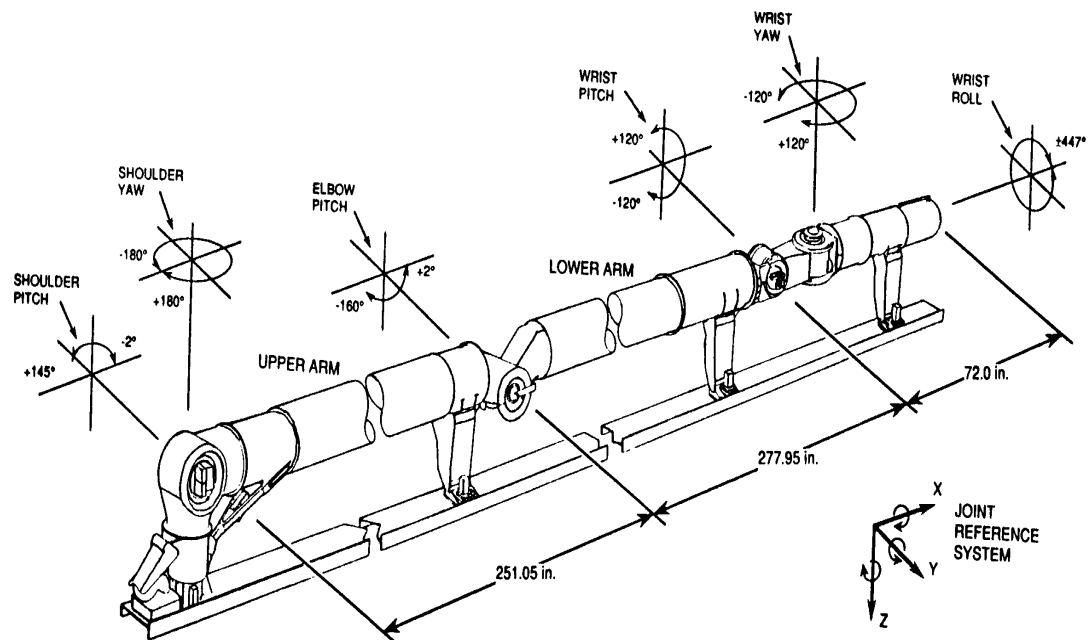


Figure 5.1.1 Space Shuttle Remote Manipulator System (RMS)

### Fixed slew rates mandated by safety operational procedures

In all reconfigurable structures there is an upper bound slew rate demanded by safety operational procedures. This slew rate is best described as a fixed velocity and acceleration rate of the servos driving the structural joints. The velocity constraint manifests itself as a finite rate at which the arm or tip can be positioned. This constraint ensures that the structure can stop within an operational envelope to prohibit a collision.

The fixed acceleration upper limit slew rate ensures that stress loads in the mechanical links do not exceed mandated safety limits. It turns out that the acceleration slew rate,

hereafter referred to as the slew rate, affects the spectrum of the vibratory energy imparted to the electromechanical structure.

Without an upper bound slew rate constraint, a step input imparts energy into the structure in a broad frequency band. With the fixed slew rate constraint, the input has a finite rate at which the servo can accelerate. Table 5.1 indicates the fixed slew rate limits for the SRMS (Ravindran, 1982). These limits were mandated to provide the ability to stop from maximum speed within 0.6 meters under all loading conditions. The fixed slew rate serves to attenuate the high frequency response, especially for heavier payloads.

<p><i>Table 5.1.1</i> Slew Rate Limits of SRMS</p>		
Load	Rate Limits	
	m/Sec	Deg/Sec
Unloaded	0.6	4.76
Loaded (15,000 Kg.)	0.06	0.476
Loaded (30,000 Kg.)	0.03	0.238

Four RMS configurations were adopted for the system identification study. These configurations are shown in Figure 5.1.2 - 5.1.5 with the Shuttle Pallet Satellite (SPAS) free-flyer spacecraft as an attached payload. The SPAS payload was used for the dynamic response studies. Depicted in the plots are the RMS configurations for various values of the elbow joint angle, with the SPAS attached payload used on the STS-07 Shuttle mission.

The time response data shown in Figure 5.1.6 are typical of the kind of RMS motions encountered during normal arm maneuvers, as predicted by the DRS. The plots depict free responses following a 10-second single joint rotation command to the shoulder-yaw joint, with the other joint positions maintained by the RMS position-hold function. Shown are the lateral displacements of the free end of the arm, the shoulder-yaw joint angle encoder response, and the shoulder-yaw joint rate derived from the motor shaft tachometer. After the command to the RMS is removed, the peak-to-peak free oscillation at the tip of the arm is about 5 inches, while the actual measured joint angle change during the same time is on the order of 0.1 degree. The discrete stepping of the encoder response is due to word length limitations in the Shuttle computer, indicating that the signal is at the limit of useful resolution. The yaw joint rate is on the order of 3.0 degrees/second, and again has discrete stepping characteristics which limit the useful resolution of data. These types of responses are an indication that the existing RMS sensors may not be adequate for active damping augmentation purposes. Because of this, the addition of another sensor in the form of a tip mounted accelerometer was considered. The DRS simulation was used to predict the response of an accelerometer package mounted near the SPAS payload. This simulated tip acceleration measurement was used in feedback studies to determine if additional sensor hardware would be beneficial for active damping augmentation of the RMS.

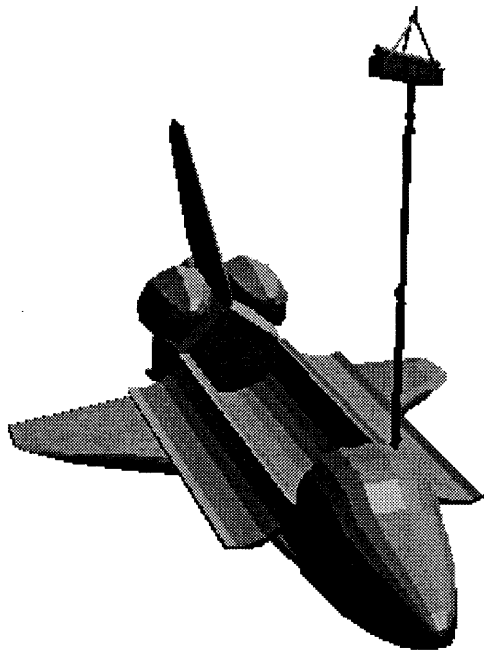


Figure 5.1.2 SRMS Configuration  $\theta = 0^\circ$

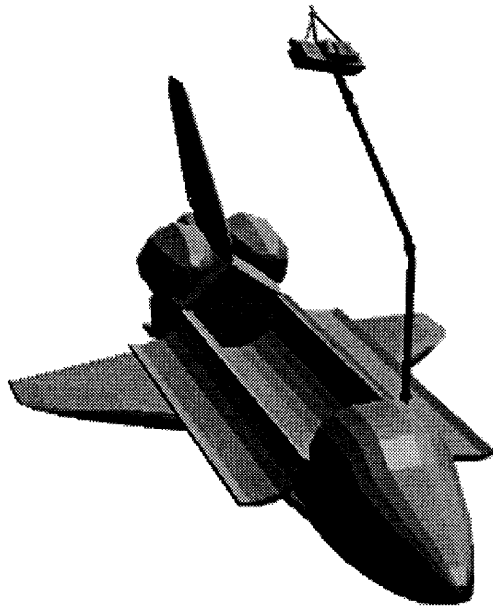


Figure 5.1.3 SRMS Configuration  $\theta = 30^\circ$

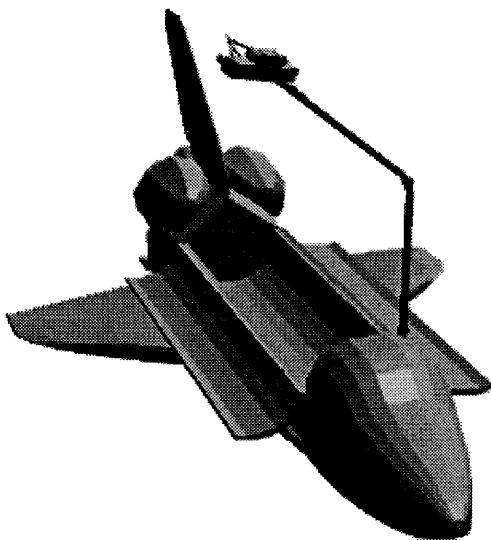


Figure 5.1.4 SRMS Configuration  $\theta = 60^\circ$

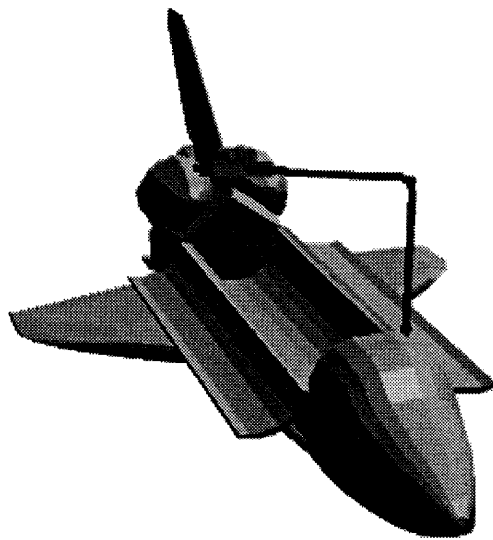


Figure 5.1.5 SRMS Configuration  $\theta = 90^\circ$

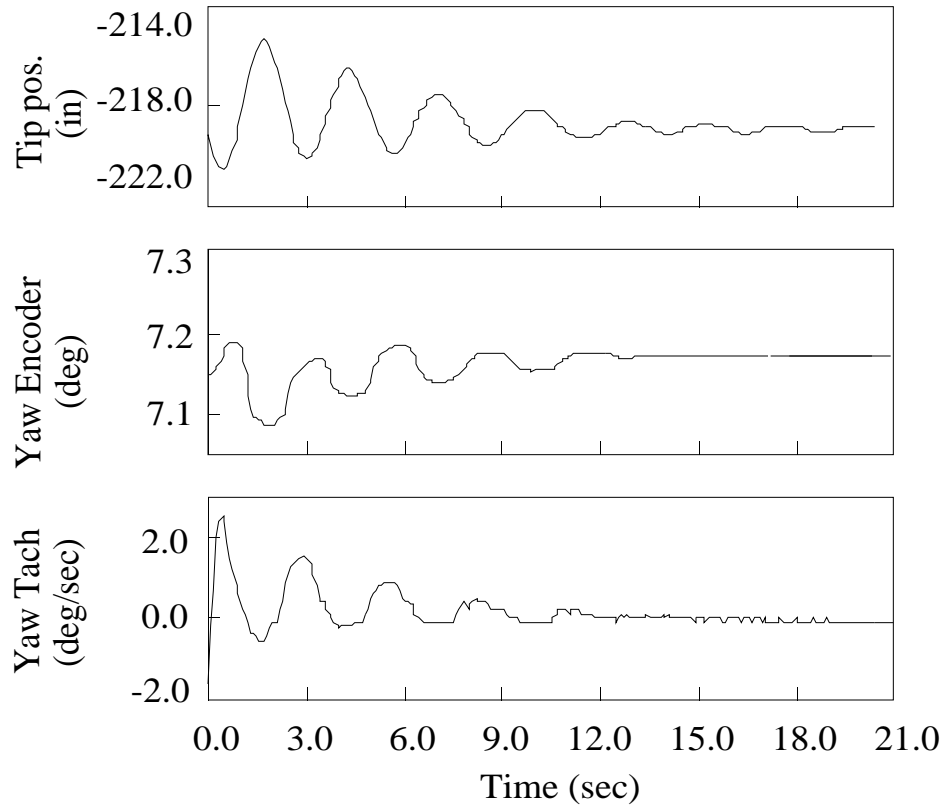


Figure 5.1.6 Typical RMS response and sensor outputs -  $\theta = 30^\circ$ .

### Global Mode Shape Analysis

Knowledge of the global mode shapes of the RMS was important in assessing the feasibility of active damping augmentation of the RMS. Since mode shapes change with arm geometry, the four configurations were studied. Appraisal was made of mode shape observability and controllability from the available sensor and actuator suites. Mode shape information was obtained using an eigenanalysis version of the DRS (Gilbert, 1992).

Figure 5.1.7 shows an exaggerated representation of the second mode of the RMS. The predicted frequency of this mode is 0.259 Hertz. This mode shape includes a significant amount of upper and lower boom bending. Other RMS modes include



Figure 5.1.7 RMS Second Structural Mode Shape

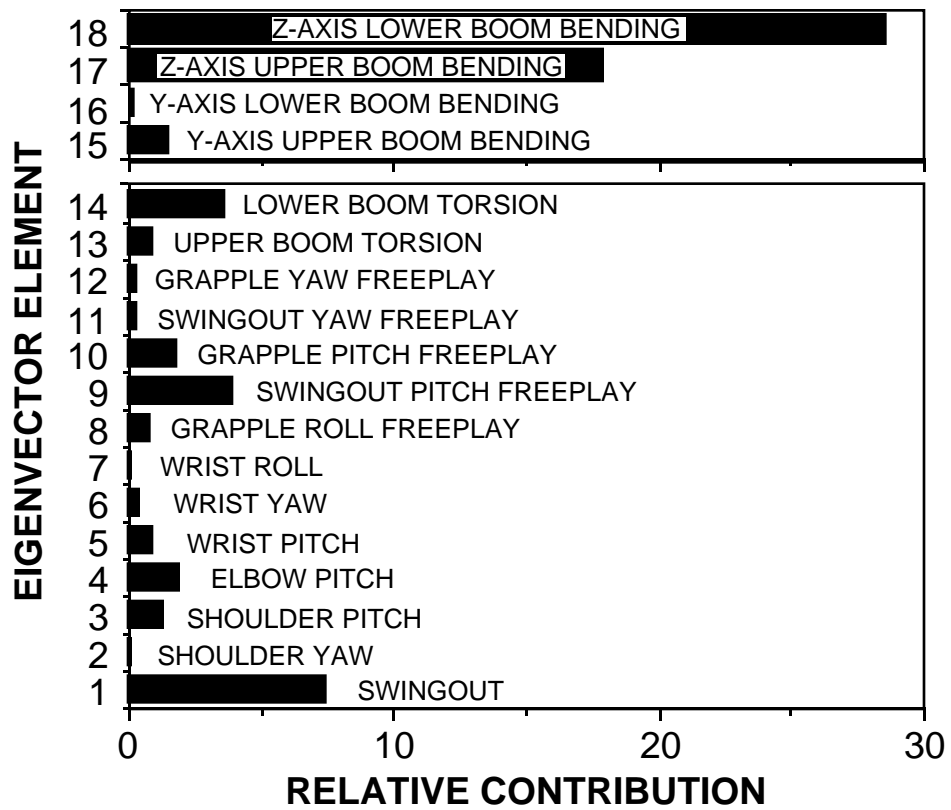


Figure 5.1.8 RMS Structural Mode Contributions

considerable amounts of joint flexibility and/or orbiter sidewall flexibility, with little boom bending contribution. In order to assess the relative contributions of each generalized coordinate in the state equations, the magnitudes of the eigenvector elements were plotted. Figure 5.1.8 is such a plot, showing the relative rotational contribution of states 1 through 13, and the relative displacement of states 14 through 17.

## **5.2 Collocated Versus Non-Collocated Control**

The existing tachometer sensors were used to feed back joint rate command signals to reduce arm tip motion following a pilot maneuver. Linear single-input, single-output (SISO), state space models were developed to investigate the damping improvement using local tachometer feedback to the respective joints and tip accelerometer feasibility studies. State-space models were developed to investigate state feedback controllers. The methods and results for both cases are presented below.

Linear SISO state-space models of the RMS were derived from DRS response data using system identification methods outlined in Chapter 3. The data have been obtained for single joint mode cases with the SPAS payload using the 3-second shoulder-yaw joint rate command pulse as the input, and either the joint tachometer or linear acceleration measurement at the tip of the arm as the output. Assuming a nominal model order of 8 states corresponding to 4 vibration modes, frequency, damping, and influence coefficient parameters were selected to make the model best match the DRS response data in a least-squares sense. The SISO system identification results for the y axis of the simulated tip accelerometer and the shoulder-yaw tachometer are shown in Figure 5.2.1 and 5.2.2 respectively. The solid line represents the nonlinear DRS predicted response and the dotted line corresponds to the identified linear model

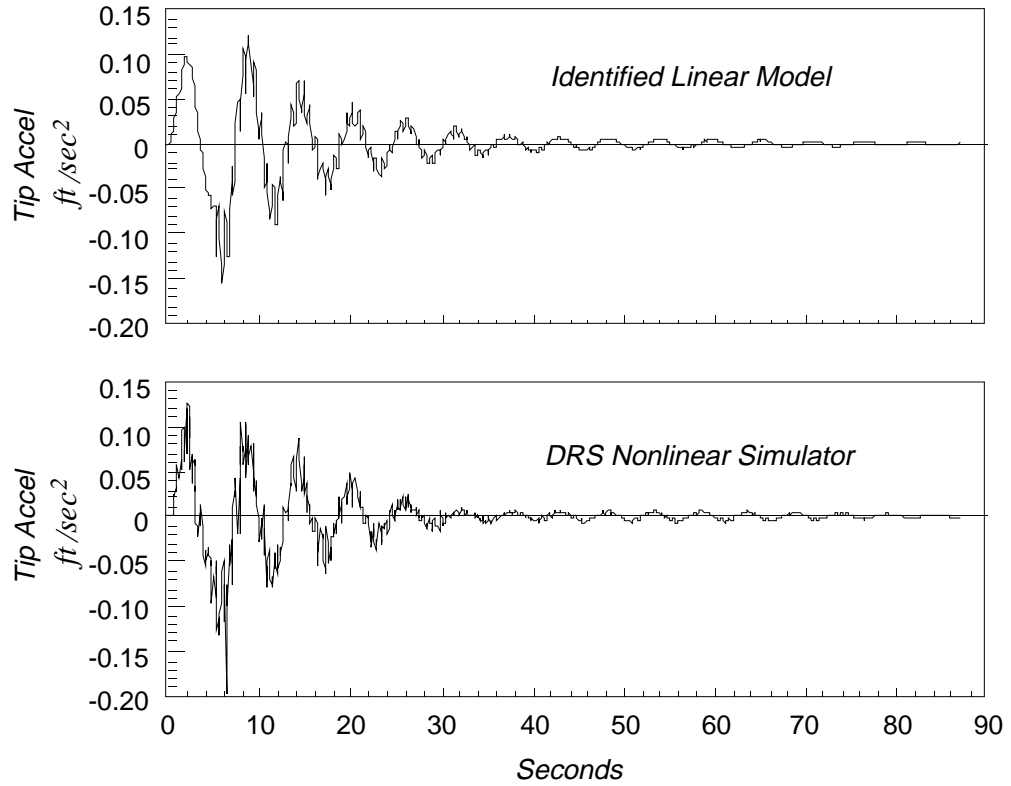


Figure 5.2.1 The SISO System Identification Results for the y Axis of the Simulated Tip Accelerometer

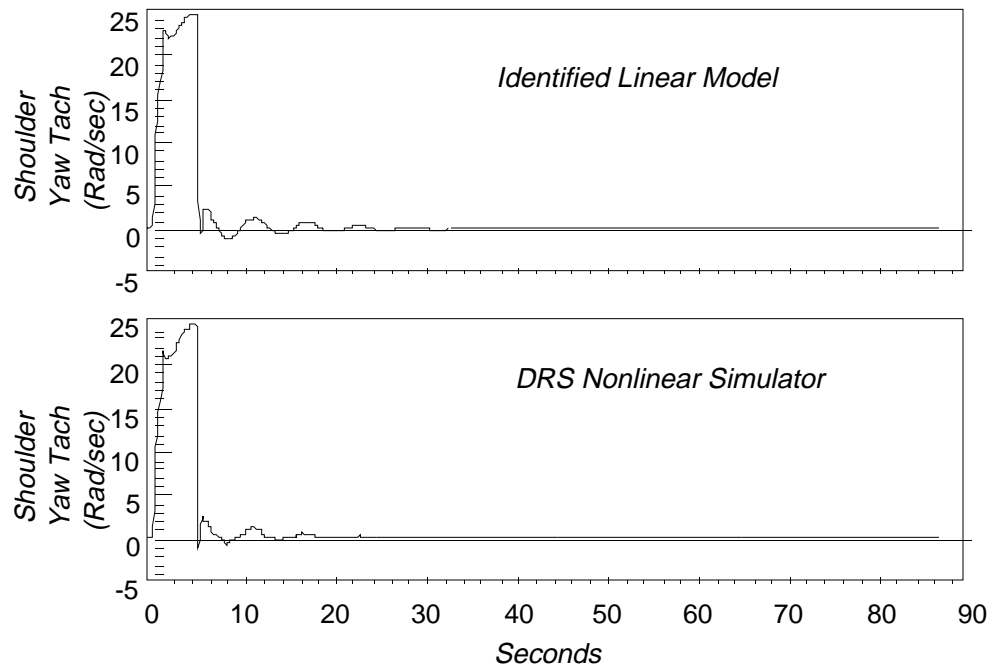


Figure 5.2.2 The SISO System Identification Results for the Simulated Shoulder-Yaw Tachometer

response. The identified linear models were used to evaluate the effect of tachometer and accelerometer feedback on system modes (i.e. damping) through simple gain loop-closures.

### Collocated and Non-Collocated Active Damping Results

Figures 5.2.3 and 5.2.4 show the RMS damping improvement as a function of a scaled gain parameter for feeding back the shoulder-yaw and pitch tachometer measurements, and tip acceleration measurement.

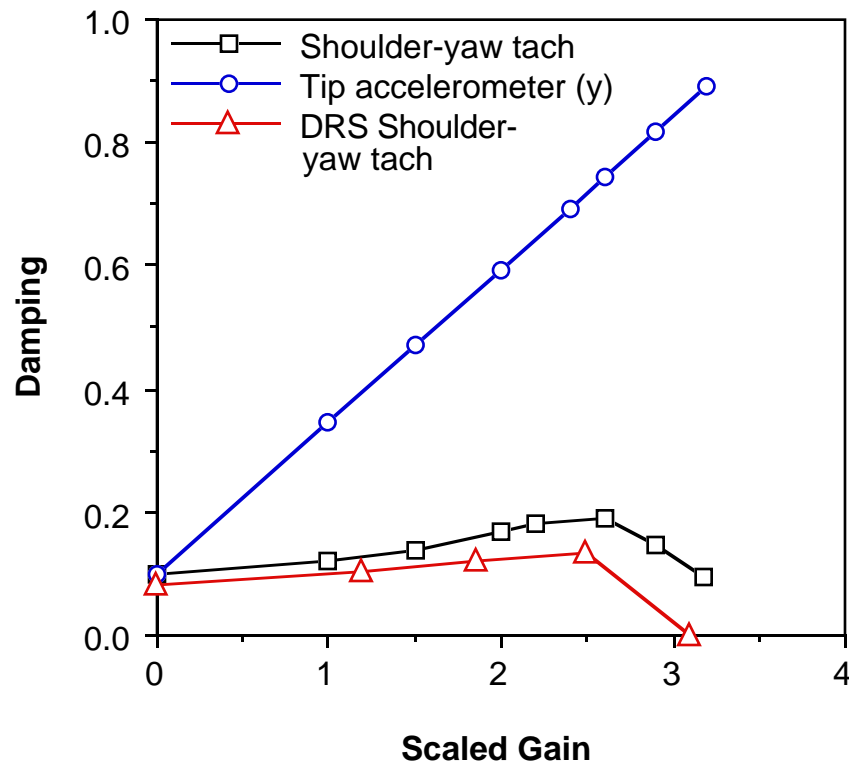


Figure 5.2.3 Damping as a Function of Scaled Gain Using the Shoulder-Yaw Joint

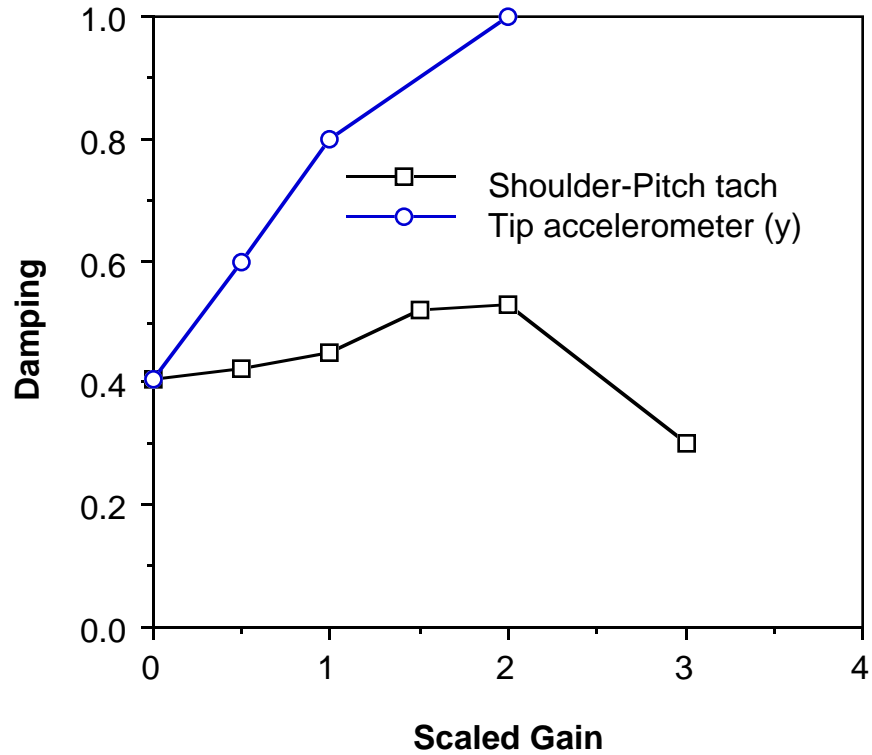


Figure 5.2.4 Damping as a Function of Scaled Gain Using the Shoulder-Pitch Joint

The initial damping values for zero gain for the two joints are different because the joints excite and are able to control different structural modes. For both joints, feedback of the tachometer measurement initially results in a small increase in RMS damping. Feedback of the acceleration measurement in both cases shows larger increases in damping. Also shown in Figure 5.2.3 is the result of tachometer feedback as predicted by the nonlinear DRS code, validating the linear model tachometer results.

### 5.3 Spline Varying System Identification

The SISO studies above investigated direct output feedback using tachometer and accelerometer measurements. Spline varying optimal controllers were also investigated. These SVO controllers were based on nonlinear models of the RMS

dynamics. The controller logic was implemented in the DRS nonlinear simulation so that candidate control laws could be evaluated including the effects of nonlinear arm dynamics, computer time delays, and existing RMS health and safety software functions. The controllers are of the form

$$\begin{aligned}x_c(k+1) &= A_c(\theta)x_c(k) + B_c(\theta)y(k) \\ u(k) &= C_c x_c(k) + D_c(\theta)y(k)\end{aligned}\tag{5.3.1}$$

where  $A_c(\theta)$  is the compensator dynamics matrix,  $B_c(\theta)$  is the control distribution matrix,  $C_c$  is the observation matrix,  $D_c(\theta)$  is the control feed-through matrix,  $x_c$  is the control state vector.

The spline varying observer models used for control law design were outlined in Chapter 3. Four models were derived, corresponding to the four study positions of the RMS in Figures 5.1.2 - 5.1.4. All four models had one input corresponding to the, shoulder-pitch, and one output corresponding to the in axis acceleration at the tip of the RMS. The shoulder joint was given a 3-second pulse rate command which was intended to excite the low frequency modes. The response data was aggregated to allow the algorithm to identify a single model representing the response of the RMS to the input. The four models are second order, corresponding to fundamental structural mode. Prior to the system identification, the DRS simulation acceleration data were processed through a first-order low-pass filter with a break frequency of 0.2 Hz.

Using the batch method, the observer Markov parameters were identified.

$$\hat{\mathbf{Y}}(\theta) = \begin{bmatrix} \hat{\beta}_0(\theta) & \hat{\beta}_1(\theta) & \hat{\alpha}_1(\theta) & \hat{\beta}_2(\theta) & \hat{\alpha}_2(\theta) \end{bmatrix}\tag{5.3.2}$$

A summary of the identified observer Markov parameters for the four study configurations are given in Table 5.3.1.

<p style="text-align: center;"><i>Table 5.3.1</i> Identified Observer Markov Parameters</p>					
Theta (Degrees)	$\hat{\beta}_0(\theta)$	$\hat{\beta}_1(\theta)$	$\hat{\alpha}_1(\theta)$	$\hat{\beta}_2(\theta)$	$\hat{\alpha}_2(\theta)$
0	2.2172e-17	-1.7278e-02	1.9842	1.7210e-02	-9.8794e-01
30	1.6627e-15	-1.7018e-02	1.9839	1.6945e-02	-9.8770e-01
60	-4.5981e-16	-1.5960e-02	1.9827	1.5876e-02	-9.8701e-01
90	1.5727e-15	-1.3153e-02	1.9810	1.3062e-02	-9.8599e-01

Notice that the identified  $\hat{\beta}_0(\theta)$  parameter is nearly zero as expected. Figures 5.3.1 - 5.3.4 show the identified observer Markov parameters plotted as a function of theta. The spline function is used to interpolate between the identified models and is shown in each figure.

$$\hat{\beta}_1(\theta) = 1.7278(10)^{-2} + 5.9333(10)^{-6} \theta - 8.500(10)^{-8} \theta^2 + 5.8704(10)^{-9} \theta^3$$

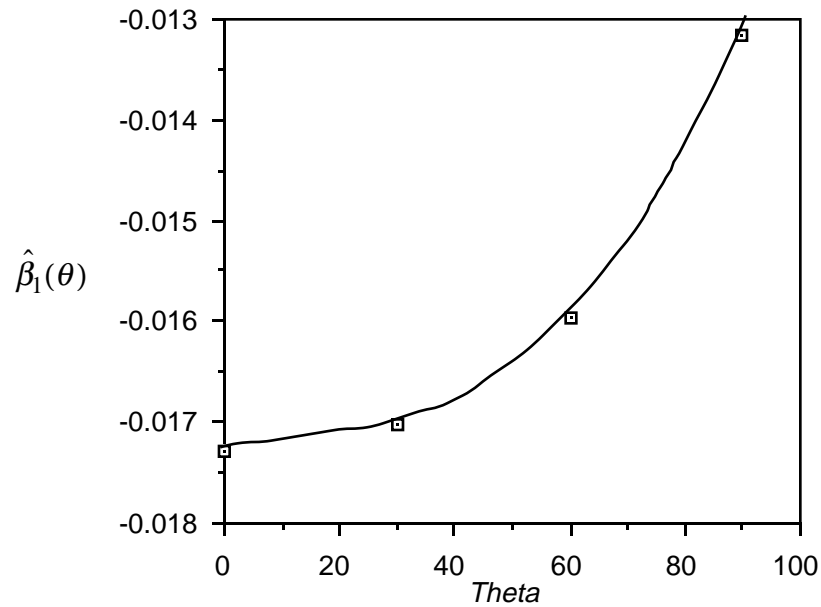


Figure 5.3.1 SVO SRMS Compensator Parameter  $\hat{\beta}_1(\theta)$

$$\hat{\alpha}_1(\theta) = 1.9842 + 9.4444(10)^{-6} \theta - 7.222(10)^{-7} \theta^2 + 2.4691(10)^{-9} \theta^3$$

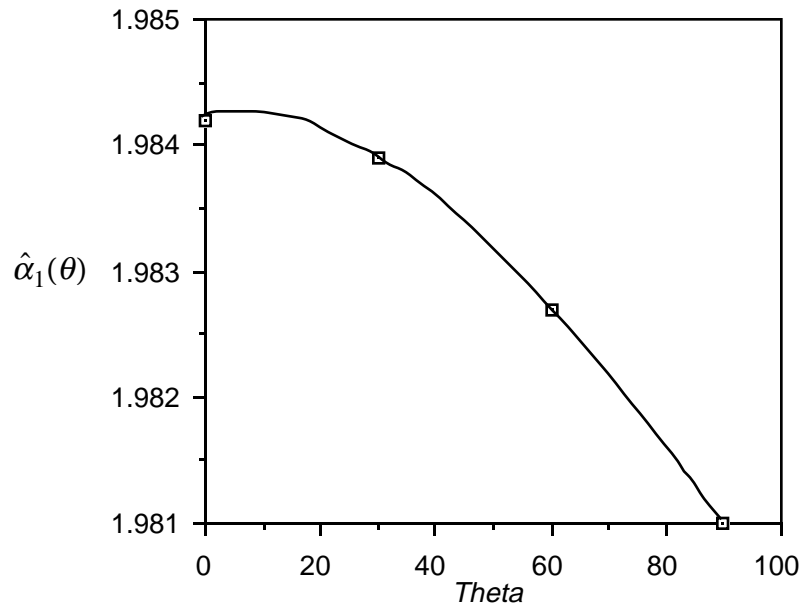


Figure 5.3.2 SVO SRMS Compensator Parameter  $\hat{\alpha}_1(\theta)$

$$\hat{\beta}_2(\theta) = 1.721(10)^{-2} - 5.8889(10)^{-6} \theta + 7.6111(10)^{-8} \theta^2 - 5.8086(10)^{-9} \theta^3$$

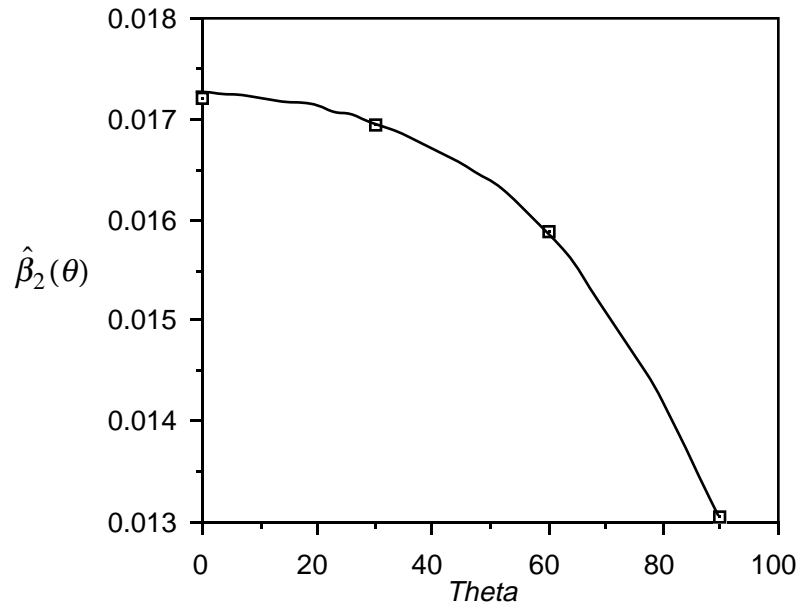


Figure 5.3.3 SVO SRMS Compensator Parameter  $\hat{\beta}_2(\theta)$

$$\hat{\alpha}_2(\theta) = -0.9879 - 8.3333(10)^{-7} \theta + 3.1667(10)^{-7} \theta^2 - 7.4074(10)^{-10} \theta^3$$

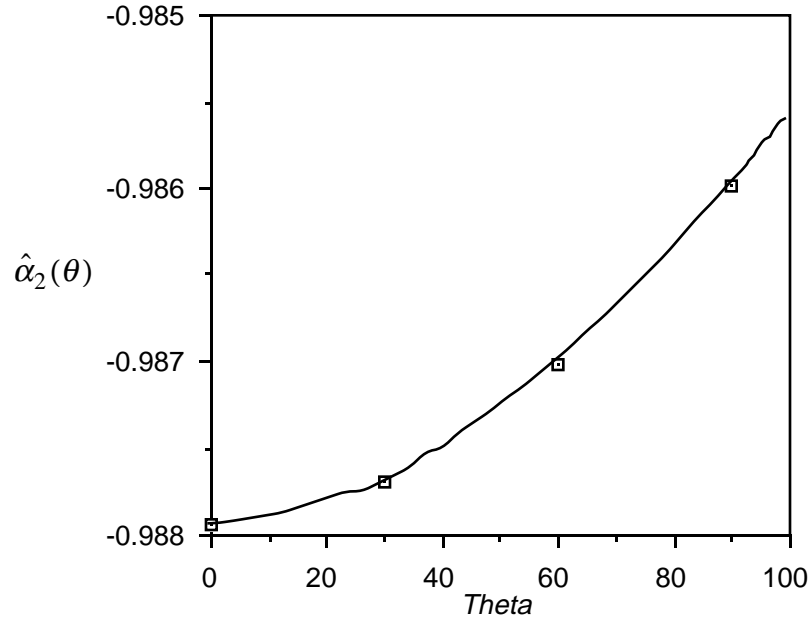


Figure 5.3.4 SVO SRMS Compensator Parameter  $\hat{\alpha}_2(\theta)$

The time domain results of the system identification are shown in Figures 5.3.5 and 5.3.6 for a nominal arm orientation. Shown are comparisons of the nonlinear DRS simulation response data with one of the identified models. Figure 5.3.5 shows the arm tip position following the 3-second pulse shoulder-pitch rate command (from 0 to 3 seconds in the plot). In this figure both the DRS nonlinear simulator (solid line) and the identified linear model (dashed line) match so closely that the curves overlap. Figure 5.3.6 illustrates the tip acceleration for both the DRS nonlinear simulator (solid line) and the identified linear model (dashed line) for the same 3-second pulse command.

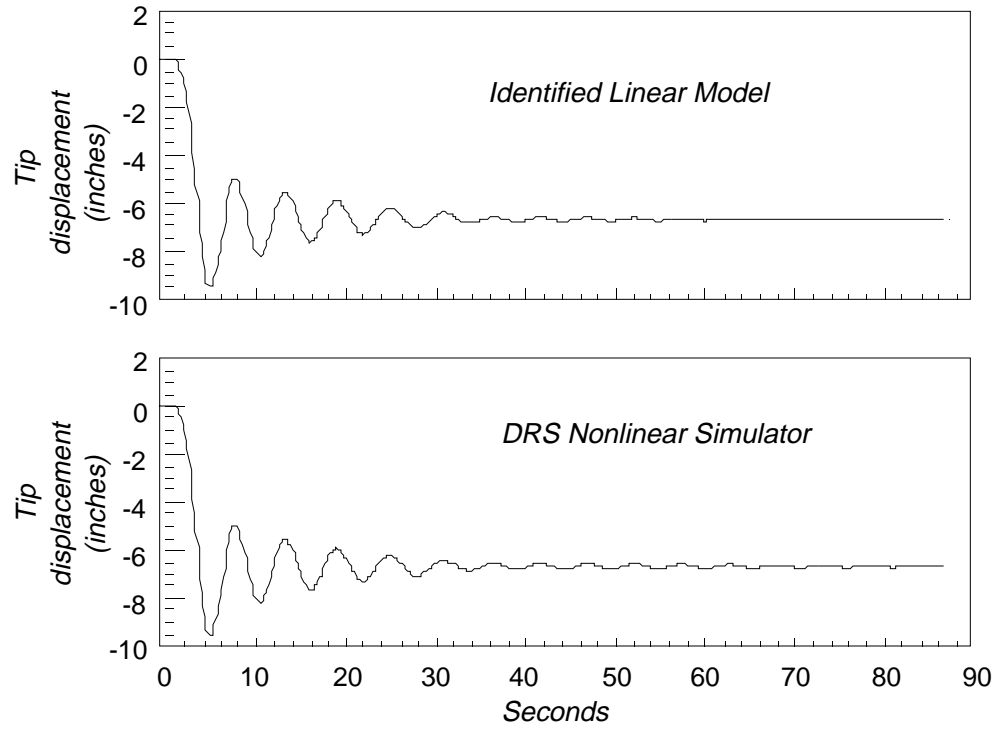


Figure 5.3.5 System Identification Results for the Tip Displacement

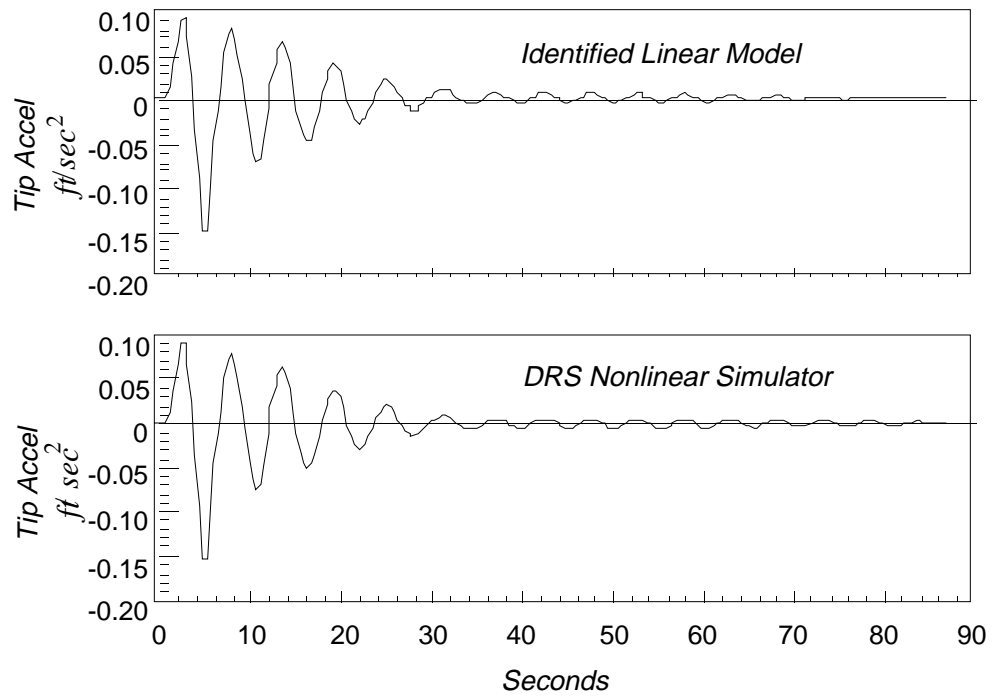


Figure 5.3.6 System Identification Results for the Tip Accelerometer (y axis)

#### 5.4 Spline Varying Optimal Controller Design and Implementation in RMS Software

The vibration suppression control law for each of the four configurations was developed using the SVO control strategy of Section 4.5. Each set point design used the frequency weighted Linear Quadratic Regulator (LQR) design method of Gupta (1980). Prior to the frequency weighted LQR regulator design, a digital high-pass prefilter was added in series to the identified model to reject steady-state bias as would be encountered in feeding back accelerometer measurements in a real system. This filter had the digital form

$$N(z) = \frac{\tau_1 z + \tau_2}{\tau_3 z + \tau_4} \quad (5.4.1)$$

where the constants  $\tau_1$  through  $\tau_4$  have the values 0.9707, -0.9707, 1, and -0.9414 respectively. The values for this filter correspond to a first order high pass filter with a break frequency of 0.12 Hz. The identified model and prefilter are described by the state-space model

$$\begin{aligned} \hat{x}(k+1) &= \hat{A}(\theta)\hat{x}(k) + \hat{B}(\theta)u(k) \\ y(k) &= \hat{C}\hat{x}(k) + \hat{D}(\theta)u(k) \end{aligned} \quad (5.4.2)$$

where

$$\hat{x}(k) = \begin{bmatrix} \hat{x}_1(k) \\ \hat{x}_2(k) \end{bmatrix} \quad (5.4.3)$$

where

$$A(\theta) = \begin{bmatrix} 0 & \alpha_2(\theta) \\ 1 & \alpha_1(\theta) \end{bmatrix}, \quad \hat{B}(\theta) = \begin{bmatrix} \beta_2(\theta) - \alpha_2(\theta)\beta_0(\theta) \\ \beta_1(\theta) - \alpha_1(\theta)\beta_0(\theta) \end{bmatrix} \quad (5.4.4)$$

and

$$\hat{C} = [0 \quad 1], \text{ and } \hat{D}(\theta) = \beta_0(\theta) \quad (5.4.5)$$

For control purposes, a fixed gain regulator of the form

$$u(k) = -C_c(\theta)\hat{x}(k) \quad (5.4.6)$$

was used where  $u$  is the joint rate command signal. The state estimate  $\hat{x}(k)$  was obtained from an observer of the form

$$\hat{x}(k+1) = \hat{A}(\theta)\hat{x}(k) + \hat{B}(\theta)u(k) + K(y(k) - \hat{x}(k)) \quad (5.4.7)$$

where  $y$  is the tip accelerometer measurement. The observer gains  $K_1(\theta)$  and  $K_2(\theta)$  were found using (3.6.16) and (3.6.17).

$$K_1(\theta) = -\alpha_2(\theta) \quad (5.4.8)$$

and

$$K_2(\theta) = -\alpha_1(\theta) \quad (5.4.9)$$

To obtain the optimal gain  $C_c(\theta)$ , the model with the prefilter was used in a frequency weighted LQR design with a weighted cost function of the form

$$J(\theta) = \sum_{k=0}^{\infty} y(k)^T Q y(k) + u(k)^T R u(k) \quad (5.4.10)$$

where  $Q$  is the output weight matrix, and  $R$  is the control weighting matrix. The numerical values of  $Q$  and  $R$  were determined using an iterative design procedure on the linear model which avoided actuator saturation. The final values used in the design are  $Q = \text{diag}\{0.002\}$  and  $R = \text{diag}\{0.02\}$ . Using

$$y(k) = \hat{C}\hat{x}(k) + \hat{D}(\theta)u(k) \quad (5.4.11)$$

the performance index Equation (5.4.10) was recast:

$$J(\theta) = \sum_{k=0}^{\infty} \hat{x}^T(k) \hat{C}^T Q \hat{C} \hat{x}(k) + 2\hat{x}(k)^T \hat{C}^T Q \hat{D}(\theta)u + u^T (\hat{D}^T(\theta) Q \hat{D}(\theta) + R)u \quad (5.4.12)$$

The optimal feedback gain  $C_c(\theta)$  which minimizes the performance index  $J(\theta)$  for the four values of  $\theta$  in Equation (5.4.10) was found using Matlab software tools (Matlab, 1992).

An implementation of the SVO controller in the Shuttle software was identified. This strategy, illustrated in Figure 5.4.1, allows use of all existing RMS health and safety monitoring functions in an effort to simplify flight development work. The SVO controller would be a software module which acts as a preprocessor to the existing

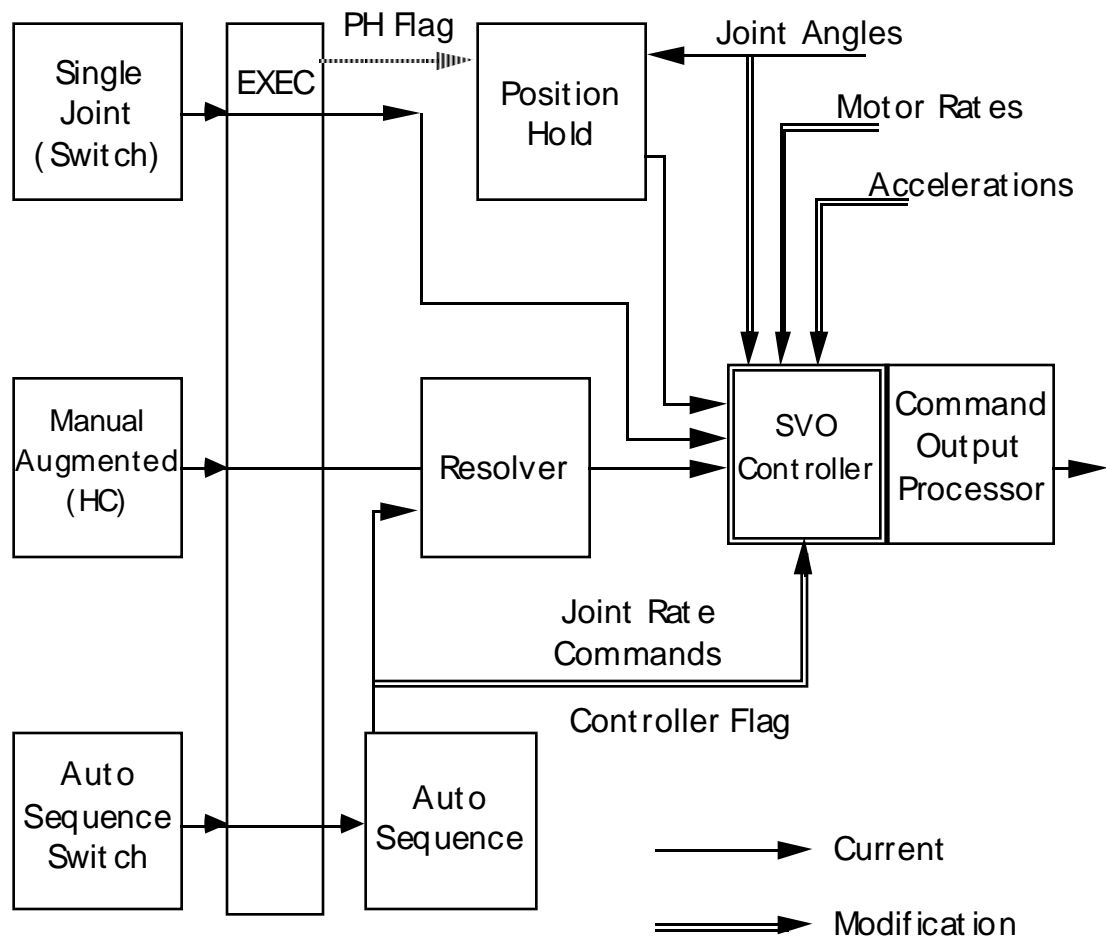


Figure 5.4.1 Proposed SVO Controller Implementation in Shuttle Software

RMS Command Output Processor (COP). It would be turned on and off using the executive function of the existing software by a flag which would activate the controller when RMS joint move commands are zeroed. Using motor rate and/or acceleration feedback measurements, the controller would damp the free response of the arm to some level at which time the normal position-hold function of the arm would be activated. With this implementation, the active damping function of the controller could be expanded to damp RMS motions following Shuttle thruster firings as well.

## **5.5 Active Damping Results**

The SVO controller was evaluated on the DRS nonlinear simulation. The tip position following a 3-second shoulder-yaw pulse rate command is shown in Figure 5.5.1. The top figure represents standard RMS operation and the bottom line represents actively damped performance. The time required to damp the tip oscillation to  $\pm 1$  inch is decreased by a factor of 3. The shoulder-pitch servo torque following the 3-second shoulder-pitch pulse rate command is shown in Figure 5.5.2. In addition, after 90 seconds a Shuttle thruster roll doublet firing was simulated for 6 seconds. The upper plot represents simulated standard RMS operation while the bottom plot represents closed-loop performance with the SVO controller. In this time history the controller has the effect of reducing the applied torque by a factor of 2. This provides the added potential benefit of reducing the structural stress in the arm following routine maneuvers involving either joint commands or Shuttle thruster firings.

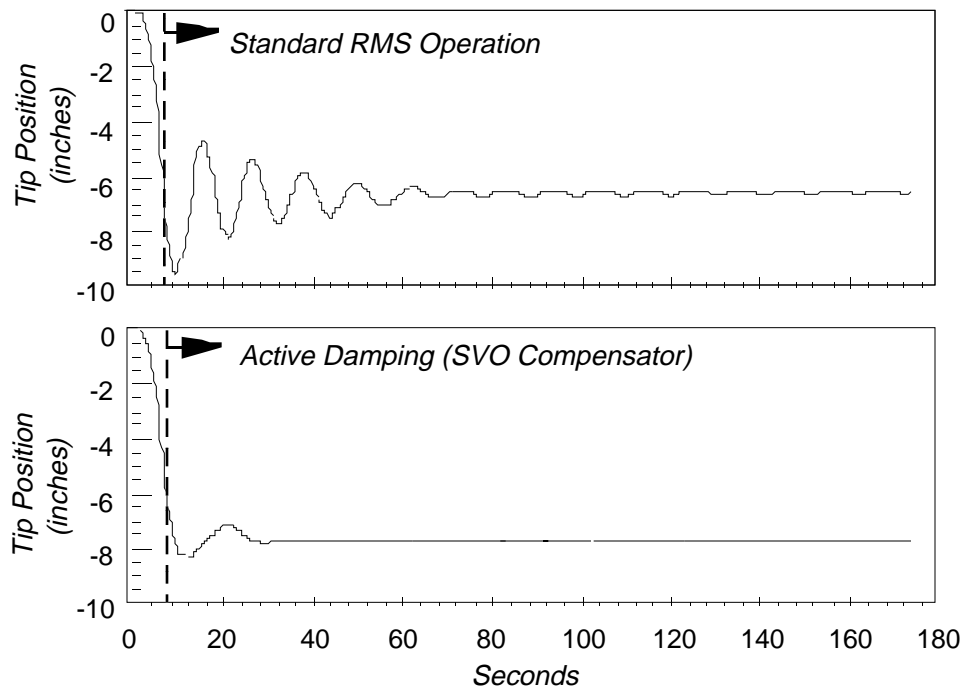


Figure 5.5.1 Tip Position Following 3-Second Pulse Command

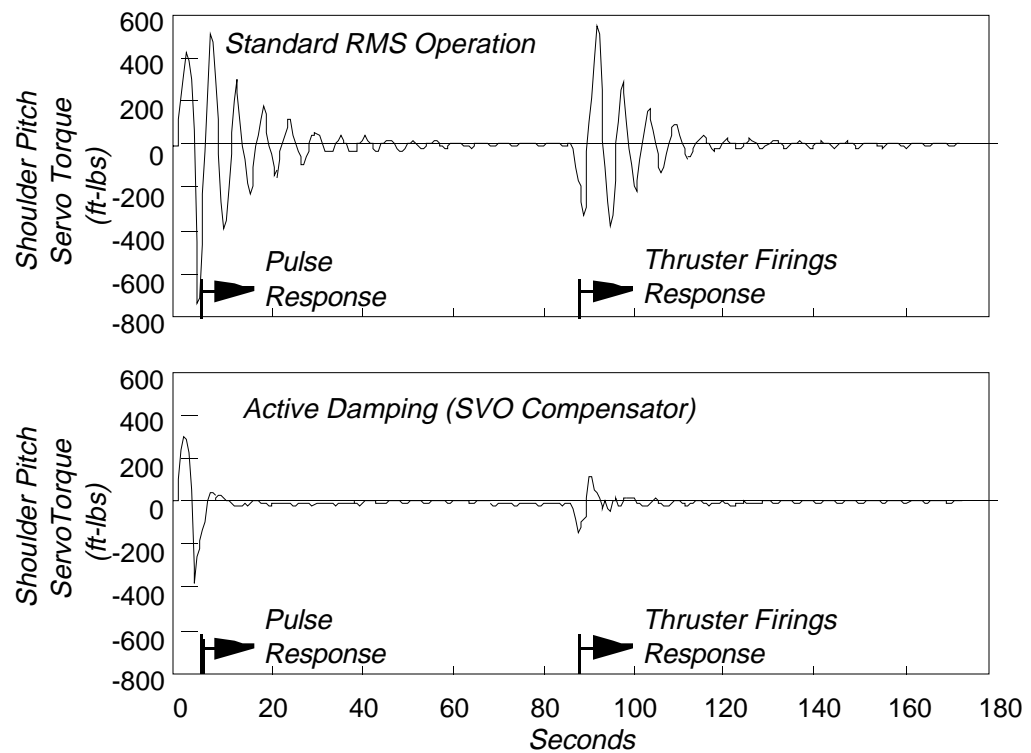


Figure 5.5.2 Shoulder Pitch Servo Torque Following 3-Second Pulse Command. After 90 Seconds the Shuttle Thrusters are Fired for 6 Seconds

## 5.6 Summary

An analytical study to determine the feasibility of actively augmenting the damping of the Shuttle remote manipulator system has been developed. System identification studies were performed to evaluate collocated direct output feedback and non-collocated dynamic spline varying controllers. The SVO controller and logic were evaluated in a nonlinear simulation which included the effects of kinetic and kinematic nonlinear arm dynamics, computer time delays, and existing Shuttle health and safety software functions. The collocated results indicate that for both shoulder yaw and pitch joints, the feedback of the tachometer measurement results in a small increase in RMS damping, with very small increases in proportional gain producing instabilities. Feedback of the acceleration measurement in both cases resulted in much larger increases in damping. SVO controllers were designed to enable improved performance over a large workspace. Based on the results, active damping of the remote manipulator system appears feasible using the existing joint actuators and Shuttle computers and software. However, some additional feedback sensors in the form of accelerometers located at the tip of the arm are required.

The SVO controller developed for this system does not change or delay the trained operator input command to move the arm, thus the “feel” of the arm has not been altered. The SVO control system, when evaluated on the nonlinear simulation, demonstrated significant improvement over the present arm performance: (1) Damping level is improved by a factor of 3; (2) Peak joint torque is reduced by a factor of 2 following Shuttle thruster firings.

## CHAPTER 6

### CONCLUSION AND RECOMMENDATIONS

The planar nonlinear dynamics of a reconfigurable electromechanical structure and controller have been studied in this thesis. Several unique and unusual nonlinear compensators have been designed, compared, and contrasted. The three main contributions of this thesis are the following:

- (1) A highly complex mathematical nonlinear reconfigurable system can be controlled with an extremely low order SVO controller. The SVO controller can accommodate the non-collocated actuator problem when kinematic nonlinearities are present.
- (2) The Markov parameters are the key to reducing the highly heterogeneous parameters in multiple fixed controllers to one simply connected SVO controller. Understanding how the essential kernel of the mathematical problem is changing with a measurable state (such as the elbow joint angle) is fundamental to designing low order high performance SVO controllers. For example, the Markov parameters were found to be extremely useful in reducing the manifold of changing parameters in the mathematical system.
- (3) The derivation of the SVO controller can be developed using linear identification techniques as opposed to high fidelity finite element

modeling. This is not to say that the high fidelity finite element based simulation is not to be used or developed. If an accurate physical model is not available or too cumbersome, identification can be accomplished for the optimal controller via a recurrent network using data gathering experiments of a minimum of four arm orientations. In addition, the observer Markov parameters can be utilized to reduce the identified parameters to a minimal set of identified network weights. All of the controller coefficients in the nonlinear optimal controller can be very closely approximated by a third order polynomial in the elbow joint angle ( $\theta_2$ ).

There is a direct way of determining the system matrices  $A(\theta)$ ,  $B(\theta)$ ,  $C$ , and  $D(\theta)$  without first computing the system Markov parameters by using the observer Markov parameters in the spline varying observer canonical state space model form. In this similarity transformation, the time varying state space model is derived quickly for control system design. There is no need for induction which unnecessarily increases control design development time.

The four advantages in using the SVO controller where the spline function approximates the system model, observer, and controller gain are listed below:

- (1) The spline function approximation is simply connected, thus the SVO controller is more continuous than traditional gain scheduled controllers when implemented on a time varying plant.
- (2) The SVO controller is easier for real time implementations in storage and computational effort when compared to traditional gain scheduled compensators.

- (3) Where system identification is required, the spline function requires fewer experiments. Namely four experiments are required to identify the four polynomials in each of the non zero elements in the controller.
- (4) Startup transients are reduced. When the estimator is determining the state at all times during the maneuver, initial estimator transients can be eliminated.

In the process of developing the SVO controller, an understanding of the physics of a two-link model of a flexible manipulator provided useful insights to the tenuous task of developing a high performance nonlinear controller. When used alone, high fidelity mathematical models obfuscate the control system designer while tackling the problem of nonlinear kinematics. High fidelity models can however, accurately predict the performance of complex systems such as the SRMS (Gray, C., et al., 1985). While a high fidelity simulator is useful to test and fine tune a low order controller prior to real time implementation, fundamental dynamics must be identified and utilized for low order control system development. For example, it is shown that the use of collocated actuator sensor pairs (on the high fidelity simulator) does not appreciably affect the damping levels when compared to an accelerometer sensor.

The two link model was useful in:

- Observing the behavior of the non-minimum phase zeroes when disparate base boundary conditions are applied.
- Identifying the predominance of the fundamental mode in the open loop performance of the slewing manipulator.
- Determining the separation in frequency between successive modes.
- Understanding the relative merits of the various compensators under study.

These conclusions are highlighted in the following paragraphs.

Transforming the open loop dynamics into modal form highlights the dominance in the open loop response of the fundamental mode. For example, the infinity norm amplitude ratio of the 1st versus the 2nd mode is 40:1, and the infinity norm ratio of the 1st versus the 3rd mode is 600:1 for medium payload weight classes. For higher order modes the infinity norm ratio is still larger. These infinity norm ratios are shown to increase further still for heavier payload masses.

In addition, the frequency separation between the first and second modal frequency for the manipulator model increases as the payload mass is increased. If no payload is used, the 2nd modal frequency is 6 times the frequency of the 1st mode. The 3rd modal frequency is 18 times the frequency of the 1st mode, etc. If a payload 100 times the mass of the arm is considered, the 2nd modal frequency is 98 times the frequency of the 1st mode. The 3rd modal frequency is 316 times the frequency of the 1st mode, etc. It is worth noting that for the SRMS a payload to arm mass ratio of 100 is considered a small to medium class in terms of payload mass.

A cost comparison of the controllers under study was summarized. All of the compensators improved the open loop performance over the workspace. The overall improvement in performance is 7:1 for the fixed gain compensator, 3:1 for the fixed robust compensator, and 20:1 for the SVO compensator. Although the stability margin for the fixed gain controller was relatively low ( $10^\circ$  phase margin), its performance was about two times better than the fixed robust compensator ( $40^\circ$  phase margin). Thus by increasing the robustness of the closed loop system, the fixed robust compensator sacrificed on performance.

As a future recommendation, it should be noted that if possible, one should use collocated sensors and actuator pairs for controlling the flexible body modes. This would facilitate the task of absorbing the flexible energy in the structure in a local manner. For example, one can design the joints such that the gearbox in the joints of the electromechanical structure allow the vibratory energy passing through the joint to be observed. This is most readily accomplished by making the joint element more compliant relative to the surrounding boom elements, or providing strain energy sensors surrounding the joint in a collocated fashion. In the case of non-existent or insufficient collocated sensor/actuator pairs, a dynamic model based controller is required to improve dynamic performance. Present adaptive control techniques cannot accommodate the non-collocated actuator problem when kinematic nonlinearities are present.

Finally, the SVO controller was evaluated on the DRS nonlinear simulation. An implementation of the SVO controller in the Shuttle software was identified. This strategy allows use of all existing RMS health and safety monitoring functions. The SVO controller developed for this system does not change or delay the trained operator input command to move the arm, thus the “feel” of the arm has not been altered. The SVO controller and logic were evaluated in a nonlinear simulation, which included the effects of kinetic and kinematic nonlinear arm dynamics, computer time delays, and existing Shuttle health and safety software functions. Based on the results, active damping of the remote manipulator system can be accomplished using the existing joint actuators and Shuttle computers and software. However, some additional feedback sensors in the form of accelerometers located at the tip of the arm are required. The accelerometer sensor location was identified which allowed the nonlinear compensator to operate over large variations in the shoulder yaw, elbow pitch, and wrist roll, yaw and pitch arm orientations. The astronaut/operators assessment of the compensator

noted that there was a “significant increase in damping.” Loads reduction for the RMS with the compensator was also cited as an important factor several times during the sessions. The SVO controller demonstrated significant improvement over the present arm performance: (1) Damping level was improved by a factor of 3; (2) Peak joint torque was reduced by a factor of 2 following Shuttle thruster firings. The time required to damp the tip oscillation to  $\pm 1$  inch is decreased by a factor of 3. This provides the added potential benefit of reducing the structural stress in the arm following routine maneuvers involving either joint commands or Shuttle thruster firings.

## List of References

- Anderson, B.D.O. (1967) "A System Theory Criterion For Positive Real Matrices," *SIAM J. Control*, vol. 5, 1967.
- Anderson, Mark, (1989) "Linear Design Models for Robust Control Synthesis," *AIAA Journal*, vol. 8., 1989, pp. 263-270.
- Asada, H., and Youcef-Toumi, K., (1987) Direct-Drive Robots, Theory and Practice, MIT Press, 1987.
- Asada, H., Ma, Z, and Tokuimaru, H., (1990) "Inverse Dynamics of Flexible Robot Arms: Modeling and Computation for Trajectory Control," *Journal of Dynamic Systems, Measurement and Control*, vol. 112, June 1990, pp. 177-185.
- Balas, M. (1978) "Feedback Control of Flexible Systems," *IEEE Transactions of Automatic Control*, vol. 23, pp. 673-679, 1978.
- Balas, M. (vol. 133) "Finite-Dimensional Controllers for Linear DPS: Exponential Stability Using Residual Mode Filters," *Journal of Math Analysis and Applications*, vol. 133. pp. 283-296.
- Balas, M., (vol. 117) "Exponentially Stabilizing Finite-Dimensional Controllers for Linear Distributed Parameter Systems (DPS): Galerkin Approximation of Infinite-Dimensional Controllers," *Journal of Math Analysis and Applications*, vol. 117. pp. 358-384.
- Balas, M., Quan, R., Davidson, R., and Das, B. (1988) "Low-Order Control of Large Aerospace Structures Using Residual Mode Filters," *Proceedings of the American Controls Conference*, 1988.
- Balestrino, A, De Maria, G., and Sciavicco, L. (1983) "An adaptive model following Control System for Robotic Manipulators," *Journal of Dynamical Systems, Measurement and Control*, vol. 105 n. 3, pp. 143-151, 1983.
- Belvin, K.W, et al. (1991) "Langley's CSI Evolutionary Model: Phase 0," NASA TM-104165, November, 1991.
- Book, W.J. (1979) "Analysis of Massless Elastic Chains with Servo Controlled Joints," *Journal of Dynamical Systems, Measurement and Control*, vol. 101, pp. 187-192, 1979.
- Book, W.J., Maizza-Neto, and Whitney, D.E. (1975) "Feedback Control of two-beam two-joint Systems with distributed Flexibility," *Journal of Dynamical Systems, Measurement and Control*, pp. 424-431, Dec. 1975.

- Cannon, R.H., Schmitz, E. (1984) "Initial Experiments on the End-Point Control of a Flexible One-Link Robot," *International Journal of Robotics Research*, vol. 3, no. 3, pp. 62-75, 1984.
- Chassiakos, A.G., and Bekey, G.A. (1985) "Pointwise Control of Flexible Manipulator Arm," SYROCO 1985, Barcelona, pp. 113-117, November 1985.
- De Luca, A. Lucibello, P., and Ulivi, G. (1989) "Inversion Techniques for Trajectory Control of Flexible Robot Arms," *Journal of Robotic Systems*, vol. 6, no. 4, pp. 325-344, 1989.
- Demeo, M.E, Gilbert, M.G., Scott, M.A., Lepanto, J.A., Bains, E.M, Jensen, M.C. (1992) "Human-in-the-Loop Evaluation of RMS Active Damping Augmentation" *Proceedings of the Guidance, Navigation and Control Conference*, 1992.
- Doyle, J.C., Wall, J.E., and Stein, G. (1982) "Performance and Robustness Analysis for Structured Uncertainty," *Proceedings of the 21st IEEE Conference on Decision and Control*, vol. 2, Orlando, FL, Dec. 1982, pp. 629-636.
- Eisler, G.R., Segalman, D.J., and Robinett, R.D. (1990) "Approximate Minimum-Time Trajectories for Two-link Flexible Manipulators," *Proceedings of the 1990 American Control Conference*, San Diego, CA, May 23-25, 1990.
- Enns, D.F. (1984) "Model Reduction for Control System Design," Ph.D. Dissertation, Department of Aeronautics and Astronautics, Stanford University, June 1984.
- Feddema, J.T., Eisler, G.R., and Segalman, D.J., (1990) "Integration of Model-Based and Sensor-Based Control for a Two-Link Flexible Robot Arm." *IEEE International Conference on Systems Engineering*, Pittsburgh, Pennsylvania, August 9-11, 1990, pp. 435-439.
- Freudenberg, J.S., Looze, D.P., and Cruz, J.B. (1982) "Robustness Analysis Using Singular Value Sensitivities," *International Journal of Control*, vol. 35, No. 1, 1982, pp. 95-116.
- Galvez, M. (1991) "On Dynamic Model Reduction and Adaptive Control of Flexible Large Space Structures," Ph.D. Thesis, Department of Electrical and Computer Engineering, University of Colorado, Boulder, June 1991.
- Gevarter, W.B (1970) "Basic Relations for Control of Flexible Vehicles," *AIAA Journal*, vol. 8., 1970, pp. 666-672.
- Gilbert, M.G., Scott, M.A, and Demeo, M.E (1992) "RMS Active Damping Augmentation," *Automation and Robotics for Space-Based Systems*, N92-27763 18-63, pp. 93-110.
- Goodson, R.E. (1970) "Distributed System Simulation Using Infinite Product Expansions," *Simulation*. Dec. 1970, pp. 255-263.
- Goodwin, G.C., and Sin, K.S. (1984) Adaptive Filtering Prediction and Control, Prentice-Hall, Inc., 1984.
- Graff, K.F. (1975) Wave Motion In Elastic Solids, Ohio State University Press, 1975.

- Gray, C., et al. (1985) "Validation of the Draper RMS Simulation (DRS) Against Flight Data," CSDL-R-1755, vol. 1-2, Cambridge, Massachusetts, April 1985.
- Gupta, N.K. (1980) "Frequency-Shaped Cost Functionals: Extensions of Linear-Quadratic Gaussian Design Methods," *Journal of Guidance and Control*, vol. 3, Nov.-Dec. 1980, pp. 529-535.
- Harashima, F., and Ueshiba, T. (1986) "Adaptive Control of Flexible Arm using the End-Point Sensing," *Proceeding of Japan-U.S.A. Symposium on Flexible Automation*, Osaka, Japan, pp. 225-229, July, 1986.
- Hasting, G.G., and Book, W.J. (1985) "Experiments in the Control of a Flexible Robot Arm," *Proceedings of 1985 American Control Conference*, pp. 728-729.
- Hasting, G.G., and Book, W.J. (1986) "Verification of a Linear Dynamic Model for Flexible Robotic Manipulators," *IEEE International Conference on Robotics and Automation*, pp. 1024-1029, April, 1986.
- Hillsley, K. L., and Yurkovich, S. (1991) "Vibration Control of a Two-Link Flexible Robot Arm," *IEEE International Conference on Robotics and Automation*, April 1991.
- Joshi, S.M.; Maghami, P.G.; Kelkar, A.G. (1991) "Dynamic Dissipative Compensator Design for Large Space Structures" Presented at AIAA Guidance, Navigation, and Control Conference, Paper No. AIAA 91-2650 New Orleans, LA, August 12-14, 1991.
- JSC, (1988) "Space Shuttle System Payload Accommodations," NASA Johnson Space Center, Houston, Texas, NSTS 00700, vol. XIV, Appendix 8, Revision J, January 27, 1988.
- Juang, J.-N., (1993) Applied System Identification, Prentice Hall, Engelwood Cliffs, NJ 07632. pp. 175.
- Juang, J.-N., Horta, L.G., Phan, M., and Longman, R.W. (1991) "Identification of Observer and Kalman Filter Markov Parameters: Theory and Experiments," *Proceedings of the AIAA Guidance, Navigation and Control Conference*, New Orleans, Louisiana, August 1991, pp. 1195-1207.
- Juang, J.-N., Horta, L.G., Robertshaw, H.H. (1986) "A Slewing Control Experiment for Flexible Structures," *Journal of Guidance, Control and Dynamics*, vol. 9, No. 5, Sept.-Oct. 1986, pp. 599-607.
- Juang, J.-N., Wu, S.C., Phan, M., Longman, R.W. (1993) "Passive Dynamic Controllers for Nonlinear Mechanical Systems" *Journal of Guidance and Control*, vol. 16, Sept.-Oct. 1993, pp. 845-851.
- Judd, R.P, and Falkenburg, D.R. (1985) "Dynamics of Non rigid Articulated Robot Linkages," *IEEE Transactions on Automatic Control*, vol. 30, pp. 499-502, 1985.
- Kanoh, H., Lee, H. (1985) "Vibration Control of a One-Link Flexible Arm" in *Proceedings of the 24th Conference of Decision and Control*, Ft. Lauderdale, Florida, December 1985, pp. 1172-1177.

- Karkkainen, P. and Halme, A. (1985) "Modal Space Control of Manipulator Vibrational Motion," SYROCO 1985, Barcelona, pp. 101-105, November 1985.
- Korolov, V.V., and Chen, Y.H., (1989) "Controller Design Robust to Frequency Variation in a One Link Flexible Robot Arm," *Journal of Dynamic Systems, Measurement, and Control*, vol. 111, 1989, pp. 9-14.
- Kotnik, P.T., Yurkovich, S. and Ozguner, U. (1988) "Acceleration Feedback for Control of a Flexible Manipulator Arm," *Journal of Robotic Systems*, 5(3) 1988, pp. 181-196.
- Kreutz, K., and Jamieson, R.S., "Linearization of Robot Manipulators," *NASA Tech Brief*, vol. 11, No. 8, Item #114, 1987.
- Lepanto, J. (1992) Draper Laboratory correspondence to NASA LaRC. Memo No: RMS/CSI-93-05. ESC-93-281. October 28, 1992.
- Liang, S.C., Balas, M.J. (1990) "Direct Model Reference Adaptive Control in Large Space Structure Using Hyperstability," IEEE Intelligent Control System Conference, Philadelphia, PA., 1990.
- Ljung, L. and Soderstrom, T (1983) Theory and Practice of Recursive Identification, MIT Press, 1983.
- Lucibello, p., Bellezza, F. (1990) "Nonlinear Adaptive Control of a Two-Link Flexible Robot Arm," *IEEE Conference on Decision and Control*, vol. 4, Honolulu, HI, December 5-7, 1990. pp. 2545-2550.
- Matlab<sup>TM</sup> for Macintosh Computers (1992) *Users Manual*, The MathWorks, Inc., South Natlick, MA, September 1992.
- Matsuno, F., Sakawa, Y. (1990) "A Simple Model of Flexible Manipulators with Six Axes and Vibration Control by Using Accelerometers," *Journal of Robotic Systems*, 7(4), 1990. pp. 575-597.
- Meirovitch, L. (1967) Analytical Methods in Vibrations, Macmillan, New York, NY, 1967.
- Meirovitch, L. (1975) Elements of Vibration Analysis, McGraw-Hill, Inc. 1975. Page 212.
- Metzinger, R.W. (1988) *DRS Users Guide*, (Revision 88-2) The Charles Stark Draper Laboratory, Massachusetts, July 21, 1988.
- Moore, B.C. (1981) "Principal Component Analysis in Linear Systems: Controllability, Observability, and Model Reductions," *IEEE Transactions on Automatic Control*, vol. AC-26, No. 1, Feb. 1981, pp. 17-32.
- Mukhopadhyay, V, Newsom, J.R. (1982) "Application of Matrix Singular Value Margins of Multiloop System," NASA TM-84524, July, 1982.

- Mukhopadhyay, V. (1989) "Digital Robust Control Law Synthesis using Constrained Optimization," *Journal of Guidance Control and Dynamics*, vol. 12, Number 2, March-April 1989, pp. 175-181.
- Newsom, J.R., Mukhopadhyay, V. (1983) "The Use of Singular Value Gradients and Optimization Techniques to Design Robust Controllers for Multiloop Systems," AIAA Paper No. 83-2191CP. AIAA Guidance and Control Conference, Gatlinburg, Tennessee, August 15-17, 1983.
- Nicosia, S., and Tomei, P. (1984) "Model Reference Adaptive Control Algorithms for Industrial Robots," *Automatica*, 20, pp. 635-644, 1984.
- Oakley, CM. and Barratt, C.H. (1990a) "End-Point Controller Design for an Experimental Two-link Flexible Manipulator using Convex Optimization," *Proceedings of the 1990 American Control Conference*, vol. 2, San Diego, CA., May 23-25, 1990, pp. 1752-1759.
- Oakley, CM. and Cannon, R.H. (1989) "End-Point Control of a Two-Link Manipulator with a Very Flexible Forearm: Issues and Experiments," *Proceedings of the 1989 American Control Conference*, vol. 2, Pittsburgh, PA., June 21-23, 1989, pp. 1381-1388.
- Oakley, CM. and Cannon, R.H. (1990b) "Anatomy of an Experimental Two-Link Flexible Manipulator under End-Point Control," *IEEE Conference on Decision and Control*, vol. 2, Honolulu, HI, December 5-7, 1990, p. 507-513.
- Phan, M., Horta, L.G., Juang, J.-N., and Longman, R.W. (1992) "Linear System Identification Via an Asymptotically Stable Observer," *NASA Technical Paper 3164*, June 1992.
- Phan, M., Juang, J.-N., Hyland, D.C. (1993) "On Neural Networks in Identification and Control of Dynamic Systems," NASA TM-107702, June, 1993.
- Postlethwaite, I. and Foo, Y.K. (1984) "Representations of Uncertainty and Robustness Tests for Multivariable Feedback Systems," Multivariable Control, S.C. Tzafestas (Ed.), D Reidel Publishing Company, 1984, pp. 151-160.
- Prakash, O., Adams, N.J., and Appleby, B.D. (1991) "Multivariable Control of Space Shuttle Remote Manipulator System," *Proceedings of the AIAA Guidance, Navigation and Control Conference*, New Orleans, Louisiana, August 1991, pp. 1923-1931.
- Ravindran, R., Doetsch, K. H. (1982) "Design Aspects of the Shuttle Remote Manipulator Control," Internal Spar Aerospace Document number 82-1581. Toronto, Ontario.
- Schaechter, D. (1982) "Hardware Demonstration of Flexible Beam Control," *Journal of Guidance and Control*, 5(1) 48-53. January 1982.
- Scott, M.A., Gilbert, M.G., Demeo, M.E. (1993) "Active Vibration Damping of the Space Shuttle Remote Manipulator System" *Journal of Guidance and Control*, vol. 16, Sept.-Oct. 1993, pp. 275-280.

- Seraji, H., Jamshidi, M., Kim, Y.T., Shahinpoor, M. (1986) "Linear Multivariable Control of Two-Link Robots," *Journal of Robotic Systems*, vol. 3, Winter 1986, p. 349-365.
- Shoenwald, D.A., Feddema, J.T., Eisler, G.R., and Segalman, D.J. (1991) "Minimum-Time Trajectory Control of a Two-Link Flexible Robotic Manipulator," *1991 IEEE International Conference on Robotics and Automation*, Sacramento, California, April 9-11, 1991, pp. 2114-2120.
- Singer, N.C., and Seering, W.P. (1990) "Preshaping Command Inputs to Reduce System Vibration" *Journal of Dynamic Systems, Measurement, and Control*, vol. 112, March 1990, pp. 76-82.
- Smart, D. (1992) "Analysis of Gravitational Effects on Flexible Multibody Systems," Masters thesis, Mechanical Engineering Department, Auburn University, Auburn Alabama, August 28, 1992.
- Smart, D. (1993) "Effect of Gravity on the Static and Dynamic Characteristics of a Single Link Component of Flexible Multibody Systems," *Proceedings of ASME 14th Biennial Conference on Mechanical Vibration and Noise*, Albuquerque, NM, September 19-22, 1993.
- Spector, V.A. (1988) "Modeling of Flexible Systems for Control System Design," Ph.D. thesis, University of Southern California, Department of Mechanical Engineering, Dec. 1988.
- Spector, V.A., and Flashner, H. (1989) "Sensitivity of Structural Models for Noncollocated Control Systems," *ASME Journal of Dynamic Systems, Measurement, and Control*, vol. 111, Dec. 1989, pp. 646-655.
- Stroud, Richard, C. (1987) "Excitation, Measurement, and Analysis Methods for Modal Testing," *Sound and Vibration*, August 1987. pp. 12-27.
- Sunada, W.H., and Dubowsky, S. (1983) "On the Dynamic Analysis and behavior of industrial Robotic Manipulator with Elastic Members," *Journal of Mechanical Design*, vol. 105, pp. 42-51, 1983.
- Truckenbrodt, A. (1982) "Control of Elastic Mechanical Systems," *Regelungstechnik*, vol. 30, pp. 277-285, 1982.
- Tzes, A.P, and Yurkovich, S. (1989) "Adaptive Precompensators for Flexible-Link Manipulator Control," *Proceedings of the 28th Conference on Decision and Control*, Tampa, Florida, December 1989, pp. 2083-2087.
- Wells, R.L, Schueller, J.K., and Tlustý, J. "Feedforward and Feedback Control of a Flexible Manipulator Arm," *IEEE Control Systems Magazine*, vol. 10.
- Wie, B. (1981) "On the Modeling and Control of Flexible Space Structures," Ph.D. Thesis, Stanford University, DUDAAR 525, June 1981.
- Yurkovich, S, Tzes, A.P., Lee, I, Hillsley, K. (1990) "Control and System Identification of a Two-link Flexible Manipulator," *1990 IEEE International Conference on Robotics and Automation*, Cincinnati, Ohio, May 13-18, 1990. pp. 1626-1631.

## Appendix A

### Hyperstability and Positive Definite Systems - Definitions

#### Hyperstable

---

The system

$$\begin{aligned}\dot{x} &= Ax + Bu \\ y &= Cx + Du\end{aligned}\tag{A.1}$$

is Hyperstable if for any  $u$  where

$$\int_0^T u'(t)y(t)dt \leq \delta[\|x(0)\|] \sup_{0 \leq t \leq T} \|x(t)\| \tag{A.2}$$

the following inequality holds

$$\|x(t)\| \leq k(\|x(0)\| + \delta) \tag{A.3}$$

where  $\delta$  and  $k$  are positive constants.

#### Asymptotically Hyperstable

---

The system is Asymptotically Hyperstable if:

$$\lim_{t \rightarrow \infty} x(t) = 0 \tag{A.4}$$

Also applies.

#### Positive Real (PR)

---

A rational transfer function matrix  $z(s)$  is Positive Real if:

- 1)  $z(s)$  has real elements
- 2)  $z(s)$  has no poles in  $\text{Re}[s] > 0$ , the poles on the  $j\omega$  axis are simple and the associated residue matrix is non-negative definite Hermitian.
- 3)  $z(j\omega) + z^*(j\omega)$  is non-negative definite Hermitian.

where  $z^*$  implies complex conjugate of  $z$

Also

If  $H(s) = M(s) / N(s)$  is a Positive Real (PR) Transfer function, then:

- 1) The order of  $M(s)$  equals the order of  $N(s) \pm 1$ .
- 2)  $1 / H(s)$  is positive real.
- 3)  $M(s)$  and  $N(s)$  have real coefficients.
- 4)  $M(s)$  and  $N(s)$  satisfy the Hurwitz criterion.
- 5)  $M(s)$  and  $N(s)$  have zeroes with negative real parts.

Note: It can also be shown that PR matrices have no transmission zeros or poles in the open right-half of the complex plane, and that the poles on the imaginary axis are simple and have non-negative definite residues (Anderson, 1967).

### **Strictly Positive Real (SPR)**

---

For a linear transfer function  $z(s)$ :

- 1) If  $z(s)$  is Positive Real  $\Leftrightarrow$  it is hyperstable.
- 2) if  $z(s)$  is Strictly Positive Real.  $\Leftrightarrow$  it is asymptotically hyperstable.

### Kalman-Yacubovich Lemma

The transfer function

$$H(s) = D + C(sI - A)^{-1}B \quad (\text{A.5})$$

is Strictly Positive Real if there exists a symmetric positive definite matrix  $P$  and a matrix  $K$  and  $L$  such that for any positive definite  $Q$ ,

$$\begin{aligned} A^T P + PA &= -Q \\ B^T P + K^T L^T &= C \end{aligned} \quad (\text{A.6})$$

If  $D=0$ , then  $H(s)$  is Strictly Positive Real if

$$\begin{aligned} A^T P + PA &= -Q \\ B^T P &= C \end{aligned} \quad (\text{A.7})$$

### Passive

If a system  $\dot{x} = \bar{A}x$  has a negative definite dynamic matrix ( $\bar{A} < 0$  or equivalently  $\bar{A} + \bar{A}^T < 0$ ) the system is *passive*. Where  $\bar{A} = T^{-1}AT$ .

Note: Geometrically,  $\bar{A} + \bar{A}^T < 0$  means:  $\angle(x, \bar{A}x) \in (90^\circ, 270^\circ)$ . Thus  $x(t)^T x(t)$  decreases as  $t \rightarrow \infty$  since the component of  $\dot{x}$  projected onto  $x$  is in a direction opposite to  $x$ . See Figure A.1.

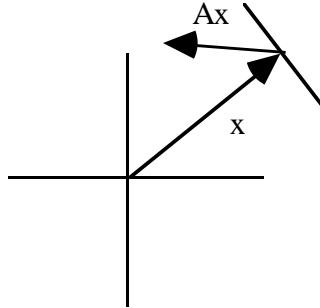


Figure A.1

Geometric Interpretation of  $\bar{A} + \bar{A}^T < 0$